University of Würzburg

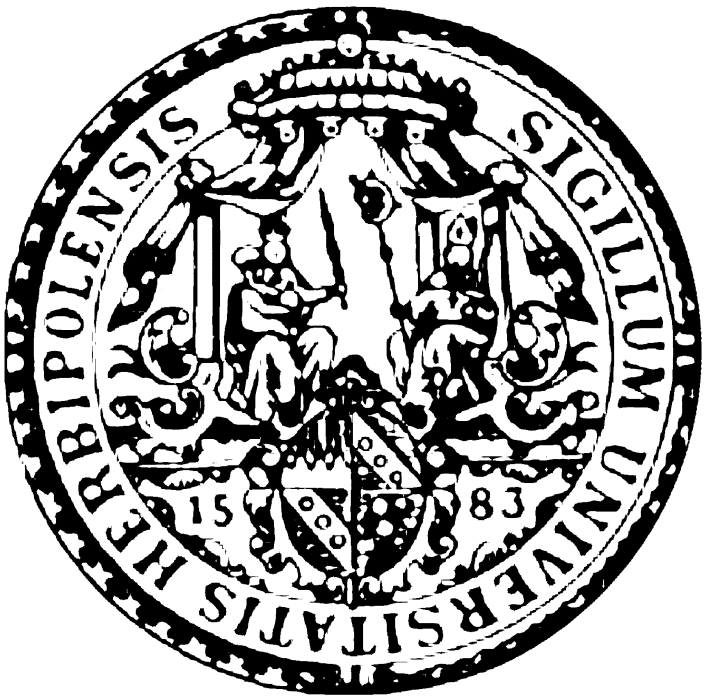

Chair for Astronomy

Bachelor Thesis

Amplitude Self-Calibration Corrections in TANAMI VLBI Experiments

Alexander Kappes

University of Würzburg

Chair for Astronomy

Bachelor Thesis

Amplitude Self-Calibration Corrections in TANAMI VLBI Experiments

* * *

Amplituden selbstkalibrations Korrekturen in TANAMI VLBI Experimenten

---

Author:
Alexander Kappes

Supervisor:
Prof. Dr. Matthias Kadler

Date of submission:
18.11.2013

Abstract

In this bachelor thesis I analyse the amplitude self-calibration corrections of the Tracking Active Galactic Nuclei with Austral Milliarcsecond Interferometry (TANAMI) experiments. Active Galactic Nuclei (AGN) are among the brightest objects over all wavelengths in the universe and some of them eject pairs of highly collimated plasma outflows, called jets. Although these jets are studied for about half a century now, they are still not well understood. The TANAMI project is the first to utilise a Very Long Baseline Interferometry (VLBI) array, that monitors a selected sample of about 80 AGNs on the southern hemisphere in the milliarcsecond regime at two frequencies (8.4 GHz and 22.3 GHz) to study the long term evolution of radio jets in combination with observations in the optical, X-ray and γ-ray regime. TANAMI uses a heterogenous array, which can differ in configuration in every observation cycle leading to strong variations in the data qualitiy. This complicates the imaging process of the VLBI data, which relies on self-calibration of the data. Here, the agreement between the clean model of the final self-calibrated image and the un-self-calibrated data is studied by applying a constant gain correction factor from amplitude self-calibration. Hereby 174 observations in X-band and 97 in K-band are investigated in total. The gain correction value distributions show that the frequently used telescopes (Parkes, ATCA, Mopra and Hobart while Ceduna does not), agree better with the clean models than the others, which is an expected result because the experienced performance is better. One interesting result of Ceduna is a constantly increased gain value in the K-band, which might be systematically motivated and requires further investigation. TIGO and O'Higgins generally need to be calibrated more intensely, while Hartebeesthoek generally seems to be in good agreement with the clean models. Most telescopes show some very high gain corrections that should be examined further. Additionally, the results suggest that the performance of the array does not seem to depend strongly on the declination of the observed sources. All conclusions reached in this thesis would benefit from more data, which motivates the repetition of this study in the future, when more data are collected. This is the first time that such a systematic study has been performed on a large number of observations within the TANAMI project. The results cannot indicate an exact amplitude uncertainty but they can be used in future to improve the estimated uncertainties of the amplitudes.

Zusammenfassung

In dieser Bachelorarbeit analysiere ich die Amplituden-Selbstkalibrations Korrekturen der TANAMI Experimente. AGN sind mitunter die über alle Wellenlängen hellsten bekannten Objekten im Universum. Einige von ihnen stoßen paare von hochgradig kollimierten Plasmaauswürfen aus, welche Jets genannt werden. Obwohl diese Jets schon seit etwa einem halben Jahrhundert untersucht werden, sind sie kaum verstanden. Das TANAMI Projekt ist das erste, welches ein VLBI Array verwendet, das eine Auswahl an etwa 80 AGNs in der südlichen Hemisphäre in der Ordnung von Millibogensekunden beobachtet. Dies findet bei zwei Frequenzen statt (8.4 GHz und 22.3 GHz), um die Langzeitentwicklung von Radiojets in Kombination zu Beobachtungen im optischen-, sowie Röntgenstrahlen- und Gammastrahlen-Bereich zu studieren. TANAMI verwendet einen heterogenen Verbund aus Teleskopen, dessen Aufstellung sich in jedem Beobachtungszeitraum ändern kann, was zu großen Unterschieden in der Datenqualität führen kann. Das erschwert den bildgebenden Prozess auf Basis der VLBI Daten, welcher auf die Amplituden-Selbstkalibration angewiesen ist. Hier kann man unter der Annahme, dass das erlangte clean model richtig sei einen Faktor errechnen welcher den Grad der Amplitudenveränderung über den gesamten Beobachtungszeitraum wiedergibt. Hier ist nun eben dieser Koeffizient untersucht worden, wobei 174 Beobachtungen im X-band und 97 im K-band herangezogen wurden. Die Verteilungen dieser Werte zeigen, dass die häufig verwendeten Teleskope, Parkes, ATCA, Mopra und Hobart (Ceduna jedoch nicht) generell Daten liefern, welche besser mit den Modellen übereinstimmen als bei anderen Teleskopen. Dieses Ergebnis ist jedoch nicht überraschend, da eben diese Teleskope erfahrungsgemäß bessere Daten liefern und aus diesem Grund häufiger eingesetzt werden. Ein interessantes Ergebnis für Ceduna ist, dass im Schnitt alle selbstkalibrations Korrekturwerte im K-band höher liegen, was auf einen systematischen Effekt hindeutet, der weiter untersucht werden muss. TIGO und O'Higgins müssen im allgemeinen intensiver kalibriert werden, während Hartebeesthoek generell scheinbar Daten liefert, welche mit dem clean model gut übereinstimmen. Die meisten Teleskope weisen zu dem ein paar wenige sehr hohe Werte auf, die weiter untersucht werden müssen. Zusätzlich scheint die Funktionsfähigkeit des Arrays nicht sonderlich von der Deklination der beobachteten Quelle abzuhängen. Alle getroffenen Schlüsse würden von einem größeren Datensatz bezüglich der Aussagekraft profitieren, weshalb diese Untersuchungen in der Zukunft wiederholt werden sollten. Diese Arbeit bildet die erste systematische Studie über die große Anzahl an Beobachtungen innerhalb des TANAMI Projektes im Hinblick auf die Amplituden Selbstkalibration. Die Ergebnisse können zwar keine exakte Amplituden Messunsicherheit angeben, jedoch schaffen sie eine Grundlage für zukünftige sinnvolle Fehlerabschätzungen.

Contents

1. Introduction

The sky has always been a magnificent subject of observation for the humans. Understanding the processes and connections has been a compelling topic since the existence of humanity. Among the most powerful objects are the AGN, galaxies with a so called 'active nucleus', emit radiation in all wavelengths. The nucleus, a small region inside the host galaxy, emits a broad part of the electromagnetic (EM) spectrum. The inner centre of the galaxy contains a Super Massive Black Hole (SMBH) with an accretion disc surrounded by a torus. Sometimes these objects emit radiation which is thousand times more than that produced in the Milky Way Galaxy (for more information see Robson (1996)).

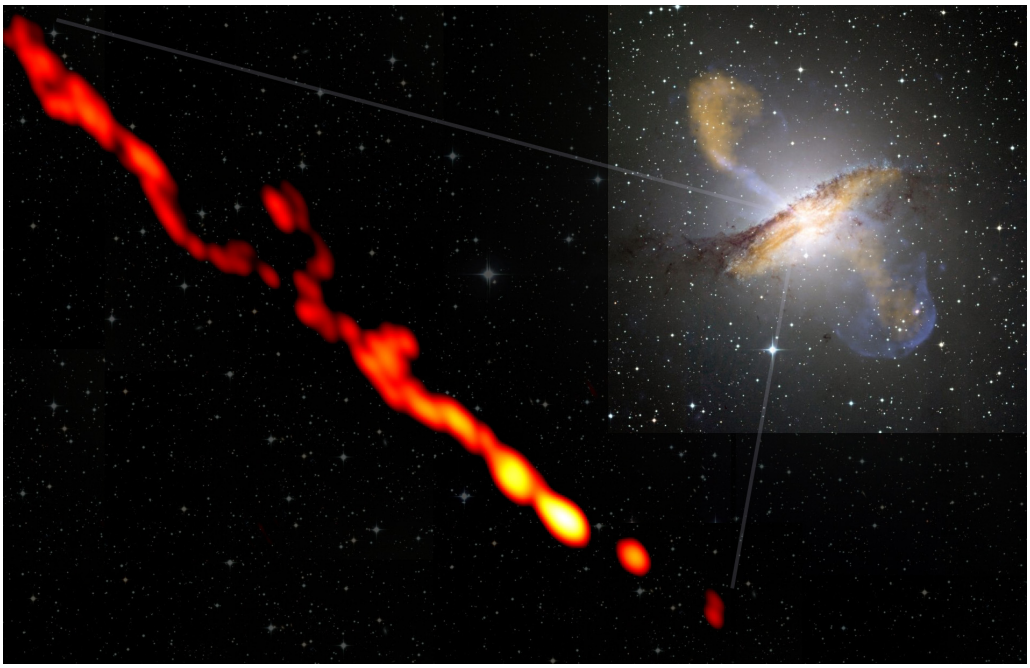

Figure 1.1.: Zoom into the inner jets of Centaurus A. Based on Müller et al. (2011). Credit: M. Kadler

In a number of cases, a jet structure, consisting of relativistic plasma that is ejected in a straight matter string, can be observed (Ghisellini (2011)). Figure 1.1 shows the AGN which is closest to us, Centaurus A. In the upper right corner, one can see a multi-wavelength (radio, optical and x-ray) image of the galaxy and its two jets, emitted from the inner region. This can be seen in radio wavelengths because the jet is very luminous compared to the host galaxy and radio waves penetrate the torus. By using a network of radio-telescopes from all over the world observing one source at a time, it is possible to acquire high-resolution images. This is achieved by the VLBI technique, which produces a resolution in the milliarcseconds regime. The jet displayed on the left side is a close look into the inner part of the galaxy with a resolution in the lightday regime. This image shows the highest resolved jet of an AGN (Müller et al. (2010)). This was accomplished through use of a network of radio telescopes in the southern hemisphere

used by the program TANAMI (see Figure1.2).

TANAMI* is a program which, among others, images and monitors AGN. The primary sample consisted of 43 blazars† that were selected as an agreement of a radio selected flux-density subsample and a γ-ray selected subsample based on the results of Energetic Gamma Ray Experiment Telescope (EGRET)(Hartman et al. (1992)). Additionally, all radio loud AGN south of $\delta = -30°$ based on the catalogue of Stickel et al. (1994) fullfilling the threshold of a radio flux density of $S_{5\ \mathrm{GHz}} > 2$ Jy and showing a flat radio spectrum between 2.7 GHz and 5 GHz are added. Since November 2007, the specific role of TANAMI has been to observe the annotated sources with a declination lower than -30 degrees at 8.4 GHz and 22.3 Ghz. To achieve the required incredible resolution the Long Baseline Array (LBA) is used in combination with other telescopes (see Table 1.1). Long-term monitoring takes place with a recurrence of about three months, which allows kinematic studies to be performed (see e.g. Trüstedt (2013)). This makes a wide field of studies in multi-wavelength observations possible, for example the connection between γ- and radio activities. A more recent description of the TANAMI sample and results of the first radio surveys can be found in Ojha et al. (2010). More recent multi-wavelength study can be found in Böck (2012). Since the program started, TANAMI has observed 93 sources, the majority of which are observed repeatedly. To improve further observation capabilities, other telescopes are joining the program, an example being the latest observations which were assisted by the Warkworth telescope in New Zealand. Important programs that operate in the northern hemisphere using VLBI techniques are Monitoring Of Jets in Active galactic nuclei with VLBA Experiments (MOJAVE) and European VLBI Network (EVN).

Due to the variation among the telescopes that are used, it is necessary to study the applied corrections in the data reduction. This thesis will examine the amplitude self-calibration corrections in all TANAMI observations through June 2013.

The structure of this work is as follows: this introduction is followed by a chapter elaborating on the fundamentals for understanding the hybrid mapping process, that is an essential part to acquire the radio image. The subsequent part presents the study of the corrections in the data reduction, leading into the final chapter with the conclusion and an outlook.

*http://pulsar.sternwarte.uni-erlangen.de/tanami/ (16.November 2013) - is the official website of the TANAMI program

†Blazars are AGN where it is assumed that the line of sight coincide with the jet axis. These objects are very luminous and show a flat spectrum.

Table 1.1.: Telescopes participating the TANAMI program

Telescope name	Diameter (in meters)	Location	Frequency bands[1]
Parkes[2]	64	Parkes, New South Wales, Australia	X, K
ATCA[2]	5 x 22	Narrabri, New South Wales, Australia	X, K
Mopra[2]	22	Coonabarabran, New South Wales, Australia	X, K
Hobart[2]	26	Mt. Pleasant, Tasmania, Australia	X, K
Ceduna[2]	30	Ceduna, South Australia, Australia	X, K
DSS34[3]	34	Tidbinbilla, ACT, Australia	X
DSS43[3]	70	Tidbinbilla, ACT, Australia	X, K
DSS45[3]	34	Tidbinbilla, ACT, Australia	X
Hartebeesthoek[4]	26	Hartebeesthoek, South Africa	X, K
O'Higgins[5]	9	O'Higgins, Antarctica	X
TIGO[5]	6	Concepción, Chile	X
Warkworth[6]	12	Warkworth, New Zealand	X

[1] X-Band: 8.4 GHz, K-Band: 22.3 GHz
[2] Operated by the Australia Telescope National Facility (ATNF) and part of the LBA
[3] Part of NASA's Deep Space Network
[4] Operated by the National Research Facility of South Africa's National Research Foundation
[5] Operated by *Bundesamt f[Pleaseinsert\PrerenderUnicode{Ãij}intopreamble]r Kartographie und Geod[Pleaseinsert\PrerenderUnicode{Ãd}intopreamble]sie* (BKG)
[6] Operated by the Institute for Radio Astronomy and Space Research

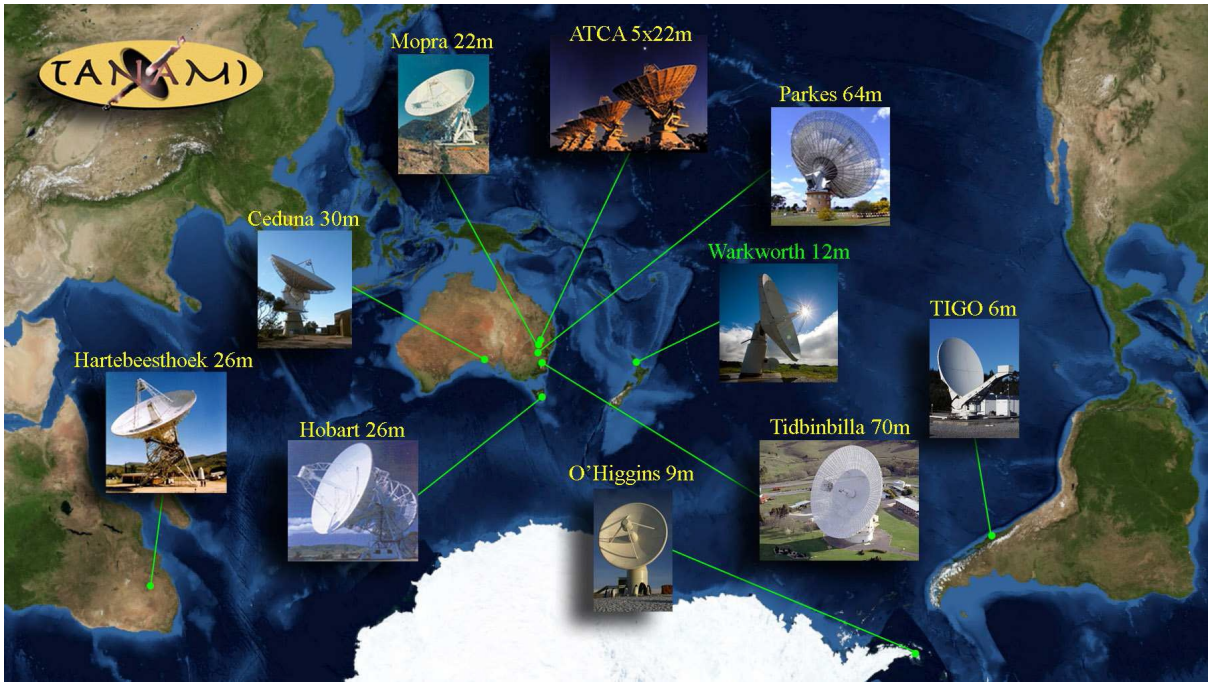

(a)

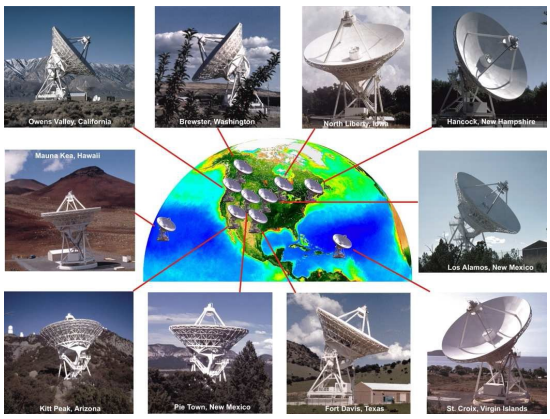

(b)

(c)

Figure 1.2.: The telescope arrays of the VLBI programs MOJAVE (1.2b), called VLBA (Credit: NRAO/AUI) and TANAMI (1.2a) (Credit: M. Kadler) and the telescope array EVN(1.2c)(Credit: The European VLBI Network)

2. Imaging of VLBI experiments

One aim of VLBI observation is a highly resolved image of the inner jet structure of the most distant objects of the known universe, the AGN. The process begins with the observation of a source, whereby all radio telescopes point simultaneously at the source. The telescopes themselves do not need to be connected, but data regarding the exact time and position of the telescopes must be collected. This information is essential for the next step of the data processing, which is the correlation of the data. Afterwards, the data need to be amplitude and phase calibrated, which will not be discussed in this thesis. For further information see Thompson et al. (2001). The data now represents the convolution of the intensity distribution with the array, the so called visibilities, which have an amplitude and a phase. The goal is now to reconstruct the image with so called *hybrid mapping*, that includes an iterative acquisition of a model and a self-calibration process. For a better understanding it is helpful to have some basic knowledge of this subject in advance. The information presented in this chapter is based on Burke & Graham-Smith (2010)(for section 2.1) and Taylor (1997)(for section 2.2) and Kadler (2011)* unless noted otherwise.

2.1. Interferometry measurement in the radio regime

Astronomical interferometry techniques date back to the optical work of Michelson and Pease (Michelson & Pease (1921)), to measure the diameter of several stars like Arcturus and Betelgeuse. Here, interferometry helped to obtain a sufficiently fine angular resolution to allow these measurements. The instrument that was used was named after the inventor - the Michelson stellar interferometer, which uses the superposition of two EM waves.

In the same way and with the same aim, radio astronomers use this technique. Figure 2.1 shows the basic application with two radio dishes as an illustration. Any angular resolution of a certain telescope system can be described by the Rayleigh criterion. For radio telescopes this can be approximated by

$$\sin(\alpha) \approx 1.22\frac{\lambda}{D} \tag{2.1}$$

where α is the angular resolution, λ the wavelength of the observed signal and D the diameter of the telescope. This says that after choosing the desired wavelength, there is only the possibility to increase the resolution by enlarging the diameter D. Building a bigger dish is a possibility, but reaches reaches its limit quite fast†. Here, interferometry helps to increase the resolution. With a telescope system, as shown in Figure 2.1, the diameter D in equation 2.1 is the distance between both telescopes b_λ. This telescope system will work like one big radio dish with the

*http://www.astro.uni-wuerzburg.de/∼mkadler/teaching.html (16.November 2013)

†the two biggest steerable radio dishes have a diameter of about 100m (Green Bank (USA) and Effelsberg (DE).

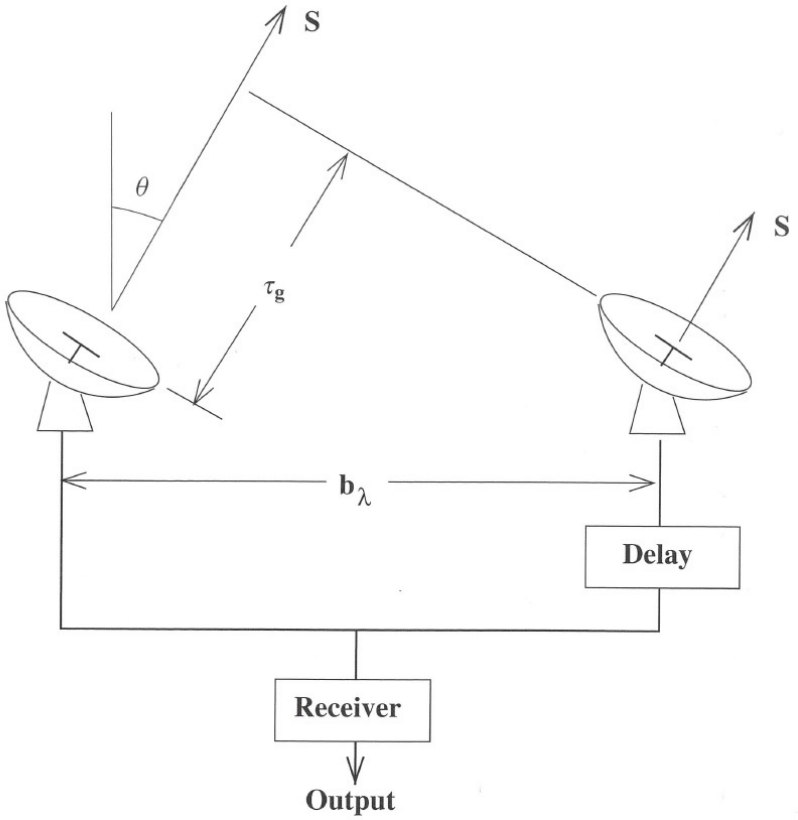

Figure 2.1.: Geometry of the two-element Michelson interferometer with the geometrical path delay τ_g that is compensated by the delay circuit in the receiver. An additional delay τ_i can be inserted by this delay circuit (Burke & Graham-Smith (2010))

diameter b_λ. One telescope receives the signal respectively to the other with the delay τ_g because of the geometrical alignment that creates a longer way to travel for the radio signal as shown in Figure 2.1. This is based on the assumption of an infinite distant compact object with a flat spectrum within the observed spectrum (compare analogy to double slit experiment Young (1802)). It can be calculated with:

$$\tau_g = \frac{b}{c} \sin\theta \tag{2.2}$$

where b is the length of the baseline and c is the speed of light. Afterwards, the correlator integrates and combines the two signals and generates an output of the two amplitudes of the time-averaged product, called *cross power product* R_{xy}.

$$R_{xy}(\tau_g) = A(\vec{s}) \cdot S \cdot \cos(2\pi\tau_g\nu) = A(\vec{s}) \cdot S \cdot \cos\left(\frac{2\pi\nu b \sin\theta}{c}\right) \tag{2.3}$$

Where $A(\vec{s})$ is the effective area, $\vec{s}$ the direction of the telescopes and S the source's flux. The correlator brings in another time delay τ_i to define a reference position $\vec{s_0}$ close to a source with the position $\vec{s}$ where $\tau_g = \tau_i$. The position $\vec{s_0}$ is called *phase-tracking centre*. τ_g compensates the geometrical time delay. The direction to the source with respect to the phase-tracking centre

can now be written as:

$$\vec{s} = \vec{s_0} + \vec{\sigma} \tag{2.4}$$

where the displacement $\vec{\sigma}$ is a vector orthogonal to $\vec{s_0}$ (see Figure 2.2).
Since the recorded signal is a convolution of the synthesized beam of the array and the observed sky, a Fourier transformation has to be applied in order to process the signal according to the convolution theorem. As the cross power product is the convolution of the array and the source, the visibility function V can be introduced as:

$$V = \int A(\sigma) B_\nu(\sigma) e^{i2\pi \vec{b}\sigma} d\Omega \tag{2.5}$$

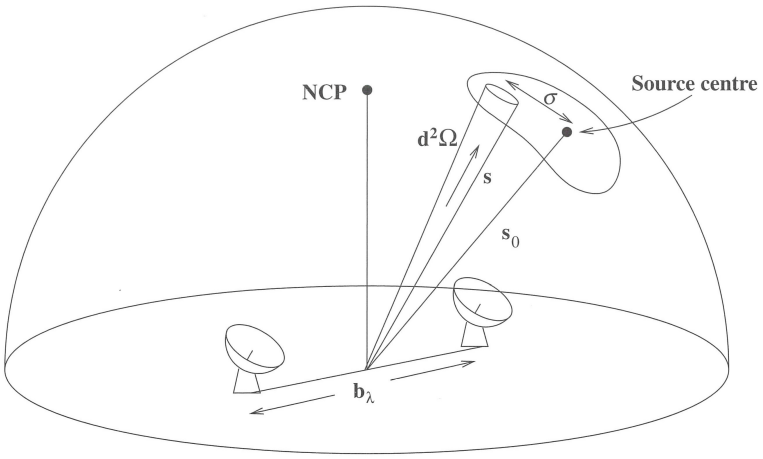

Figure 2.2.: Contribution of a small receiving element in the direction $\vec{s}$ and solid angle $d\Omega$; NCP stands for the North Celestial Pole (Burke & Graham-Smith (2010))

$B_\nu(\sigma)$ is the brightness of the source and $\vec{b}$ represents the baseline vector between two telescopes. Since the correlator output is a signal for each synthesized baseline, it is helpful to introduce another coordinate system (see Figure 2.3). One defines a right-handed rectilinear coordinate system (u,v,w) in units of the observed wavelength. The baselines are parallel to the (u,v)-plane respectively, and the w-axis is collinear to the $\vec{s_0}$ vector. $\vec{\sigma}$ is also parallel to the (u,v)-plane. To form this plane, l and m are used for the directions of the cosines of u,v.

$$u = \frac{\nu b \cos\theta}{c} \tag{2.6}$$

$$v = \frac{\nu b \sin\theta}{c} \tag{2.7}$$

$$\Rightarrow V = \int_{4\pi} A(l,m) B_\nu(l,m) e^{i2\pi(ul+vm)} \frac{dl\,dm}{\sqrt{1-l^2-m^2}} \tag{2.8}$$

The visibilities are measured in the (u,v)-plane that corresponds to a Fourier transformation of the brightness distribution convolved with the synthesized beam of the array as mentioned above. More telescopes lead to more baselines, meaning a better coverage of the (u,v)-plane.

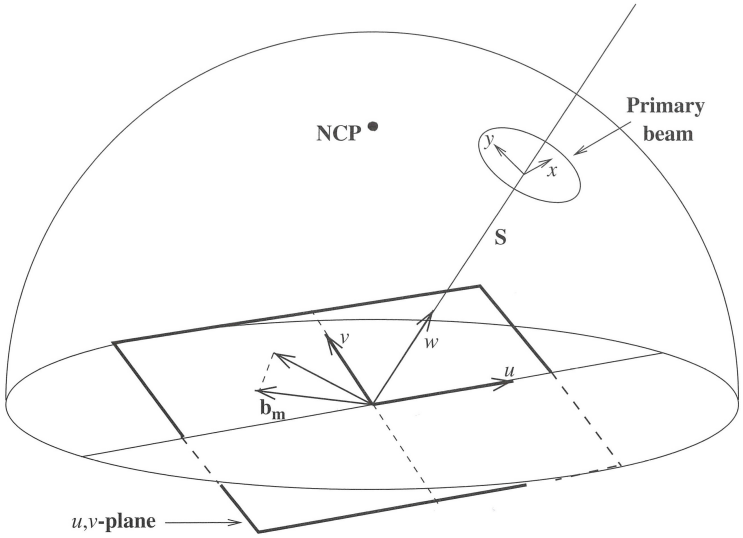

Figure 2.3.: The geometrical relation of the (u,v)-plane to the interferometer. x, y are used for the small-angle approximation of l, m parallel to u,v. (Burke & Graham-Smith (2010))

The coverage of the plane can also be altered by the angle to the observed source and improved by a longer observation time due to the rotation of the Earth, that also rotates the baseline vectors. Because the earth rotates during the experiment and the telescopes track the source, the baseline vector is time-dependent. This leads to a denser coverage in the (u,v)-plane and is called *earth rotation synthesis*. This is shown in Figure 2.4. It is important to mention that the telescopes recorded the signal for ten minutes and changed their objective to two other sources whereupon the first object is in focus again. This is done to compromise observing as many sources as possible with an optimal coverage of the plane. This leads to arcs cut in pieces, as shown in Figure 2.4. If one observes continuously a single source, drawn-through -arcs will be seen.

2.2. Hybrid imaging with DIFMAP

Since one has a Fourier transformed image of the source, it has to be deconvolved. During onward progress, point sources are used for the modelling because they are simple to apply. The so called self-calibration is applied during the modelling, where the amplitude may be altered, however the total flux should stay constant. Because self-calibration occurs alongside the modelling, this step is referred to as *hybrid mapping*. For later use, the point sources may be replaced by Gaussian sources, which allow for kinematic studies to be performed. One has worked out a good model if the subtraction of the intensity distributions between model and observation is only a weak noise background. The model can now produce the image of the source as shown on the left side of Figure 1.1. This is called a clean model.
Following these steps, the use of computational methods is unavoidable due to the amount

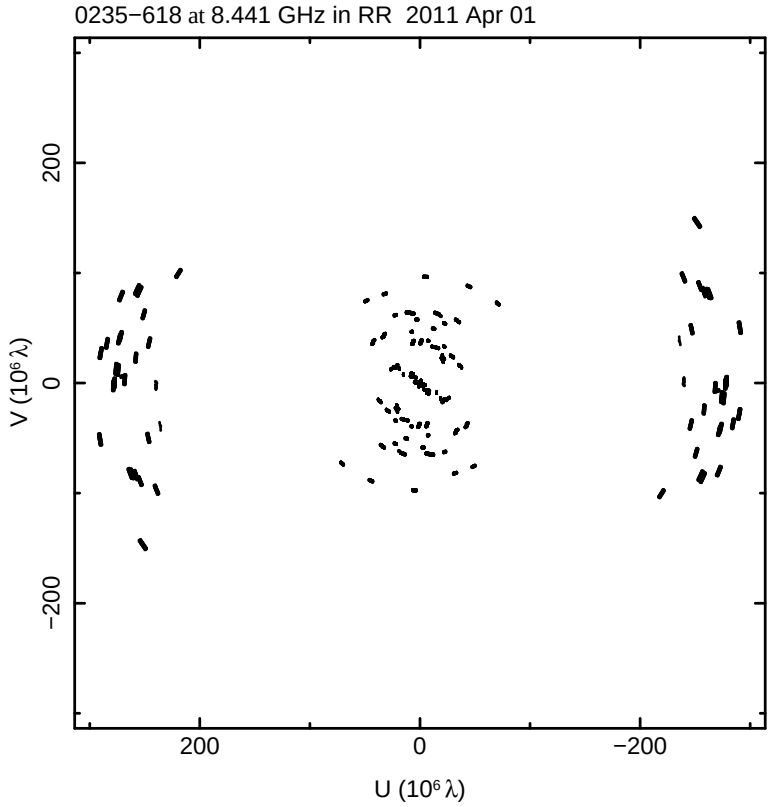

Figure 2.4.: (u,v)-plane coverage of the TANAMI VLBI experiment on source *PKS 0235-618*

of data. The implemented Software DIFMAP[‡] can process the data after the correlation and calibration up to receiving the final image. After the data is loaded, it can be inspected in various ways. Figure 2.4 shows an example, a plot of the (u,v)-plane. At first, the data is being averaged with 32 seconds and then weighted to shape the dirty beam[§]. The most common weighting schemes are either *natural weighting* or *uniform weighting*, where the *natural* option weights every visibility with:

$$W_{j,k} = 1 \tag{2.9}$$

where j,k is the j,k-th cell. This leads to minimisation of the noise and a maximisation of the signal-to-noise ratio.
The *uniform weighting* is defined as:

$$W_{j,k} = \frac{1}{the\ number\ of\ visibilities\ in\ j,k} \tag{2.10}$$

It gives less weighting to densely-sampled regions of the (u,v)-plane, which increases the resolution, but also increases the noise. Note that parallel to all steps in this process, single data can be flagged, which means it will be ignored for the further process. This happens to data

[‡]ftp://ftp.astro.caltech.edu/pub/difmap/difmap.html (16.November 2013) official homepage for more details and downloading DIFMAP
[§]The dirty beam is the Fourier transformed (u,v)-plane

that show an obvious measurement error or an unusually large uncertainty. The final part of the data processing is the Fourier inversion of the visibility that leads to the so called *dirty image* and the deconvolution of this image. The most common procedure follows the CLEAN algorithm after Högbom (1974). The algorithm is presented here following the lecture by Kadler (2011):

1. Execute a Fast Fourier transformation (FFT) of the interpolated (*u,v*)-plane to acquire the *dirty image*.
2. Determine the brightest pixel in the *dirty image* and subtract the dirty beam response of a point source.
3. This depicts a model which is just a point source in the first run-through. This is stored in a new map that will be modified in the following loops.
4. Loop the steps 2 and 3 by using the maxima of the *dirty image* at any one time. This is now called *residual map*.
5. End the loop when the *residual map* no longer shows clear localized maxima.
6. Convolve the developed *clean* model with a synthesized Gaussian beam (*clean beam*). The full width at half maximum (FWHM) equals the width of the main lobe of the dirty beam. This yields a *clean image*.
7. Add the *residual map* to the *clean image*.

A modified way to use the CLEAN algorithm is the previously mentioned *hybrid imaging* that is widely used especially in VLBI imaging. This modification takes advance of the closure relationship between the visibility phases and amplitudes that is given by every triangle of antennas for the phase calibration and a set of four antennas in case of amplitude calibration (in more detail see Thompson et al. (2001)). This relationship is independent of the errors introduced by the atmosphere and ionosphere that cause phase shifts or amplitude changes, that can not be simply measured or calculated. The general applied modifications are listed following the lecture by Kadler (2011):

- From the point one has acquired a first model that reproduces the (*u,v*)-plane reasonably well, a phase self-calibration is performed. The acquired data yields to a second model that is used in the further process.
- The *clean* process of the CLEAN algorithm is repeated with the phase self-calibration (*clean-selfcal*) until there is no further improvement of the model. Here, the amplitude self-calibration is applied, that uses a long solution interval. This corrects only constant or slowly varying errors in the visibility amplitudes.
- Afterwards, a new cycle begins, where the previous model is waived and a new one is developed with the new amplitude and phase calibrated data. Again, the best acquired model is being amplitude self-calibrated, this time with a smaller solution interval.
- After iteratively improving the data with a smaller and smaller solution interval, one has obtained a self-consistent model that reproduces the calibrated data.

Unfortunately, this technique waives the information about the absolute source position because applying the phase self-calibration does not tell whether one single phase error was corrected for one telescope or multiple phase errors at multiple telescopes.

2.3. Example

To illustrate section 2.2, this part will feature an observation of *PKS 0235-618* recorded by TANAMI on 1 April 2011 in the X-Band, as an example of *hybrid imaging* in praxis. As mentioned before, during the whole process data will be flagged if they show a clear discrepancy to the trend of all the other data, or if the uncertainty is too high.
Figure 2.4 shows the (u,v)-plane of this experiment. After applying the *natural weighting* and averaging the data and calculating errors from the internal scatter, one acquires the *dirty image* (shown in Figure 2.5).

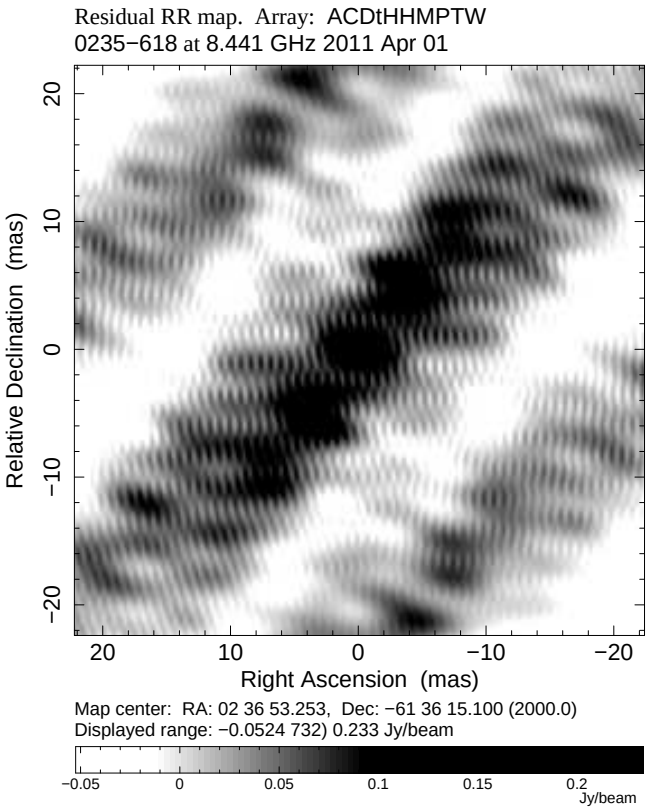

Figure 2.5.: Residual map of *PKS 0235-618* after averaging the data (*dirty image*)

Following the CLEAN algorithm and determining the brightest pixel, the residual map is altered after subtracting the dirty beam response of a point source, as shown in Figure 2.6a and 2.6c. One can define windows where the point sources can be placed to evaluate the model with prior knowledge. By adding more model elements, following the algorithm instructions, the jet components are being formed, whereas the amplitude of the fluctuations in the residual map decreases. Figure 2.6b shows the residual map where a satisfying model has been achieved. The complementary map of the components is shown in Figure 2.6d. On the first look there is not that much difference in the morphology to Figure 2.6a. This is due to the fact that the most luminous feature is the central region (compare number of contours of central region and a component) and therefore is the major contribution of the flux in the residual map. The following components have a clearly smaller influence. Comparing the displayed range of both maps (2.6a and 2.6b), one can see a clear decrease of the positive flux that is explainable with the further model components.

Based on the current model, the amplitudes of the telescopes are being corrected, while the flux is conserved. Here, one can compute an amplitude correction value that tells the percentage of the altering per telescope per data stream (or a sub-band, as in this case) for the total observation time. The function *gscale* in DIFMAP that outputs the gain (correction) value. This thesis investigates these values in chapter 3.1. An important feature of the gain correction values is their correlation among themselves. Later in this process, a further amplitude and phase self-calibration is performed with a specified solution interval based on the current model. Here, the interval is chosen for 180 minutes. This will be repeated for shorter and shorter intervals (here 180, 60, 20, 5, 1, 0 minutes). Now a self-consistent model is acquired that reproduces the calibrated data. The remaining residual map and clean map are shown in Figure 2.7. Figure 2.7a shows the residual map remaining after the subtraction of the clean model. The displayed range is from about -0.0013 to 0.0014 Jy/beam. This is very symmetric about 0, which is an indication of a good model, because no more flux is expected that is missing in the model. Figure 2.7b shows the clean map, which is the convolution of the beam with the created model. The beam has a FWHM of 1.74 x 0.543 (mas) at 3.13°. The brightest flux reaches 0.258 Jy/beam, while it is subdivided in nine contours, namely -0.47%, 0.47%, 0.93%, 1.88%, 3.76%, 7.52%, 15%, 30.1% and 60.2% of the peak value. In the figure, a luminous core can be seen (indicated by many contours) along with fainter features (indicated by few contours). The morphology can be double-checked by observing the source a second time and repeating the *hybrid mapping* process.

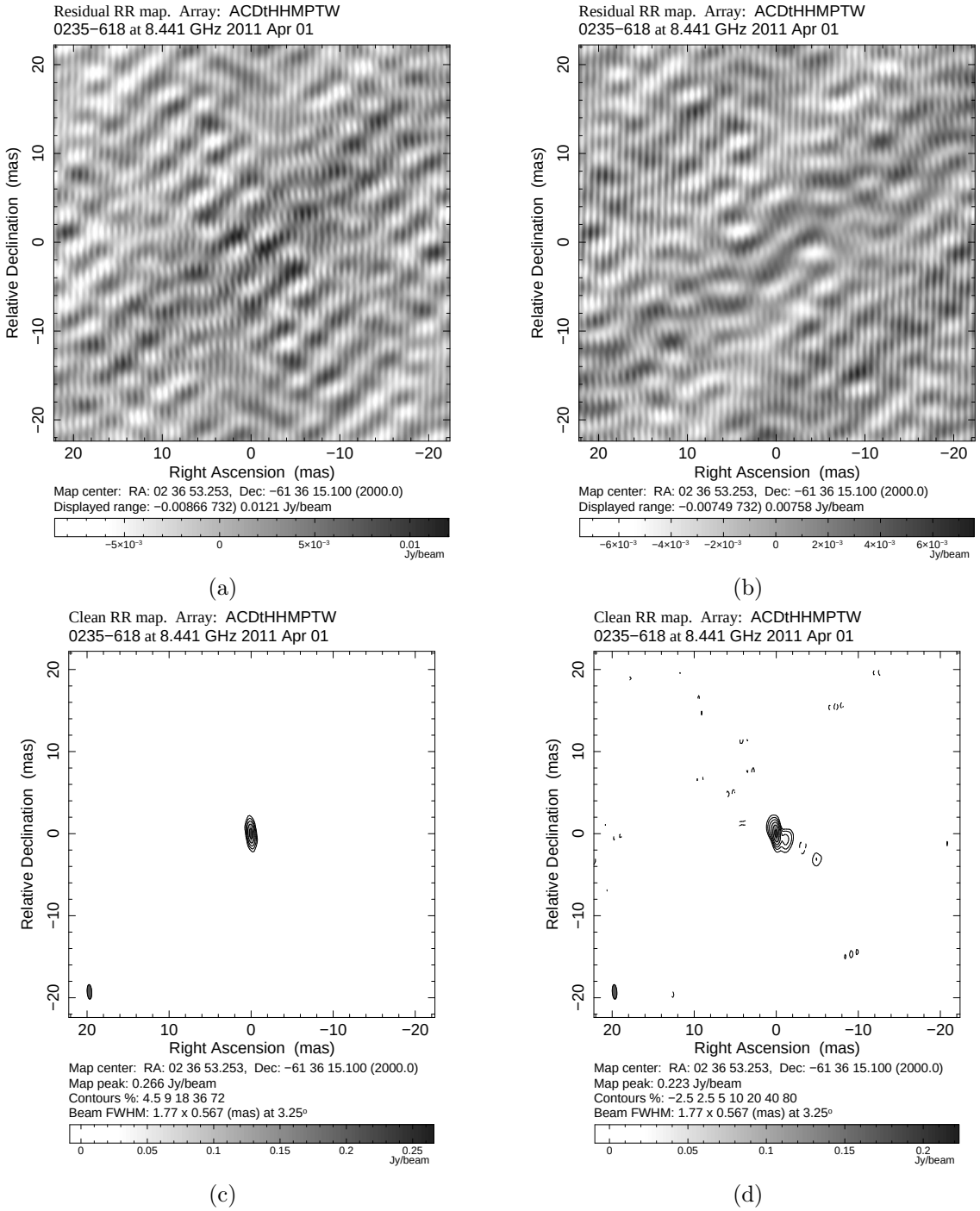

Figure 2.6.: Residual map of *PKS 0235-618* applying one (2.6a) and many (2.6b) components in the model. Complementary the map of the components applying one (2.6c) and many (2.6d) components in the model

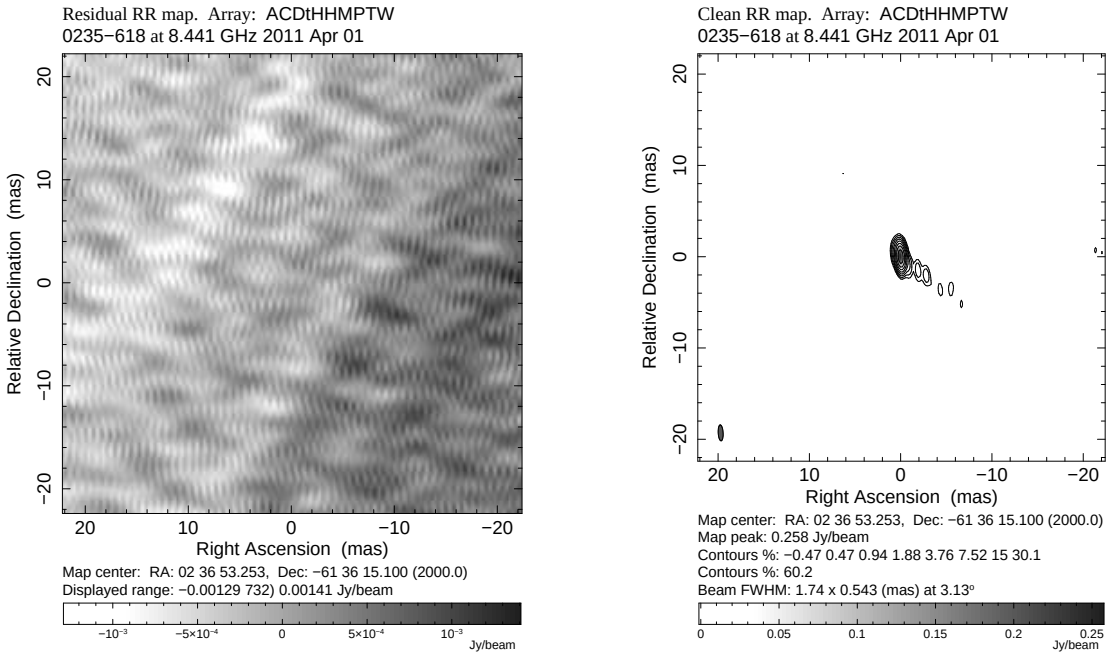

(a) (b)

Figure 2.7.: Final residual (2.7a) and clean map (2.7b) of *PKS 0235-618* passing trough the hybrid mapping

3. Study of the corrections in the data reduction

As described in Chapter 2.2 and shown in an example in Chapter 2.3, self-calibration is an important part of the *hybrid mapping* process. The function representing the alteration of the amplitude over the total observing time is called *gscale* in DIFMAP. Studying the resulting gain correction factors can show possible systematic errors which may be caused by calibration errors, station specific technical reasons or errors within the data processing.
In the following section, these values are analysed over all observations for each telescope (Chapter 3.2.1), for each telescope in each observation cycle (Chapter 3.2.2) and for each observation cycle (Chapter 3.2.3). Additionally one may think of an unknown influence that is dependent on the source's declination (Chapter 3.2.4). The next chapters describe the precise implementation of the issue, followed by a discussion of the results.

3.1. Processing the data

The first step is to collect the available clean models, which were compiled by C. Müller. A total of 174 and 97 clean models in X- and K-band respectively will be used in this analysis. This work uses the clean models registered in this file. With this amount of data, it is convenient to use computational methods to automatise iterative steps. Scripts were implemented that are programmed in SLANG[*], which provides a multi-platform programmer's library to access DIFMAP by running the scripts in ISIS[†].
The first script reads the clean model and the associated observation data from the file by C. Müller. Then, the following steps (known from chapter 2.3) are performed:

1. Loading the data prior to self-calibration.
2. Defining the map size from the saved clean model.
3. Selecting all IFs.
4. Enabling the natural weighting.
5. Averaging the data over 32 seconds.

Afterwards the clean model is read in and the *gscale* function is performed, which outputs the gain values that are of interest for the following process. A file is created that contains the resulting correction values (or gain values) due to amplitude self-calibration in X- and K-band for all observations that have a validated model. These data are printed in the appendix in Table A.1 for the X-band and Table A.2 for the K-band. The sources are named after the Parkes Radio Cataloge (PKS)[‡]. The so called "*epoch*" is used throughout the rest of the thesis as an synonym for observation time and observation band. Table 3.1 displays this information for all

[*] http://www.jedsoft.org/slang/index.html (16.November 2013)
[†] http://space.mit.edu/cxc/isis/ (16.November 2013)
[‡] ftp://cdsarc.u-strasbg.fr/cats/VIII/15/ (16.November 2013)

relevant observation cycles in this thesis, and additionally the telescopes that were operating in the respective *epoch* and the number of observed sources of each observation that has a clean model. Because more clean models in one cycle means a better application for statistics, the *epochs* A to J and L are better to analyse.
The *IF* listed in the Tables A.1 and A.2 indicate the data channel of the observation. They divide the observing band into sub-bands to gather more data, but by assuming, that spectral properties do not depend on the frequency of the sub-bands. Values with an asterisk mark that no data from this telescope were available, hence no gain corrections were calculated. Values with an "–" indicates no participation in the observation. This is sensible, because the channels conflate in the clean models.
For further analysis, the *IF*s for each telescope in each experiment are averaged. This data is studied in the following chapters.

Obs. code	Obs. band	Date of obs (YYYY-MM-DD)	ref. *epoch*	obs. sources*	PA	AT	MO	HO	CE	DSS34	DSS43	DSS45	HA	OH	TI
V252A	X	2007-11-07	A	21(21)	✗	✗	✗	✗	✗				✗		
V252B	K	2008-02-06	B	23(23)	✗	✗	✗	✗	✗		✗				
V252C	X	2008-02-07	C	24(24)	✗	✗	✗	✗	✗		✗		✗		
V252D	K	2008-03-26	D	23(23)	✗	✗	✗	✗	✗		✗				
V252E	X	2008-03-28	E	23(23)	✗	✗	✗	✗	✗		✗		✗		
V252F	X	2008-06-09	F	13(22)	✗	✗	✗	✗	✗				✗		
V252G	K	2008-08-08	G	22(23)	✗	✗	✗	✗	✗				✗		
V252H	X	2008-08-08	H	22(23)	✗	✗	✗	✗	✗			✗			
V252I	X	2008-11-27	I	21(22)	✗	✗	✗	✗	✗		✗			✗	✗
V252J	K	2008-11-29	J	21(22)	✗	✗	✗	✗	✗		✗				
V252K	X	2009-02-23	K	7(22)	✗	✗	✗	✗	✗		✗			✗	✗
V252L	X	2009-02-27	L	21(23)	✗	✗	✗	✗	✗			✗		✗	✗
V252N	X	2009-09-05	N	8(24)	✗	✗	✗	✗	✗		✗				✗
V252O	X	2009-12-14	O	7(23)	✗	✗	✗	✗	✗						✗
V252P	X	2010-03-12	P	1(26)	✗	✗	✗	✗	✗		✗				
V252Q	K	2010-05-05	Q	8(25)	✗	✗	✗	✗	✗						
V252R	X	2010-05-07	R	2(25)	✗	✗	✗	✗	✗		✗				✗
V252S	X	2010-07-24	S	3(24)	✗	✗	✗	✗	✗		✗				✗
V252T	X	2010-08-28	T	1(24)	✗	✗	✗	✗	✗	✗		✗	✗		✗

Table 3.1.: TANAMI observations used in this thesis (K,X-band) with a list of telescopes participating in each observation. The ref. *epoch* will be used as an acronym for each observation. PA = Parkes, AT = ATCA, MO = Mopra, HO = Hobart, CE = Ceduna, HA = Hartebeesthoek, OH = O'Higgins and TI = TIGO.
*number of observed sources of each observation, for which clean models are available. The values in brackets are the total number of observed sources.

3.2. Gain value distributions

The gain values are studied in the next chapters in the following way:

- Chapter 3.2.1 evaluates gain distributions for a single telescope over all *epochs* (see appendix on pages 65 to 67 for all corresponding histograms)
- Chapter 3.2.2 evaluates gain distributions for single telescopes in single *epochs* (see appendix on pages 71 to 86 for all corresponding histograms)
- Chapter 3.2.3 evaluates gain distributions for a single epoch over all telescopes (see appendix on pages 68 to 71 for all corresponding histograms)
- Chapter 3.2.4 evaluates the declination dependency of sources (see appendix on pages 87 to 90 for all corresponding histograms)

For all distributions, it has to be mentioned that an antilogarithm representation was chosen because the chance of getting a ten times higher amplitude or one tenth of the amplitude should be ideally equal. Therefore, an antilogarithm plot would create a symmetric distribution if the number of data points goes to infinity. Conclusively, the bin sizes are not constant and need to be calculated. Histograms that have fewer than 4 data points are not created, because this would be too few data for an appropriate discussion. The desired case is a narrow distribution in the region of the gain value of 1, which indicates a very good match of the observed amplitude and the amplitude given by the clean model. The chosen range of the created histograms reaches from a gain value of 0.1 to 10, because values that are not in this interval are usually statistical outlier. The amount and position (<0.1 or >10) are indicated with a blue arrow on the top with a number (amount of outliers) above.
To point out details, selected histograms from the appendix will be shown individually. In the end of every chapter, tables list the important statistical parameters for every histogram e.g. the mean and median and the number of counts in the histograms in the certain context. The median and mean are both important here. The median shows a good representation of the value where the distribution scatters while neglecting few outliers, which is a helpful quantity here. The mean, in combination with the median, can be used to estimate the influence of the outliers. The more median and mean coincide, the more the distribution is uniformly shaped. In the case that the coincidence is the value of 1, the examined case shows a very well operating telescopes.
Ojha et al. (2010) uses a conservative estimation of the error in flux density of 20%. The following will improve the estimation of amplitude errors will ascertain whether the error from Ojha is a sensible one.

3.2.1. Distributions for one telescope over all *epochs*

As mentioned above, the first topic of interest is creating histograms for the gain values corresponding to one telescope, while not differentiating between observation cycles. One count in the histograms created for this section represents the gain value of one experiment in an arbitrary observation cycle for the telescope of interest. Figure 3.1 shows two selected histograms for the discussion.

Figure 3.1a displays the gain value distribution for the ATCA telescope in the X-band. There is a narrow spreading in the region of the gain value of 1, which indicates a well operating telescope. This is reflected in the median with a value of 1.04. The blue arrow on the top right

with the number 2 indicates two gain values transcend the axis range. This influences the mean and lifts it up to a value of 9.42. Big differences between the median and mean indicate drastic outliers like in the case of 3.1a, however the amount of such outliers is generally low. This may be a result of only a minor contribution of one telescope to the observation, as seen in Figure 3.2, which shows a time-plot of the observation of PKS 1322-428 in the N cycle. Also possible reasons in those cases are bad clean models or technical problems (which is in general uncommon). A reasonable explanation is that small changes in the clean model may affect a drastic gain correction to the recorded data of one telescope that had nearly no contribution to the whole experiment. These artefacts in the histograms are generally negligible. More important in the case of finding systematic problems are distributions like Figure 3.1b. Here, the distribution seems to gather around a value clearly not even to 1. This requires further investigation that will take place in Chapter 3.2.2.
The Tables 3.2 and 3.3 list the following information of the histograms: the telescope of interest, the observed band, the median, mean and counts of the distribution, the number of observed sources and the frequency of total observations where the telescope was participating. Comparing band specific properties, less telescopes are operating in the K-band (5 to 6 per observation) than in X-band (6 to 9 per observation). In addition less sources are in the K-band sample (49) than in the X-band (75) for which clean models were available. Nevertheless the telescopes work well in both bands although the reception works in a different way. As stated earlier the distributions with only few counts are less representative and can be neglected.
As one can see in Table 3.1, the telescopes Parkes, ATCA, Mopra, Hobart and Ceduna are operating in all observation cycles in both bands. This leads to well calibrated data which is as well represented in the median of all telescopes, close to a value of 1. Only Ceduna tends to higher values for the median, especially in the K-band. Generally the data suggests that these telescopes seem to work best in general and are well calibrated. This can be evaluated in the next section in more detail.

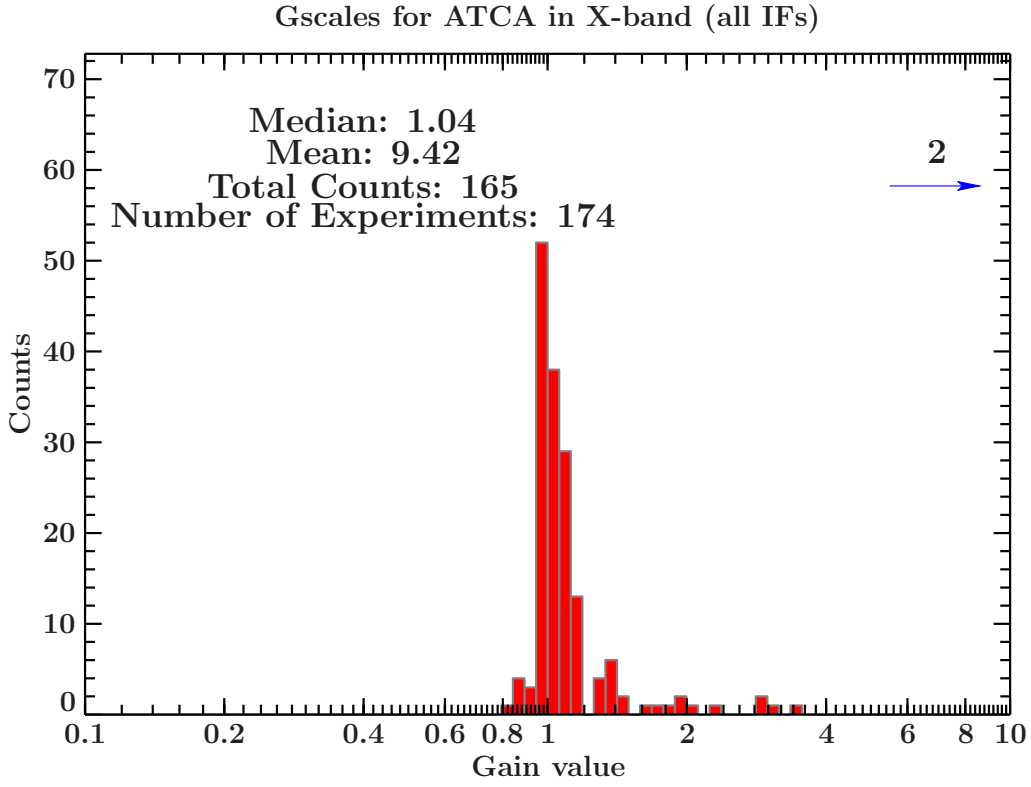

(a)

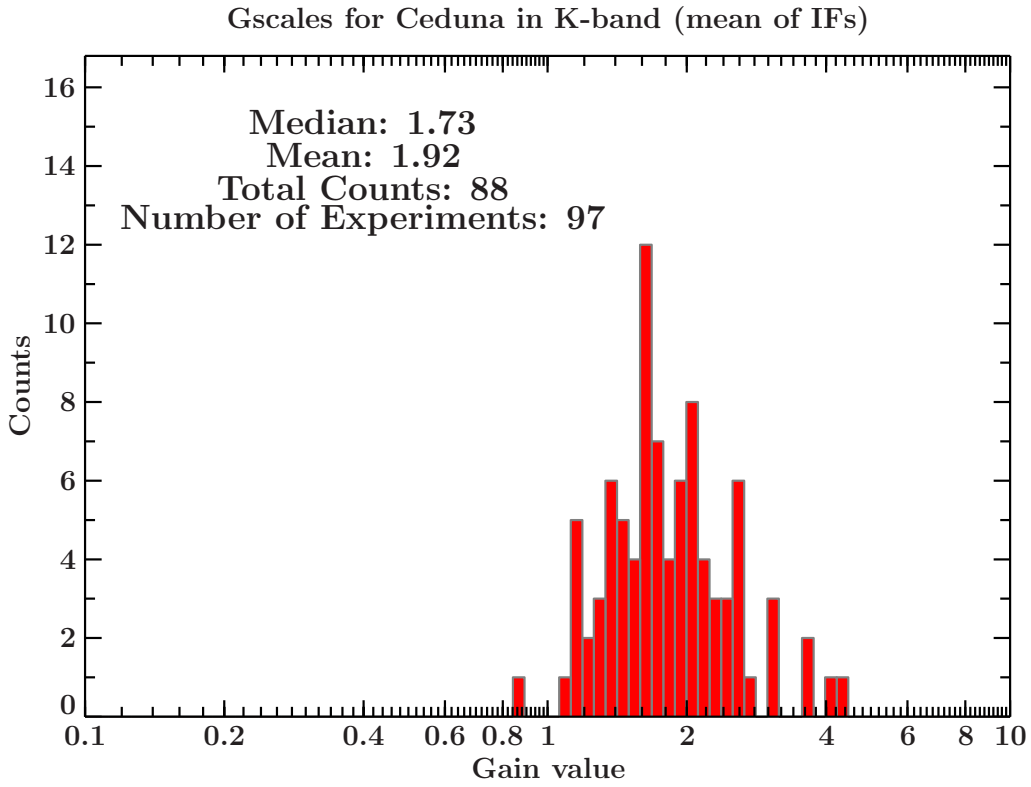

(b)

Figure 3.1.: The gain value distribution as histograms for (3.1a) the ATCA telescope for observations in the X-band and (3.1b) the Ceduna telescope for observations in the K-band

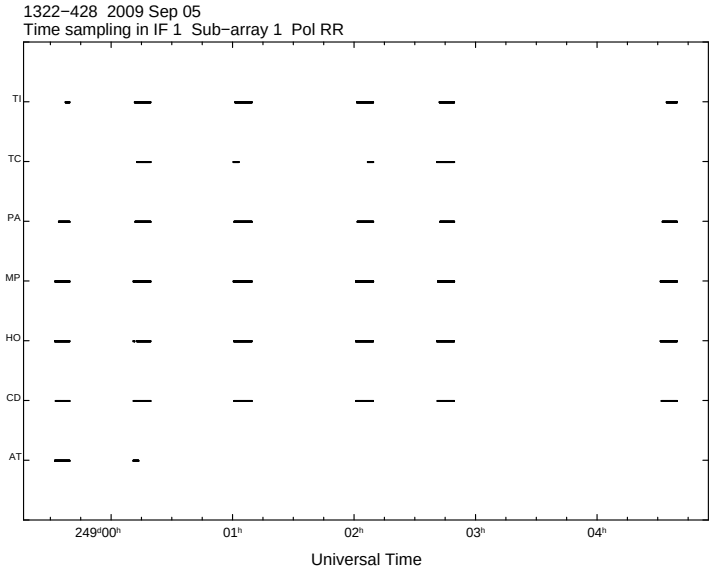

Figure 3.2.: Timeplot of the observation of the source 1322-428 in observation cycle N in X-band. The ordinate shows the initials for the operating telescopes for this experiment, where AT stands for ATCA.

Telescope	Band	Median	Mean	Counts	observed sources	total observations
Parkes	X	1.02	1.55	170	75	174
ATCA	X	1.04	9.42	165	75	174
Mopra	X	1.00	1.07	170	75	174
Hobart	X	1.00	1.19	170	75	174
Ceduna	X	1.22	2.81	167	75	174
DSS34	X	1.56	11.14	2	8	8
DSS43	X	1.51	71.25	57	51	82
DSS45	X	1.04	45.68	36	43	51
Hartebeesthoek	X	1.04	120.60	100	46	104
O'Higgins	X	1.29	13.14	50	45	49
TIGO	X	1.91	9.30	62	56	70

Table 3.2.: Median and Mean of gain correction factor for each telescope in the X-band (8.4 GHz) with the corresponding number of observed sources. The counts mark the number of gain values, which are collected from total observations.

Telescope	Band	Median	Mean	Counts	observed sources	total observations
Parkes	K	1.04	1.06	94	49	97
ATCA	K	1.06	1.11	94	49	97
Mopra	K	1.04	1.05	94	49	97
Hobart	K	1.01	1.04	94	49	97
Ceduna	K	1.73	1.92	88	49	97
DSS43	K	2.19	2.89	19	43	67
Hartebeesthoek	K	15.45	13.97	8	22	22

Table 3.3.: Median and Mean of gain correction factor for each telescope in the K-band (22.3 GHz) with the corresponding number of observed sources. The counts mark the number of gain values, which are collected from total observations.

3.2.2. Distributions for one *epoch* over one telescope

This chapter takes consequentially a closer look on the gain value distributions, because here every operating telescope in every *epoch* is examined separately. Getting a general idea of the distributions, one concludes that most of them show the desired scattering around the value of 1 both in X-band and K-band. Again some telescopes have very few counts, that do not allow reliable conclusions. The distributions' parameters are listed in the Table 3.4 for the X-Band and Table 3.5 for the K-Band .
Evaluating the median values in X-band, shows some conspicuous ones like for the telescope Ceduna. Here the median occurs always lifted a little except of the observation cycle O. But here are only few data, available so that this might not be representative, as well as in the *epochs* K, N, O, P, R, S and T. This behaviour can be seen in a clear anomaly in observation cycle E, where the telescope Ceduna has a clear lifted median value of 3.94.
Although DSS43 has a relatively high median in E with a value of 6.43, there is no further systematic noticeable. Especially in this *epoch* it is conspicuous, that DSS43 is the only telescope with 15 counts, instead of 23, which may indicate problems with the telescope during the observation or that DSS43 stopped observing.
The highest median is given by the telescope Hartebeesthoek in the observation cycle H with a value of 9.29. Also the mean is here the highest with 345.36. The major influence is given

by the experiment with the source 1323-526. As seen in the Table A.1 the telescope has very high gain values also in the *epoch* E, which may indicate a systematic problem like a very faint source, where Hartebeesthoek does not contribute good data.
TIGO has very few data because it participated in the program only in the later observation cycles, but all median values show a tendency to be lifted noticeable. The telescopes TIGO and O'Higgins might be responsible for increasingly lifted medians beginning in the *epoch* I. Including the tendencies of O'Higgins telescope, both telescopes definitely should influence the distributions, discussed in the next chapter. A sustainable statement, that gives information about possible systematic behaviour can be made, when more data is acquired, because here are especially the last observation cycles interesting and it would also be necessary to have a look at the logfiles for each station. But in fact we have only few validated model, that are represented in the counts.
Like Chapter 3.2.1 mentioned, Ceduna shows in the K-Band a significantly shifted distribution. Now we can additionally see in Table 3.5, that this tendency is present for all *epochs* for median values from 1.57 to 2.17 with respect to the stochastic comparability. Figure 3.3a shows the gain value distribution for Ceduna in the observation cycle J in the K-band. It shows a representative histogram for this band. Figure 3.3b, which shows a gain value distribution also for Ceduna, but in the *epoch* C in X-band, makes a comparison between the K- and X-band possible. This allows to prove the previous made assumption to be true, namely that Ceduna has a persistent tendency for a higher mean for the gain values in K-band.
However the highest median is given by Hartebeesthoek in the observation cycle G with a value of 15.45, but due to no further operation in the K-band and only 8 counts in the histogram, no clear conclusions can be drawn. DSS43 shows a lifted median with a value of 2.19 in the J *epoch*, but must also be left uncommented because of few data (observing only in one observation cycle in the K-band).
Parkes appears to be working very well over all observations except in *epoch* F, which has a mean of 3.23 and a median of 5.04. The available 13 counts are clearly less than usually in the *epochs* in X-band A to I (about 20). Including the fact, that Ceduna has in general a lifted mean and median, whereas in the F cycle a very good mean of 1.02 and median 1.00, probably this outcome is a result of measuring problems. Generally all gain correction values tend to be higher than the value 1 with less being lower.
ATCA seems to work very well both in X- and K-band. The biggest deviation of the median is in the L *epoch* with a value of 1.14 (not considering the cases with low counts), which is still a good median. The mean appears very high with 66.73, which is a result of one single gain correction value of the observation of the source 1325-558 (see Table A.1). Because this is a single anomaly, a further investigation should take place outside of this thesis.
Also Hobart and Mopra seem to werk very well in K- and X-band, which is indicated by means and medians close to the value of 1, except of Hobart in *epoch* K, L and O, though K and O have very few counts and the deviations are not that great (highest value for mean is 1.87).
The performance of DSS stations vary over all *epochs*. Nevertheless in observation cycle H DSS45 has an excellent agreement between clean models and the data (median = 0.99, mean = 1.00), but still compared to the other telescopes there are only 16 counts instead of 22.
Investigating all numbers of counts one sees that in *epochs* with higher numbers the telescopes Ceduna, any DSS station and Hartebeesthoek usually have lower counts. These data was probably dismissed because they did not observe although they were listed to observe or calibration errors were too big or the telescope had detection problems.

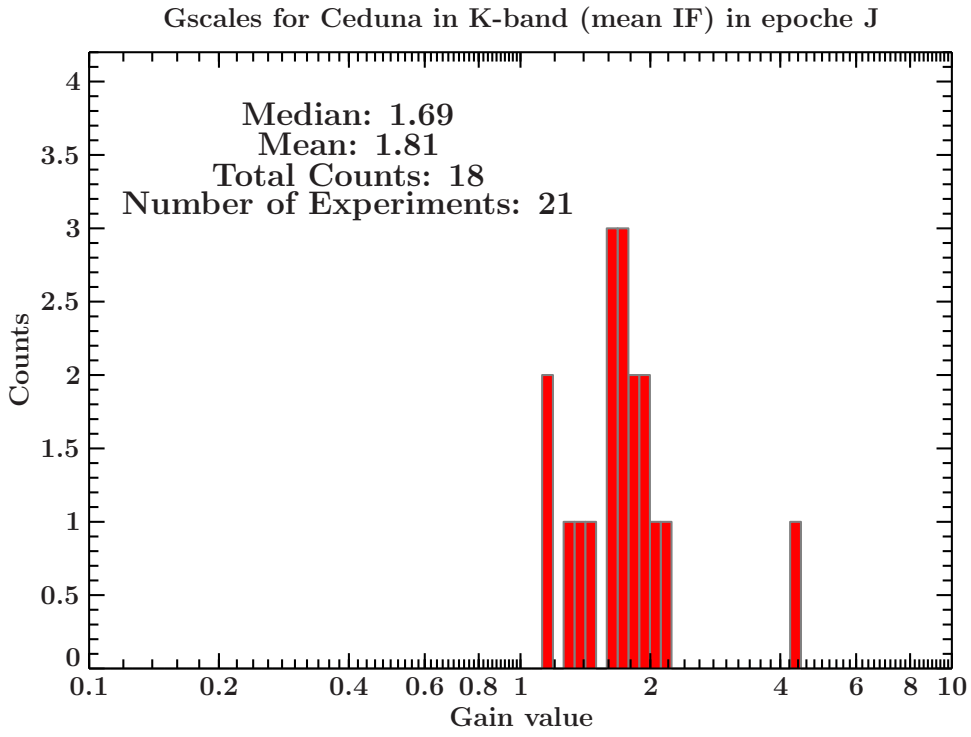

(a)

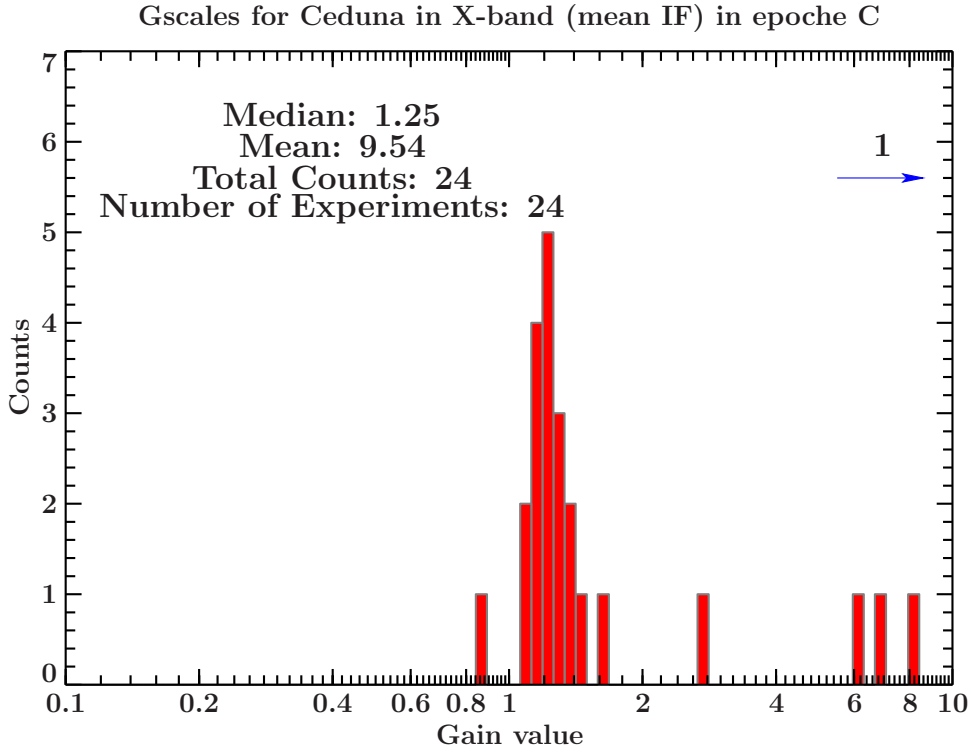

(b)

Figure 3.3.: The gain value distribution as histograms for the Ceduna telescope in (3.3a) in the observation cycle J in the K-band and (3.3b) in the observation cycle C in the X-band

Epoch	Telescope	Band	Median	Mean	Counts
A	Parkes	X	1.07	1.42	21
A	ATCA	X	1.02	1.05	21
A	Mopra	X	0.99	1.02	21
A	Hobart	X	1.02	1.02	21
A	Ceduna	X	1.09	1.34	21
A	Hartebeesthoek	X	1.00	1.27	20
C	Parkes	X	1.02	1.25	24
C	ATCA	X	1.05	1.48	24
C	Mopra	X	1.00	1.00	24
C	Hobart	X	1.00	0.98	24
C	Ceduna	X	1.25	9.54	24
C	Hartebeesthoek	X	1.01	1.16	18
E	Parkes	X	1.03	1.04	23
E	ATCA	X	0.98	0.98	23
E	Mopra	X	0.98	0.99	23
E	Hobart	X	1.03	1.03	23
E	Ceduna	X	3.94	3.52	23
E	DSS43	X	6.43	136.25	15
E	Hartebeesthoek	X	1.00	96.84	23
F	Parkes	X	3.23	5.04	13
F	ATCA	X	0.97	0.99	13
F	Mopra	X	1.06	1.07	13
F	Hobart	X	1.04	1.07	13
F	Ceduna	X	1.02	1.00	13
F	Hartebeesthoek	X	1.55	31.57	11
H	Parkes	X	1.01	1.02	22
H	ATCA	X	1.06	1.15	22
H	Mopra	X	0.98	0.98	22
H	Hobart	X	0.97	1.01	22
H	Ceduna	X	1.19	1.19	22
H	DSS45	X	0.99	1.00	16
H	Hartebeesthoek	X	9.29	345.36	22
I	Parkes	X	1.00	1.85	21
I	ATCA	X	1.09	1.27	21
I	Mopra	X	1.05	1.40	21
I	Hobart	X	0.98	0.98	21
I	Ceduna	X	1.10	2.23	21
I	DSS43	X	1.18	2.37	21
I	O'Higgins	X	1.08	1.27	20
I	TIGO	X	2.11	16.34	16
K	Parkes	X	0.94	1.01	6
K	ATCA	X	0.96	0.96	6
K	Mopra	X	0.89	1.02	6
K	Hobart	X	1.03	4.12	6
K	Ceduna	X	1.15	1.18	6
K	DSS34	X	1.56	11.14	2

Continued on the next page

Epoch	Telescope	Band	Median	Mean	Counts
K	DSS45	X	2.60	62.96	4
K	O'Higgins	X	1.39	2.21	5
K	TIGO	X	4.73	9.48	5
L	Parkes	X	0.91	0.95	20
L	ATCA	X	1.14	66.73	20
L	Mopra	X	1.00	1.14	20
L	Hobart	X	0.98	1.32	20
L	Ceduna	X	1.34	3.29	20
L	DSS45	X	1.06	86.05	16
L	O'Higgins	X	2.58	34.00	18
L	TIGO	X	2.17	12.34	18
N	Parkes	X	0.94	0.98	7
N	ATCA	X	1.41	29.41	2
N	Mopra	X	1.05	1.04	7
N	Hobart	X	0.99	1.00	7
N	Ceduna	X	1.20	3.21	6
N	DSS43	X	1.06	1.06	7
N	TIGO	X	1.43	1.42	7
O	Parkes	X	1.11	1.16	7
O	ATCA	X	1.02	1.20	7
O	Mopra	X	1.01	1.02	7
O	Hobart	X	1.79	1.87	7
O	Ceduna	X	0.95	0.97	5
O	TIGO	X	1.66	2.22	7
P	Parkes	X	0.97	0.97	1
P	ATCA	X	1.04	1.04	1
P	Mopra	X	1.04	1.04	1
P	Hobart	X	0.99	0.99	1
P	Ceduna	X	1.27	1.27	1
R	Parkes	X	0.97	0.97	1
R	ATCA	X	1.01	1.01	1
R	Mopra	X	0.99	0.99	1
R	Hobart	X	1.05	1.05	1
R	Ceduna	X	1.40	1.40	1
R	TIGO	X	1.13	1.13	1
S	Parkes	X	1.01	1.01	3
S	ATCA	X	1.02	1.02	3
S	Mopra	X	1.00	1.01	3
S	Hobart	X	0.96	0.98	3
S	Ceduna	X	1.21	1.18	3
S	DSS43	X	1.03	1.04	2
S	TIGO	X	1.77	1.62	3
T	Parkes	X	1.04	1.04	1
T	ATCA	X	0.99	0.99	1
T	Mopra	X	0.95	0.95	1
T	Hobart	X	0.97	0.97	1

Continued on the next page

Epoch	Telescope	Band	Median	Mean	Counts
T	Ceduna	X	1.30	1.30	1
T	Hartebeesthoek	X	1.26	1.26	1

Table 3.4.: Median and mean of gain correction factor fore each telescope in each observation cycle in X-band (8.4 GHz). Counts mark the number of gain values which are collected from the observations of the telescope in the *epoche*.

Epoch	Telescope	Band	Median	Mean	Counts
B	Parkes	K	1.12	1.13	21
B	ATCA	K	1.08	1.06	21
B	Mopra	K	1.15	1.10	21
B	Hobart	K	0.99	1.04	21
B	Ceduna	K	1.60	1.78	20
D	Parkes	K	1.06	1.10	22
D	ATCA	K	1.05	1.08	22
D	Mopra	K	1.06	1.08	22
D	Hobart	K	1.08	1.11	22
D	Ceduna	K	1.57	1.65	21
G	Parkes	K	1.00	1.00	22
G	ATCA	K	1.06	1.26	22
G	Mopra	K	1.04	1.05	22
G	Hobart	K	0.92	0.97	22
G	Ceduna	K	2.17	2.21	21
G	Hartebeesthoek	K	15.45	13.97	8
J	Parkes	K	0.96	1.02	21
J	ATCA	K	1.08	1.10	21
J	Mopra	K	0.96	0.97	21
J	Hobart	K	0.97	0.99	21
J	Ceduna	K	1.69	1.81	18
J	DSS43	K	2.19	2.89	19
Q	Parkes	K	1.00	1.02	8
Q	ATCA	K	0.96	0.97	8
Q	Mopra	K	1.07	1.08	8
Q	Hobart	K	1.12	1.10	8
Q	Ceduna	K	2.35	2.48	8

Table 3.5.: Median and mean of gain correction factor fore each telescope in each observation cycle in K-band (22.3 GHz). Counts mark the number of gain values which are collected from the observations of the telescope in the *epoche*.

3.2.3. Distributions for one *epoch* over all telescopes

The examined case here is compiling gain corrections for each observation cycle, merging the data of all telescopes. Table 3.6 lists the stochastic relevant values for the X-band and Table 3.7 for the K-band. Only a few show a nice distribution with the centre at the value of 1. Figure 3.4a shows the gain value distribution for the observation cycle B in K-band and represents the best distribution, whereas most of the others show a tail in direction of higher gain values, like one can see in Figure 3.4b, where the gain value distribution is shown for the *epoch* L in X-band. This is likely because of the superposition of the different telescopes. This effect is not seen that obvious in the case of Chapter 3.2.1 because the variations between *epochs* for a single telescope are clearly smaller than the different telescope designs. This was also shown in the previous chapter in the Tables 3.4 and 3.5. Additionally there are distributions, that have only few counts and therefore are not usable to conclude any definite behaviour. This will change, when more observations will be run through the imaging process and achieve a validated clean model.
One cheerful result is for example *epoch* A in X-band which shows a very good agreement of median and mean. In general all medians look very good in X- and K-band in terms of being close to the value of 1. In case of means the K-band performs better, than the X-band. This indicates less outlier in the K-band what is probably because here less telescopes are operating, while those that operate, work fine. In X-band many telescopes are used, that do not operate frequently and also in the most cases need to be gain calibrated more intense than others.
One interesting trend is that the median is increasing in the observation cycles I to L in the X-band. However, since the availible data for K is less than for I and L, this trend cannot be clearly validated. Looking up Table 3.1 one sees that the telescopes O'Higgins and TIGO joined the first time in these *epochs* (I, K and L). It might be that only one telescope is causing that trend, or both in combination. Considering the Table 3.2, TIGO has the highest median of all telescopes in this band, which indicates that TIGO might be the major influence. This was already mentioned in the Chapter 3.2.2, why this feature confirms the previous discussion. More data, especially the later observations, where TIGO was taking part, would provide further information referring to the telescope. At this point there are not enough data to make sustainable assumptions, but this point should be kept in mind.
Conclusively this categorization shows only few information to determine systematic influences, but gives a possibility to confirm the previous found features. One should also keep in mind that the distributions among themselves may vary because the observed sample is generally not the same. A more specific investigation of this point can be achieved by comparing the gain value distributions depending on the declination of the sources, what will be done in Chapter 3.2.4.

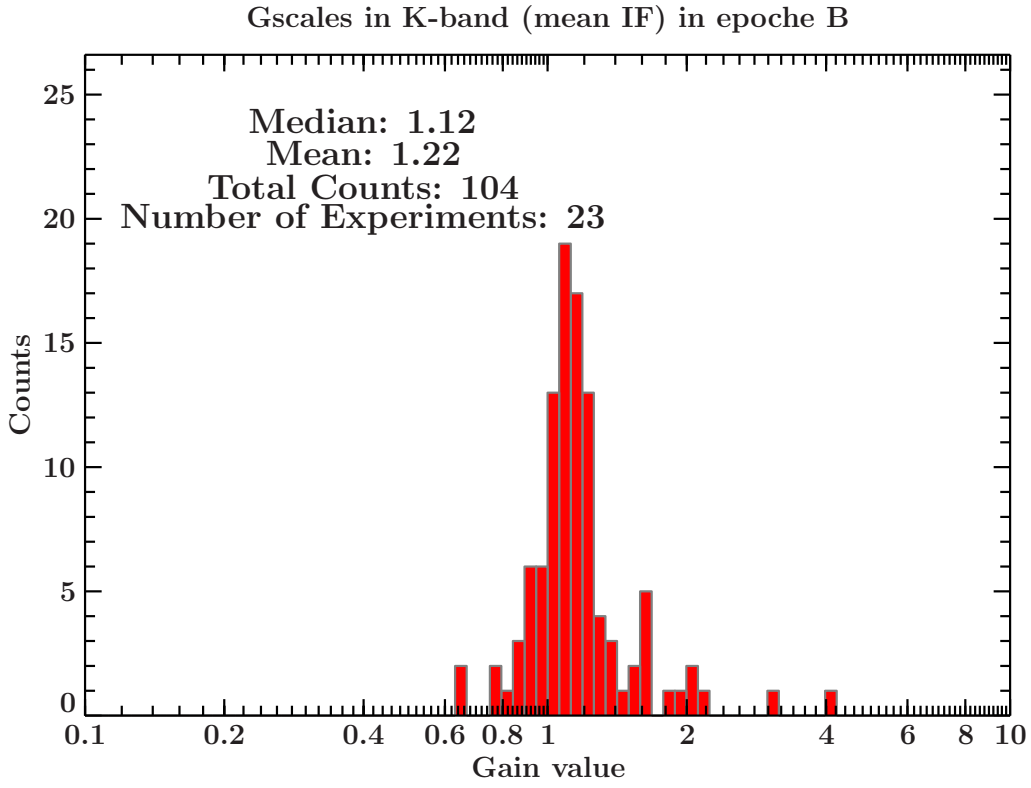

(a)

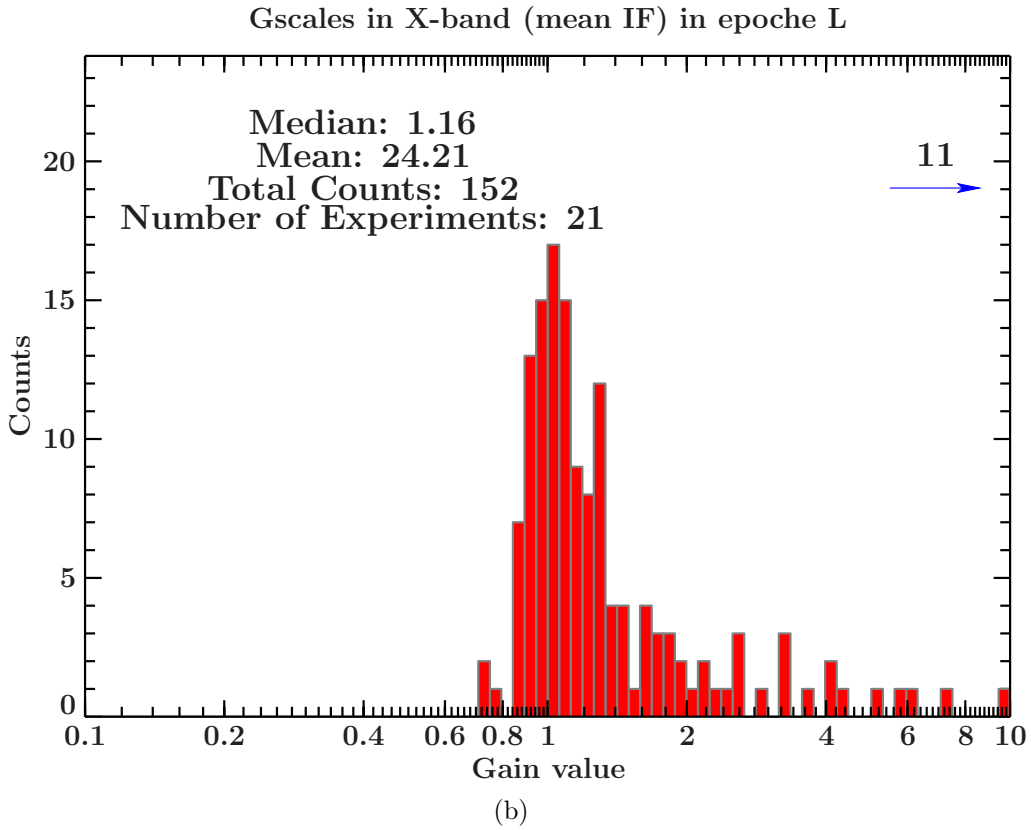

(b)

Figure 3.4.: The gain value distribution as histograms for (3.4a) the B observation cycle in the K-band and (3.4b) the L observation cycle in the K-band

Epoch	Band	Median	Mean	Counts
A	X	1.02	1.18	125
C	X	1.02	2.63	138
E	X	1.02	29.05	153
F	X	1.06	6.14	76
H	X	1.03	52.24	148
I	X	1.09	3.08	162
K	X	1.13	8.31	46
L	X	1.16	24.21	152
N	X	1.06	2.71	43
O	X	1.06	1.43	40
P	X	1.04	1.06	5
R	X	1.01	1.09	6
S	X	1.02	1.13	20
T	X	0.99	1.09	6

Table 3.6.: Median and mean of gain correction factors for each *epoche* in X-band (8.4 GHz). Counts mark the number of gain values which were collected in the relevant observation cycle.

Epoch	Band	Median	Mean	Counts
B	K	1.12	1.22	104
D	K	1.10	1.20	109
G	K	1.06	2.16	117
J	K	1.08	1.43	121
Q	K	1.07	1.33	40

Table 3.7.: Median and mean of gain correction factors for each *epoche* in K-band (22.3 GHz). Counts mark the number of gain values which were collected in the relevant observation cycle.

3.2.4. Distributions for sources with a declination in an interval

This chapter investigates the declination dependency of the gain correction values. For this purpose the observed sky by TANAMI was cut in stripes whereat the solid angle measures in every stripe the same value. So the source distribution is for X- and K-band the same, but the K-band has less data. Moreover the sources per solid angle are fluctuating, because of the sample chosen by TANAMI, that is not homogeneous, besides the sources are not observed equal times which makes it harder to compare stripes among each other. The sources' gain values in any *epoch* from any telescope are compiled for each stripe for X- and K-band in histograms. The mean and median of each histogram is listed in Table 3.8 and 3.9, such as the counts in the certain histogram, which indicates the number of gain values collected from the sources in the given declination interval regardless of the *epoch* and telescope. The sources in the last column indicate number of sources in the sample that lie in the particular stripe.
Figure 3.5 shows two gain value distributions for sources between -44.4° and -48.6° in X- and K-band. Comparing both histograms one recognises in both cases a nice distribution around the value of 1 and the tendency of X-band to show more outliers, which is seen well in Table 3.8 and 3.9. The mean shows clear variations in contrary to the K-band, where no mean is bigger than the value of 2. This agrees with the results of 3.2.2 and 3.2.3. This might be a statistic effect in the case that the corrections are more scattered but compensate each other. The agreement

between mean and median is not that good in most cases. The best is between -58.2° and -64.2° in the K-band (median=1.08, mean=1.19). Overall the median shows very good values in X- and in K-band. Minor deviations do not appear systematically and do not coincide with the other observation band. The highest median is in K-band with a value of 1.15, while in general the median indicates a smaller gain correction than 10%. Because usually telescopes and arrays show a declination dependent performance, it is surprising, that no clear trend can be seen in X- or K-band. Maybe the general influence is not that big for these arrays or some telescopes compensate the influences among themselves.
These information show, that averaged over all telescopes and all *epochs* the array seems to work fine in the given declination range or at least our models describe the data prior to the self-calibration well. Nevertheless, a closer inspection of those outliers responsible for the elevated means is necessary.

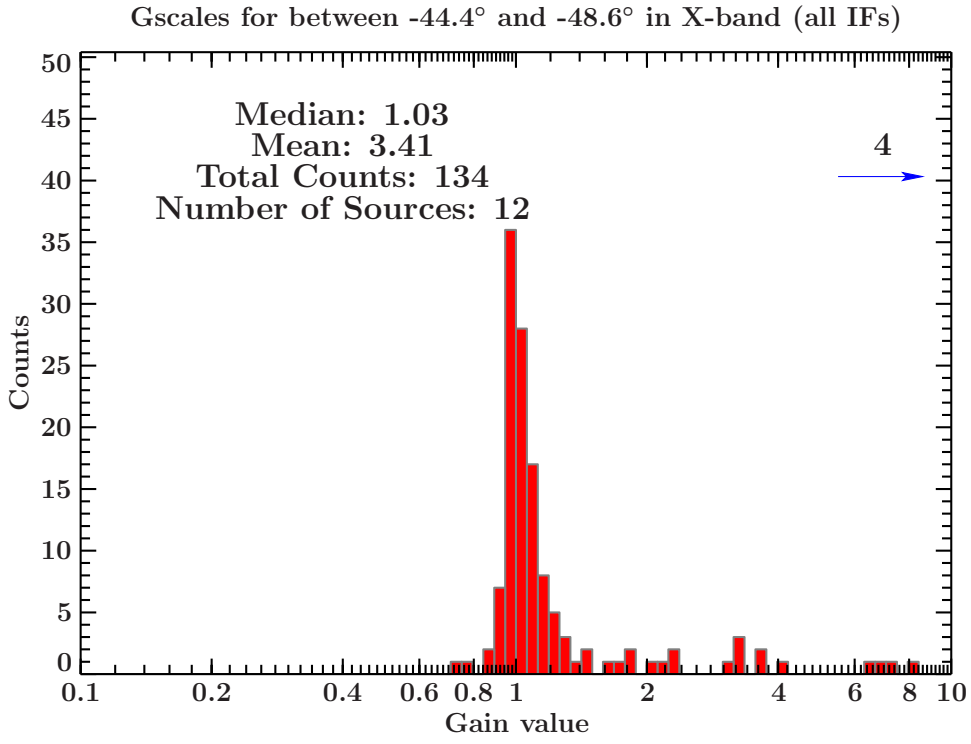

(a)

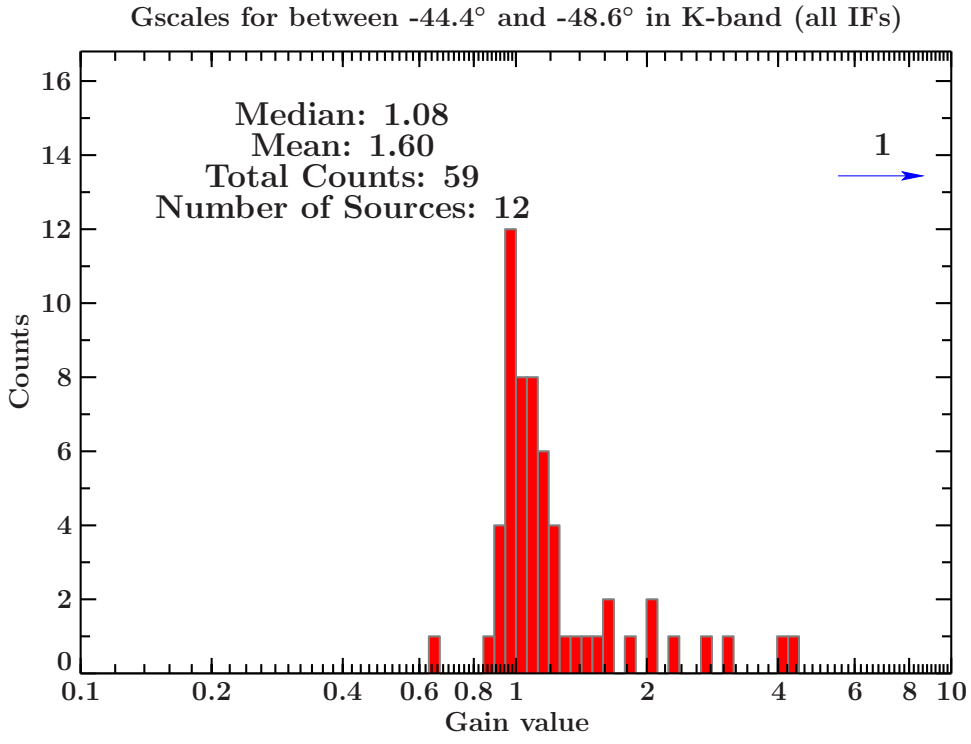

(b)

Figure 3.5.: The gain value distribution as histograms for the sources between -44.4° and -48.6° in X- (3.5a) and K-band (3.5b)

Range in degrees	Band	Median	Mean	Counts	Sources
-30.0 to -33.4	X	1.04	22.30	82	9
-33.4 to -36.9	X	1.04	1.46	159	11
-36.9 to -40.5	X	1.04	11.74	134	12
-40.5 to -44.4	X	1.04	4.59	138	8
-44.4 to -48.6	X	1.03	3.41	134	12
-48.6 to -53.1	X	1.03	81.79	104	9
-53.1 to -58.2	X	1.05	16.10	98	8
-58.2 to -64.2	X	1.13	2.31	103	9
-64.2 to -71.8	X	1.06	1.79	55	5
-71.8 to -90.0	X	1.04	24.06	108	9

Table 3.8.: Mean and median for gain correction distributions for sources in a certain declination interval in X-band (8.4 GHz). The counts indicate the number of collected gain correction values for the given criteria. The number of observed sources of the given sample in a particular declination interval is given in the last column.

Range in degrees	Band	Median	Mean	Counts	Sources
-30.0 to -33.4	K	1.04	1.73	31	9
-33.4 to -36.9	K	1.08	1.65	70	11
-36.9 to -40.5	K	1.12	1.57	69	12
-40.5 to -44.4	K	1.15	1.59	54	8
-44.4 to -48.6	K	1.08	1.60	59	12
-48.6 to -53.1	K	1.06	1.34	46	9
-53.1 to -58.2	K	1.11	1.40	47	8
-58.2 to -64.2	K	1.08	1.19	41	9
-64.2 to -71.8	K	1.07	1.27	22	5
-71.8 to -90.0	K	1.09	1.44	52	9

Table 3.9.: Mean and median for gain correction distributions for sources in a certain declination interval in K-band (22.3 GHz). The counts indicate the number of collected gain correction values for the given criteria. The number of observed sources of the given sample in a particular declination interval is given in the last column.

4. Summary and outlook

The TANAMI project offers milliarcsecond resolution and longterm monitoring to study radio jets in a sample of AGN on the southern hemisphere at two frequencies (8.4 and 22 GHz) since 2007. It uses a VLBI array with changing configuration, while utilising telescopes with different technical specifications. This results in variations of the data quality, which complicates the data reduction process. In order to gain high quality images of these jets, *hybrid mapping* is used, which relies on amplitude and phase self-calibration. As an example, the first observation of *PKS 0235-618* by TANAMI has been imaged as part of this thesis, showing a one-sided jet in south-west direction and a total flux density of the image of ~ 0.33 Jy. However, it is important to test the reliability of the resulting images by comparing them to the data prior to self-calibration. To this purpose, this thesis investigates the application of a gain correction from amplitude self-calibration on a total of 174 observations at 8.4 GHz and 97 observations at 22.3 GHz. The gain correction is assumed to be constant over the individual observation time of each source, but allowed to vary for each telescope and each *IF*. The resulting gain value distributions are examined from different points of views, which allows a good estimation for the amplitude calibration tendencies in certain experiments or telescopes. Chapter 3.2.2 presents a detailed view on the gain value distributions of each telescope in each observation.
The general performance of the telescopes Parkes, ATCA, Mopra and Hobart achieves the best results in the K- and in the X-band, which is less surprising, because these telescopes are operating in every *epoch* because they show from experience better data. Ceduna is also observing in every *epoch* but the data's amplitudes need to be calibrated more intensely. In addition, Ceduna shows a shifted distribution in the K-band which requires further investigation. Here, it might be that a systematic influence is the reason.
Furthermore, a more stable mean is visible over all telescopes in the K-band in contrary to the X-band. This observation repeats in every chapter, but it is also expected because in the K-band, most telescopes make frequent observations, in contrast to in the X-band..
There is a consistent trend of increasing gain values with TIGO and O'Higgins, but can not be validated because of lack of data especially in the last *epochs*. This can be monitored in the future for confirming or dismissing the assumption.
Hartebeesthoek shows apart from a few drastic outliers a similar performance like ATCA. The problematic observations should be further investigated, especially with respect to the luminosity dependence. This should not be only performed for Hartebeesthoek, but the smaller telescopes should show a more obvious effect due to the effective are.
Summing up the DSS stations is with the available data not possible because the means and medians seem to fluctuate uncommitted.
The median of the gain value distributions for a single telescope does not transcend the value of 2 in the most cases, it is for many telescopes even not higher than 1.10. Very interesting is also that all medians are bigger than the value of 1. Even in all distributions, shown in this thesis, the median is generally higher than the value of 1.
Regarding the gain value distributions for certain *epochs* no prominent one can be found. The medians in all *epochs* show similar good values (highest median 1.16 in L *epoch*) which indicates a good performance throughout the array.

The analysis of the declination dependency showed no mentionable tendencies for lifted or lowered medians in X- and K-band. The deviations of mean and median seem to be uncorrelated to the declination of the observed sources.
All in all this thesis depicts in various ways the gain value distributions, which allows to get an idea of the performance of the array and single telescopes. Still further research should be done to get an deeper understanding of the performance of the array. In this thesis all *IF*s were averaged. The consecutive analysis should check for differences of the gain values between the *IF*s. Another interesting study would be to check if some telescopes show a worse performance with less luminous sources, due to limited baseline sensitivity. This should be the case because of the different telescope designs, but could also become negligible if the sources are very bright in the observing band and similar among themselves.

Bibliography

Böck M., 2012, Ph.D. thesis

Burke B.F., Graham-Smith F., 2010, An Introduction to Radio Astronomy, Cambridge University Press

Ghisellini G., 2011, arXiv preprint arXiv:1104.0006

Hartman R.C., Bertsch D.L., Fichtel C.E., et al., 1992, In: Shrader C.R., Gehrels N., Dennis B. (eds.) NASA Conference Publication, Vol. 3137. NASA Conference Publication, p.116

Högbom J.A., 1974, A&AS 15, 417

Kadler M., 2011, Modern astrophysics - Extragalactic jets, Lecture on modern astrophysics with spotlight on extragalactic jets held in the summer term

Michelson A.A., Pease F.G., 1921, ApJ 53, 249

Müller C., Kadler M., Ojha R., et al., 2010, Sub-parsec scale imaging of Centaurus A

Müller C., Kadler M., Ojha R., et al., 2011, A&A 530, L11

Ojha R., Kadler M., Böck M., et al., 2010, A&A 519, A45

Robson I., 1996, Active galactic nuclei, Wiley-Praxis Series in Astronomy and Astrophysics, New York

Stickel M., Meisenheimer K., Kuehr H., 1994, VizieR Online Data Catalog 410, 50211

Taylor G., 1997, The Difmap Cookbook

Thompson A.R., Moran J.M., Swenson, Jr. G.W., 2001, Interferometry and Synthesis in Radio Astronomy, 2nd Edition, New York : Wiley

Trüstedt J., 2013, Masterthesis, Julius-Maximilians-Universität Würzburg

Young T., 1802, Philosophical Transactions of the Royal Society of London 92, pp. 12

Declaration

I hereby acknowledge that I independently authored this thesis and only used the sources specified.

Würzburg, November 17, 2013

.....
(signature of the candidate)

A. Appendix

Source name	*Epoch*	IF	Parkes	ATCA	Mopra	Hobart	Ceduna	DSS34	DSS43	DSS45	Hartebeesthoek	O'Higgins	TIGO
0047-579	A	1	1.01	0.98	1.02	0.99	1.12	–	–	–	1.14	–	–
0047-579	A	2	1.01	0.98	1.01	0.98	1.13	–	–	–	1.13	–	–
0047-579	E	1	1.01	0.97	1.00	1.06	2.14	–	9.05	–	0.99	–	–
0047-579	E	2	1.01	0.98	1.00	1.05	2.22	–	1.00*	–	0.98	–	–
0047-579	H	1	1.00	1.07	0.98	0.97	1.18	–	–	0.97	8.36	–	–
0047-579	H	2	1.00	1.08	0.97	0.96	1.12	–	–	0.99	7.89	–	–
0047-579	H	3	1.02	1.03	0.99	0.94	1.11	–	–	0.99	8.02	–	–
0047-579	H	4	1.02	1.02	0.99	0.93	1.18	–	–	1.01	8.92	–	–
0055-328	L	1	0.90	1.14	0.93	1.06	1.31	–	–	1.06	–	47.98	6.11
0055-328	L	2	0.89	1.18	0.95	0.98	1.30	–	–	1.10	–	4.83	1.80
0055-328	L	3	0.93	1.16	1.22	1.06	1.34	–	–	1.06	–	36.45	2.24
0055-328	L	4	0.92	1.15	1.17	0.90	1.58	–	–	1.13	–	4.70	2.79
0208-512	A	1	1.02	1.00	1.03	0.99	1.04	–	–	–	1.00	–	–
0208-512	A	2	1.02	1.00	1.02	0.99	1.03	–	–	–	1.00	–	–
0208-512	F	1	9.37	1.08	1.21	1.07	1.08	–	–	–	0.97	–	–
0208-512	F	2	9.27	1.08	1.21	1.07	1.09	–	–	–	0.99	–	–
0208-512	I	1	1.00	0.97	0.97	0.95	11.33	–	1.13	–	–	0.98	1.76
0208-512	I	2	1.01	0.99	0.98	0.91	10.06	–	1.07	–	–	0.93	1.08
0208-512	I	3	0.98	0.99	1.08	1.00	6.96	–	1.13	–	–	0.87	1.00*
0208-512	I	4	1.00*	1.03	1.07	0.99	5.35	–	1.00*	–	–	1.00*	1.00*
0208-512	S	1	1.03	0.98	1.01	0.97	1.25	–	1.04	–	–	–	1.38
0208-512	S	2	1.03	0.97	1.01	0.96	1.18	–	1.03	–	–	–	0.91
0208-512	S	3	0.99	1.05	1.04	0.94	1.17	–	1.03	–	–	–	0.93
0208-512	S	4	1.00	1.04	1.04	0.94	1.24	–	1.03	–	–	–	0.95
0227-369	L	1	0.97	1.12	0.96	0.97	1.30	–	–	1.03	–	2.07	1.00*
0227-369	L	2	0.94	1.13	0.96	0.94	1.28	–	–	1.06	–	1.85	1.00*
0227-369	L	3	0.96	1.16	1.05	0.93	1.26	–	–	1.06	–	1.99	1.00*
0227-369	L	4	0.95	1.17	1.05	0.94	1.26	–	–	1.10	–	1.77	1.00*
0227-369	O	1	1.06	1.02	0.99	3.28	1.00*	–	–	–	–	–	2.02
0227-369	O	2	1.03	1.05	0.97	2.23	1.00*	–	–	–	–	–	1.01
0227-369	O	3	1.07	1.03	1.01	2.64	1.00*	–	–	–	–	–	1.10
0227-369	O	4	1.09	1.02	1.00	2.37	1.00*	–	–	–	–	–	0.98
0244-470	L	1	0.90	1.03	0.86	0.88	1.31	–	–	1.34	–	1.32	2.58
0244-470	L	2	0.89	1.04	0.87	0.88	1.28	–	–	1.38	–	1.18	1.45
0244-470	L	3	0.91	1.05	0.96	0.87	1.22	–	–	1.55	–	1.09	1.43

Continued on the next page

Source name	*Epoch*	IF	Parkes	ATCA	Mopra	Hobart	Ceduna	DSS34	DSS43	DSS45	Hartebeesthoek	O'Higgins	TIGO
0244-470	L	4	0.89	1.06	0.97	0.89	1.25	–	–	1.49	–	1.16	1.44
0302-623	L	1	0.88	1.07	0.99	1.09	1.52	–	–	1.00*	–	1.09	2.26
0302-623	L	2	0.88	1.09	0.99	1.08	1.47	–	–	1.00*	–	1.03	1.49
0302-623	L	3	0.89	1.08	1.09	1.09	1.44	–	–	1.00*	–	0.96	2.44
0302-623	L	4	0.89	1.08	1.11	1.09	1.47	–	–	1.00*	–	0.97	1.45
0302-623	R	1	0.97	1.00	0.97	1.06	1.52	–	1.00*	–	–	–	1.17
0302-623	R	2	0.98	1.02	0.97	1.06	1.45	–	1.00*	–	–	–	1.08
0302-623	R	3	0.98	1.00	1.03	1.03	1.37	–	1.00*	–	–	–	1.14
0302-623	R	4	0.97	1.02	1.00	1.05	1.26	–	1.00*	–	–	–	1.14
0308-611	N	1	0.97	1.00*	1.02	0.96	11.60	–	1.01	–	–	–	1.64
0308-611	N	2	0.97	1.00*	1.02	0.96	11.22	–	1.03	–	–	–	1.01
0308-611	N	3	0.99	1.00*	1.11	0.95	17.31	–	1.00	–	–	–	1.08
0308-611	N	4	0.99	1.00*	1.10	0.94	9.72	–	1.01	–	–	–	1.06
0332-403	C	1	1.02	0.97	1.18	1.02	1.10	–	1.00*	–	1.00*	–	–
0332-403	C	2	1.03	0.96	1.03	1.01	1.12	–	1.00*	–	1.00*	–	–
0332-403	C	3	1.00*	1.00*	1.00*	1.00*	1.00*	–	1.00*	–	1.00*	–	–
0332-403	E	1	1.02	0.97	1.01	1.08	1.67	–	1.00*	–	0.94	–	–
0332-403	E	2	1.03	0.97	1.02	1.07	1.72	–	1.00*	–	0.94	–	–
0332-403	H	1	1.03	1.06	0.97	0.95	1.15	–	–	0.98	8.06	–	–
0332-403	H	2	1.03	1.07	0.97	0.95	1.09	–	–	0.99	7.76	–	–
0332-403	H	3	1.04	1.02	0.99	0.94	1.09	–	–	0.99	7.35	–	–
0332-403	H	4	1.05	1.01	0.99	0.93	1.09	–	–	1.01	8.37	–	–
0332-376	L	1	0.91	1.05	0.88	0.91	1.41	–	–	0.99	–	2.38	3.87
0332-376	L	2	0.91	1.05	0.87	0.90	1.33	–	–	1.02	–	1.76	1.59
0332-376	L	3	0.92	1.11	0.95	0.90	1.31	–	–	1.01	–	2.19	1.67
0332-376	L	4	0.91	1.10	0.97	0.91	1.30	–	–	1.05	–	1.94	1.53
0402-362	N	1	0.97	1.00*	1.01	0.96	1.00*	–	1.08	–	–	–	1.63
0402-362	N	2	0.97	1.00*	1.01	0.96	1.00*	–	1.08	–	–	–	1.03
0402-362	N	3	0.99	1.00*	1.09	0.93	1.00*	–	1.06	–	–	–	1.05
0402-362	N	4	1.01	1.00*	1.08	0.92	1.00*	–	1.08	–	–	–	1.04
0405-385	C	1	1.02	0.97	1.06	1.02	1.13	–	1.00*	–	1.00*	–	–
0405-385	C	2	1.02	0.98	0.93	1.01	1.17	–	1.00*	–	1.00*	–	–
0405-385	C	3	1.00*	1.00*	1.00*	1.00*	1.00*	–	1.00*	–	1.00*	–	–
0405-385	E	1	1.03	0.98	1.01	1.01	1.38	–	1.00*	–	0.88	–	–
0405-385	E	2	1.03	0.98	1.02	1.01	1.42	–	1.00*	–	0.88	–	–
0405-385	H	1	1.03	1.07	0.96	0.99	1.26	–	–	0.96	5.58	–	–

Continued on the next page

Source name	*Epoch*	IF	Parkes	ATCA	Mopra	Hobart	Ceduna	DSS34	DSS43	DSS45	Hartebeesthoek	O'Higgins	TIGO
0405-385	H	2	1.02	1.08	0.96	0.98	1.21	–	–	0.98	5.61	–	–
0405-385	H	3	1.04	1.02	1.00	0.98	1.19	–	–	1.03	6.10	–	–
0405-385	H	4	1.05	1.02	0.98	0.98	1.21	–	–	1.02	5.26	–	–
0412-536	O	1	1.48	2.60	1.33	2.07	1.00*	–	–	–	–	–	0.58
0412-536	O	2	1.05	1.45	1.02	1.59	1.00*	–	–	–	–	–	1.79
0412-536	O	3	0.93	2.79	0.96	3.87	1.13	–	–	–	–	–	1.58
0412-536	O	4	1.67	2.55	0.94	3.17	1.00*	–	–	–	–	–	3.14
0426-380	L	1	0.96	1.15	0.88	0.95	1.34	–	–	1.03	–	2.03	2.19
0426-380	L	2	0.96	1.16	0.88	0.94	1.28	–	–	1.05	–	1.89	1.44
0426-380	L	3	0.96	1.20	0.97	0.95	1.27	–	–	1.05	–	1.90	1.45
0426-380	L	4	0.95	1.20	0.97	0.95	1.28	–	–	1.08	–	1.54	1.46
0438-436	C	1	1.05	0.98	1.06	1.01	1.07	–	1.00*	–	1.00*	–	–
0438-436	C	2	1.04	0.99	0.93	1.00	1.09	–	1.00*	–	1.00*	–	–
0438-436	C	3	1.00*	1.00*	1.00*	1.00*	1.00*	–	1.00*	–	1.00*	–	–
0438-436	F	1	2.46	1.03	1.02	1.02	0.97	–	–	–	1.57	–	–
0438-436	F	2	2.55	1.03	1.02	1.02	0.96	–	–	–	1.53	–	–
0438-436	I	1	1.04	1.01	1.05	1.21	6.53	–	1.06	–	–	1.15	1.00*
0438-436	I	2	1.00	0.98	1.00	1.07	9.00	–	1.11	–	–	1.07	1.15
0438-436	I	3	0.97	1.01	1.06	1.06	7.51	–	1.16	–	–	1.00	1.00*
0438-436	I	4	1.00*	1.04	1.07	1.03	6.91	–	1.00*	–	–	1.00*	1.00*
0447-439	L	1	0.93	1.10	0.92	1.03	1.65	–	–	1.02	–	3.24	145.75
0447-439	L	2	0.93	1.10	0.92	1.03	1.33	–	–	1.06	–	2.62	6.77
0447-439	L	3	0.93	1.14	0.99	1.13	1.36	–	–	1.05	–	2.57	2.71
0447-439	L	4	0.95	1.12	0.99	1.13	1.43	–	–	1.08	–	1.87	12.89
0454-463	A	1	1.29	1.16	0.96	0.94	1.03	–	–	–	1.09	–	–
0454-463	A	2	1.41	1.17	0.94	0.93	1.02	–	–	–	1.04	–	–
0454-463	F	1	3.04	0.97	1.03	0.99	0.71	–	–	–	1.42	–	–
0454-463	F	2	3.06	0.98	1.03	0.98	0.71	–	–	–	1.44	–	–
0454-463	I	1	1.01	0.98	0.93	0.96	1.02	–	19.80	–	–	3.51	407.90
0454-463	I	2	1.00	0.99	0.93	0.96	0.99	–	21.35	–	–	3.21	18.54
0454-463	I	3	1.00	1.04	1.00	0.98	0.99	–	17.44	–	–	3.23	1.00*
0454-463	I	4	1.00*	1.03	1.03	1.02	1.01	–	1.00*	–	–	1.00*	1.00*
0506-612	A	1	0.99	0.99	1.02	1.00	1.03	–	–	–	1.01	–	–
0506-612	A	2	1.00	1.00	1.01	0.99	1.02	–	–	–	1.01	–	–
0506-612	E	1	1.00	0.97	0.96	1.31	2.70	–	1.00*	–	1.02	–	–
0506-612	E	2	1.02	0.96	0.96	1.32	2.71	–	1.00*	–	1.02	–	–

Continued on the next page

Source name	*Epoch*	IF	Parkes	ATCA	Mopra	Hobart	Ceduna	DSS34	DSS43	DSS45	Hartebeesthoek	O'Higgins	TIGO
0506-612	H	1	1.00	1.08	0.96	1.02	1.41	–	–	0.96	6.97	–	–
0506-612	H	2	1.00	1.09	0.96	1.02	1.34	–	–	0.97	7.41	–	–
0506-612	H	3	1.02	1.04	0.97	0.98	1.34	–	–	0.97	6.49	–	–
0506-612	H	4	1.03	1.02	0.99	0.97	1.37	–	–	1.00	7.39	–	–
0516-621	K	1	0.97	0.95	0.79	1.13	1.19	1.00*	–	1.22	–	1.04	5.85
0516-621	K	2	0.98	0.97	0.78	1.13	1.11	1.00*	–	1.23	–	0.96	4.55
0516-621	K	3	1.00	0.96	0.83	1.17	1.14	1.00*	–	1.26	–	0.93	5.04
0516-621	K	4	0.98	0.97	0.85	1.17	1.15	1.00*	–	1.25	–	0.94	3.50
0518-458	A	1	1.01	0.98	1.02	1.02	1.07	–	–	–	1.12	–	–
0518-458	A	2	1.01	0.98	1.00	1.01	1.06	–	–	–	1.11	–	–
0518-458	F	1	3.24	1.02	1.03	1.00	0.97	–	–	–	1.00	–	–
0518-458	F	2	3.22	1.03	1.02	0.99	0.95	–	–	–	1.02	–	–
0518-458	I	1	0.92	0.94	1.00	1.00	6.89	–	1.22	–	–	1.24	0.88
0518-458	I	2	0.92	0.95	1.00	1.00	9.25	–	1.21	–	–	1.14	0.82
0518-458	I	3	0.93	0.99	1.08	1.03	5.55	–	1.23	–	–	1.10	1.00*
0518-458	I	4	1.00*	1.00	1.05	1.03	4.40	–	1.00*	–	–	1.00*	1.00*
0521-365	A	1	1.23	1.09	0.95	0.92	1.10	–	–	–	0.94	–	–
0521-365	A	2	1.23	1.09	0.94	0.91	1.08	–	–	–	0.94	–	–
0521-365	E	1	1.04	1.00	1.01	1.00	1.99	–	6.78	–	1.04	–	–
0521-365	E	2	1.04	1.00	1.02	1.00	2.18	–	1.00*	–	1.03	–	–
0521-365	H	1	1.02	1.08	0.95	0.99	1.25	–	–	1.00	11.96	–	–
0521-365	H	2	1.01	1.10	0.95	0.98	1.19	–	–	1.02	13.38	–	–
0521-365	H	3	1.02	1.05	0.96	0.96	1.19	–	–	1.05	11.32	–	–
0521-365	H	4	1.03	1.03	0.97	0.96	1.21	–	–	1.04	14.59	–	–
0521-365	K	1	0.89	1.04	1.08	1.03	1.14	1.00*	–	1.00*	–	1.62	2.30
0521-365	K	2	0.91	1.04	1.05	1.02	1.10	1.00*	–	1.00*	–	1.38	1.41
0521-365	K	3	0.91	1.05	1.13	1.03	1.05	1.00*	–	1.00*	–	1.35	1.37
0521-365	K	4	0.92	1.04	1.14	1.03	1.06	1.00*	–	1.00*	–	1.63	1.42
0524-485	L	1	0.92	1.06	0.87	0.98	1.25	–	–	1.07	–	2.55	2.72
0524-485	L	2	0.92	1.07	0.87	0.97	1.17	–	–	1.09	–	2.87	1.55
0524-485	L	3	0.92	1.14	0.96	1.01	1.18	–	–	1.09	–	2.19	1.60
0524-485	L	4	0.99	1.19	1.11	0.95	1.38	–	–	1.19	–	1.82	1.50
0527-359	O	1	1.09	0.95	1.09	2.13	1.02	–	–	–	–	–	2.32
0527-359	O	2	1.36	0.91	0.99	1.62	0.90	–	–	–	–	–	4.90
0527-359	O	3	1.59	1.15	1.32	1.61	0.97	–	–	–	–	–	4.93
0527-359	O	4	1.63	0.98	1.04	1.78	0.90	–	–	–	–	–	1.81

Continued on the next page

Source name	*Epoch*	IF	Parkes	ATCA	Mopra	Hobart	Ceduna	DSS34	DSS43	DSS45	Hartebeesthoek	O'Higgins	TIGO
0537-441	A	1	5.08	1.06	0.98	0.96	1.18	–	–	–	0.92	–	–
0537-441	A	2	4.16	1.07	0.97	0.95	1.16	–	–	–	0.92	–	–
0537-441	E	1	1.02	0.98	1.01	1.01	3.51	–	46.13	–	1.04	–	–
0537-441	E	2	1.02	0.98	1.02	1.01	3.64	–	1.00*	–	1.04	–	–
0537-441	H	1	1.00	1.08	0.96	0.98	1.22	–	–	0.98	28.39	–	–
0537-441	H	2	1.00	1.09	0.96	0.97	1.16	–	–	1.00	29.96	–	–
0537-441	H	3	1.02	1.04	0.98	0.96	1.16	–	–	0.99	28.43	–	–
0537-441	H	4	1.02	1.03	0.98	0.96	1.18	–	–	1.02	26.33	–	–
0537-441	K	1	0.98	0.98	0.84	16.20	1.33	1.00*	–	221.99	–	1.22	2.69
0537-441	K	2	0.99	1.00	0.83	18.78	1.27	1.00*	–	234.89	–	1.13	2.01
0537-441	K	3	0.99	0.99	0.90	20.13	1.27	1.00*	–	232.96	–	1.11	1.98
0537-441	K	4	1.00	1.00	0.89	22.72	1.31	1.00*	–	199.91	–	1.15	2.07
0625-354	A	1	2.43	0.97	1.94	1.40	5.95	–	–	–	5.30	–	–
0625-354	A	2	2.54	0.99	1.83	1.35	5.95	–	–	–	7.44	–	–
0625-354	C	1	1.02	0.99	1.07	1.01	1.26	–	1.00*	–	1.00*	–	–
0625-354	C	2	1.03	0.99	0.93	1.00	1.26	–	1.00*	–	1.00*	–	–
0625-354	C	3	1.00*	1.00*	1.00*	1.00*	1.00*	–	1.00*	–	1.00*	–	–
0625-354	F	1	3.33	1.11	1.13	1.11	1.16	–	–	–	0.70	–	–
0625-354	F	2	3.33	1.12	1.11	1.10	1.16	–	–	–	0.70	–	–
0625-354	I	1	1.01	1.07	1.04	0.99	1.01	–	1.21	–	–	1.61	1.00*
0625-354	I	2	0.96	1.01	1.01	0.97	0.95	–	1.24	–	–	1.47	1.00*
0625-354	I	3	0.96	1.03	1.08	1.00	0.95	–	1.26	–	–	1.41	1.00*
0625-354	I	4	1.00*	1.02	1.06	1.03	1.02	–	1.00*	–	–	1.00*	1.00*
0637-752	C	1	1.01	0.98	1.04	1.01	1.19	–	1.00*	–	1.04	–	–
0637-752	C	2	1.00	0.98	0.92	1.00	1.28	–	1.00*	–	1.02	–	–
0637-752	C	3	1.00*	1.00*	1.00*	1.00*	1.00*	–	1.00*	–	1.00*	–	–
0637-752	E	1	1.00	0.98	0.98	1.05	2.96	–	1924.00	–	1.04	–	–
0637-752	E	2	1.00	0.98	0.99	1.05	3.05	–	1.00*	–	1.02	–	–
0637-752	H	1	1.01	1.10	0.98	1.00	1.38	–	–	1.00*	6.50	–	–
0637-752	H	2	1.01	1.12	0.98	1.00	1.33	–	–	1.00*	6.48	–	–
0637-752	H	3	1.02	1.06	1.00	0.96	1.32	–	–	1.00*	6.54	–	–
0637-752	H	4	1.02	1.05	0.99	0.96	1.34	–	–	1.00*	8.17	–	–
0637-752	K	1	0.92	0.84	0.98	0.93	1.20	1.00*	–	21.60	–	6.06	32.87
0637-752	K	2	0.91	0.86	0.98	0.96	1.12	1.00*	–	25.21	–	6.14	23.01
0637-752	K	3	0.89	0.85	1.05	0.99	1.08	1.00*	–	29.42	–	5.75	32.11
0637-752	K	4	0.91	0.85	1.07	0.99	1.18	1.00*	–	26.05	–	6.15	25.39

Continued on the next page

Source name	*Epoch*	IF	Parkes	ATCA	Mopra	Hobart	Ceduna	DSS34	DSS43	DSS45	Hartebeesthoek	O'Higgins	TIGO
0637-752	P	1	0.98	1.04	1.02	1.01	1.30	–	1.00*	–	–	–	–
0637-752	P	2	0.97	1.04	1.03	1.01	1.26	–	1.00*	–	–	–	–
0637-752	P	3	0.96	1.03	1.05	0.97	1.23	–	1.00*	–	–	–	–
0637-752	P	4	0.97	1.03	1.05	0.97	1.28	–	1.00*	–	–	–	–
0700-661	L	1	0.89	1.03	0.98	0.93	1.27	–	–	1.02	–	2.57	4.63
0700-661	L	2	0.89	1.05	0.91	0.94	1.19	–	–	1.05	–	2.46	1.79
0700-661	L	3	0.90	1.11	1.03	0.96	1.18	–	–	1.04	–	2.39	1.83
0700-661	L	4	0.91	1.10	1.09	1.05	1.22	–	–	1.06	–	2.38	1.92
0717-432	L	1	0.93	1.34	1.29	2.46	7.64	–	–	1.38	–	2.67	3.42
0717-432	L	2	0.90	2.08	1.86	2.65	2.51	–	–	1.12	–	3.25	8.11
0717-432	L	3	1.37	1.48	1.06	2.68	6.43	–	–	1.28	–	7.52	9.82
0717-432	L	4	0.99	1.65	1.79	3.92	7.06	–	–	1.17	–	3.12	3.74
0736-770	O	1	1.18	0.92	1.03	1.75	0.93	–	–	–	–	–	2.50
0736-770	O	2	1.10	0.99	0.99	1.56	0.85	–	–	–	–	–	1.34
0736-770	O	3	1.09	0.96	1.03	1.65	0.86	–	–	–	–	–	1.44
0736-770	O	4	1.19	0.98	1.01	1.71	0.86	–	–	–	–	–	1.37
0745-330	O	1	1.17	0.96	1.00	2.17	0.90	–	–	–	–	–	1.87
0745-330	O	2	1.10	0.98	0.99	2.54	0.87	–	–	–	–	–	1.08
0745-330	O	3	1.06	0.94	1.04	1.92	0.87	–	–	–	–	–	1.11
0745-330	O	4	1.12	1.00	1.01	2.29	0.86	–	–	–	–	–	1.14
0812-736	L	1	0.84	1.21	1.54	1.61	10.35	–	–	0.96	–	4.35	3.13
0812-736	L	2	0.86	1.12	1.33	1.69	21.80	–	–	1.32	–	6.65	5.35
0812-736	L	3	0.93	1.31	2.14	4.00	46.12	–	–	0.98	–	7.66	4.25
0812-736	L	4	0.97	1.42	1.57	13.40	52.58	–	–	1.14	–	10.82	4.53
1057-797	L	1	0.96	1.08	1.30	0.86	1.31	–	–	0.95	–	156.67	1.70
1057-797	L	2	0.97	1.07	1.31	0.86	1.22	–	–	0.97	–	351.63	1.05
1057-797	L	3	0.92	1.08	1.31	0.84	1.12	–	–	1.02	–	446.36	0.96
1057-797	L	4	0.96	1.13	1.50	0.86	1.25	–	–	0.99	–	295.42	1.08
1101-536	N	1	0.94	1.39	0.99	1.01	1.21	–	1.04	–	–	–	2.16
1101-536	N	2	0.93	1.40	0.97	1.01	1.16	–	1.06	–	–	–	1.29
1101-536	N	3	0.95	1.40	1.08	1.00	1.20	–	1.02	–	–	–	1.46
1101-536	N	4	0.95	1.46	1.02	1.00	1.20	–	1.03	–	–	–	1.56
1104-445	A	1	1.01	0.99	1.02	1.04	1.05	–	–	–	0.99	–	–
1104-445	A	2	1.01	1.00	1.01	1.03	1.04	–	–	–	0.99	–	–
1104-445	C	1	0.99	0.94	1.02	0.94	1.13	–	1.00*	–	1.05	–	–
1104-445	C	2	0.99	0.95	0.88	0.93	1.16	–	1.00*	–	1.04	–	–

Continued on the next page

Source name	*Epoch*	IF	Parkes	ATCA	Mopra	Hobart	Ceduna	DSS34	DSS43	DSS45	Hartebeesthoek	O'Higgins	TIGO
1104-445	C	3	1.00*	1.00*	1.00*	1.00*	1.00*	–	1.00*	–	1.00*	–	–
1104-445	F	1	3.67	1.09	1.06	1.06	1.17	–	–	–	7.38	–	–
1104-445	F	2	3.76	1.08	1.07	1.06	1.17	–	–	–	7.48	–	–
1104-445	I	1	0.96	1.07	1.12	0.99	1.04	–	1.31	–	–	1.17	2.41
1104-445	I	2	1.01	1.03	1.14	0.99	1.41	–	1.18	–	–	1.08	1.81
1104-445	I	3	0.96	1.13	1.20	1.03	0.99	–	1.26	–	–	1.04	1.00*
1104-445	I	4	1.00*	1.10	1.29	1.03	1.01	–	1.00*	–	–	1.00*	1.00*
1144-379	C	1	1.02	0.98	1.08	1.00	1.15	–	1.00*	–	0.98	–	–
1144-379	C	2	1.01	0.98	0.92	0.99	1.16	–	1.00*	–	0.96	–	–
1144-379	C	3	1.00*	1.00*	1.00*	1.00*	1.00*	–	1.00*	–	1.00*	–	–
1144-379	E	1	1.06	0.98	0.99	1.07	4.28	–	1.00*	–	1.04	–	–
1144-379	E	2	1.06	0.98	1.00	1.07	4.35	–	1.00*	–	1.04	–	–
1144-379	H	1	1.02	1.08	1.00	0.95	1.09	–	–	1.00*	511.41	–	–
1144-379	H	2	1.02	1.09	0.99	0.95	1.05	–	–	1.00*	761.66	–	–
1144-379	H	3	1.04	1.04	1.01	0.92	1.02	–	–	1.00*	3666.73	–	–
1144-379	H	4	1.03	1.02	1.01	0.91	1.05	–	–	1.00*	338.33	–	–
1257-326	C	1	1.02	0.98	1.07	1.05	1.24	–	1.00*	–	1.06	–	–
1257-326	C	2	1.01	0.99	0.92	1.05	1.25	–	1.00*	–	1.03	–	–
1257-326	C	3	1.00*	1.00*	1.00*	1.00*	1.00*	–	1.00*	–	1.00*	–	–
1257-326	F	1	0.65	0.86	0.93	0.95	0.88	–	–	–	32.89	–	–
1257-326	F	2	0.92	0.89	0.92	0.92	0.90	–	–	–	611.32	–	–
1257-326	I	1	1.24	10.31	1.19	1.11	1.18	–	0.81	–	–	1.45	5.01
1257-326	I	2	1.03	1.01	1.25	0.98	1.02	–	0.99	–	–	1.05	2.16
1257-326	I	3	1.02	1.09	1.27	1.12	1.00	–	0.94	–	–	1.00	1.00*
1257-326	I	4	1.00*	1.34	1.18	1.00	0.98	–	1.00*	–	–	1.00*	1.00*
1313-333	C	1	1.02	1.00	1.07	1.02	1.19	–	1.00*	–	0.97	–	–
1313-333	C	2	1.02	1.00	0.92	1.02	1.20	–	1.00*	–	0.96	–	–
1313-333	C	3	1.00*	1.00*	1.00*	1.00*	1.00*	–	1.00*	–	1.00*	–	–
1313-333	E	1	1.03	0.96	0.97	1.03	4.26	–	1.00*	–	1.01	–	–
1313-333	E	2	1.03	0.96	0.97	1.03	4.34	–	1.00*	–	1.01	–	–
1313-333	H	1	1.00	1.09	0.98	0.97	1.17	–	–	1.00*	8.74	–	–
1313-333	H	2	0.99	1.10	0.99	0.98	1.13	–	–	1.00*	8.51	–	–
1313-333	H	3	1.01	1.04	1.00	0.94	1.09	–	–	1.00*	9.74	–	–
1313-333	H	4	1.01	1.03	1.00	0.93	1.11	–	–	1.00*	10.25	–	–
1322-428	A	1	1.93	1.44	0.77	0.93	1.26	–	–	–	0.85	–	–
1322-428	A	2	1.60	1.31	0.83	0.94	1.41	–	–	–	0.86	–	–

Continued on the next page

Source name	*Epoch*	IF	Parkes	ATCA	Mopra	Hobart	Ceduna	DSS34	DSS43	DSS45	Hartebeesthoek	O'Higgins	TIGO
1322-428	F	1	5.64	0.97	1.01	1.07	1.06	–	–	–	1.77	–	–
1322-428	F	2	5.76	0.98	0.99	1.05	1.06	–	–	–	1.54	–	–
1322-428	I	1	0.97	1.00	1.50	1.00	1.10	–	0.98	–	–	1.10	16.01
1322-428	I	2	1.04	1.26	1.23	1.03	0.96	–	0.92	–	–	1.04	12.50
1322-428	I	3	0.93	1.04	1.33	1.03	1.00	–	0.95	–	–	0.99	1.00*
1322-428	I	4	1.00*	1.19	1.28	0.93	1.10	–	1.00*	–	–	1.00*	1.00*
1322-428	N	1	0.94	60.80	1.02	1.02	1.22	–	1.07	–	–	–	2.62
1322-428	N	2	0.94	59.01	1.01	1.06	1.17	–	1.08	–	–	–	1.49
1322-428	N	3	0.94	59.17	1.16	1.27	1.16	–	1.03	–	–	–	1.30
1322-428	N	4	0.95	50.67	1.03	1.08	1.21	–	1.09	–	–	–	1.34
1322-428	O	1	1.01	1.01	0.95	1.00	1.05	–	–	–	–	–	1.95
1322-428	O	2	1.06	1.05	0.91	0.98	1.00	–	–	–	–	–	1.17
1322-428	O	3	1.01	0.98	0.97	0.99	0.99	–	–	–	–	–	1.81
1322-428	O	4	1.04	1.03	0.95	0.98	1.02	–	–	–	–	–	1.25
1322-428	S	1	1.04	1.00	0.99	1.05	1.14	–	1.00*	–	–	–	1.00*
1322-428	S	2	1.04	1.00	0.99	1.04	1.06	–	1.00*	–	–	–	1.75
1322-428	S	3	1.01	1.07	1.01	1.01	1.05	–	1.00*	–	–	–	2.15
1322-428	S	4	1.00	1.06	1.01	1.00	1.13	–	1.00*	–	–	–	2.26
1323-526	A	1	0.99	1.06	1.01	1.03	1.00	–	–	–	1.04	–	–
1323-526	A	2	1.00	1.07	1.01	1.02	0.99	–	–	–	1.03	–	–
1323-526	C	1	1.03	0.99	1.06	0.98	1.19	–	1.00*	–	1.00*	–	–
1323-526	C	2	1.03	0.99	0.91	0.98	1.20	–	1.00*	–	1.00*	–	–
1323-526	C	3	1.00*	1.00*	1.00*	1.00*	1.00*	–	1.00*	–	1.00*	–	–
1323-526	E	1	1.02	0.99	0.96	1.06	3.97	–	1.00*	–	1822.01	–	–
1323-526	E	2	1.02	1.00	0.96	1.05	3.91	–	1.00*	–	2586.02	–	–
1323-526	H	1	1.00	1.07	0.98	0.99	1.26	–	–	1.00*	391.56	–	–
1323-526	H	2	1.00	1.08	0.97	0.98	1.20	–	–	1.00*	6720.18	–	–
1323-526	H	3	1.01	1.03	0.99	0.96	1.18	–	–	1.00*	919.28	–	–
1323-526	H	4	1.01	1.03	0.99	0.96	1.23	–	–	1.00*	15848.50	–	–
1323-526	L	1	1.06	1.21	0.98	0.99	1.50	–	–	1.17	–	43.95	5.12
1323-526	L	2	1.06	1.22	0.98	0.98	1.41	–	–	1.20	–	40.11	3.10
1323-526	L	3	1.05	1.31	1.11	0.98	1.49	–	–	1.18	–	70.22	2.36
1323-526	L	4	1.05	1.31	1.13	0.98	1.48	–	–	1.21	–	44.93	2.63
1325-558	K	1	0.95	0.86	0.84	0.94	1.12	1.45	–	2.27	–	1.40	6.76
1325-558	K	2	0.97	0.85	0.83	0.93	1.15	1.64	–	2.49	–	1.35	4.63
1325-558	K	3	0.94	0.86	0.94	0.98	1.10	1.62	–	2.16	–	1.34	4.37

Continued on the next page

Source name	*Epoch*	IF	Parkes	ATCA	Mopra	Hobart	Ceduna	DSS34	DSS43	DSS45	Hartebeesthoek	O'Higgins	TIGO
1325-558	K	4	0.90	0.94	0.94	1.00	1.05	1.55	–	3.48	–	1.46	26.36
1325-558	L	1	0.72	0.87	0.73	0.72	1.12	–	–	0.86	–	42.80	1.49
1325-558	L	2	0.93	5245.84	0.64	0.70	1.30	–	–	0.89	–	14.79	1.05
1325-558	L	3	0.75	0.97	0.80	0.71	1.23	–	–	0.88	–	33.85	1.72
1325-558	L	4	0.75	0.95	0.80	0.76	1.15	–	–	0.87	–	319.48	0.97
1333-337	C	1	1.00	0.99	1.05	1.07	1.21	–	1.00*	–	1.14	–	–
1333-337	C	2	1.00	1.00	0.91	1.07	1.22	–	1.00*	–	1.12	–	–
1333-337	C	3	1.00*	1.00*	1.00*	1.00*	1.00*	–	1.00*	–	1.00*	–	–
1333-337	F	1	1.75	0.92	1.08	1.04	1.06	–	–	–	1.00*	–	–
1333-337	F	2	1.77	0.92	1.06	1.03	1.07	–	–	–	1.00*	–	–
1333-337	I	1	1.38	0.87	1.29	0.85	0.96	–	1.68	–	–	1.21	1.00*
1333-337	I	2	1.51	0.83	1.32	0.76	0.94	–	1.65	–	–	1.44	1.00*
1333-337	I	3	1.50	0.86	1.87	0.81	1.03	–	1.76	–	–	1.22	1.00*
1333-337	I	4	1.00*	1.04	1.85	1.05	0.89	–	1.00*	–	–	1.00*	1.00*
1344-376	L	1	0.97	1.13	0.95	0.97	1.79	–	–	1.02	–	55.49	1.64
1344-376	L	2	0.98	1.12	0.92	0.98	1.49	–	–	1.05	–	76.65	1.06
1344-376	L	3	0.94	1.14	1.00	1.05	1.57	–	–	1.07	–	27.56	1.11
1344-376	L	4	0.95	1.13	1.00	0.96	1.50	–	–	1.11	–	38.08	1.15
1424-418	A	1	1.01	1.00	1.03	1.03	0.98	–	–	–	1.03	–	–
1424-418	A	2	1.01	1.01	1.04	1.02	0.97	–	–	–	1.03	–	–
1424-418	E	1	1.04	0.97	0.98	1.02	4.01	–	1.00*	–	1.00	–	–
1424-418	E	2	1.04	0.97	0.99	1.01	4.03	–	1.00*	–	1.00	–	–
1424-418	H	1	0.99	1.06	0.98	0.98	1.17	–	–	1.00*	10.44	–	–
1424-418	H	2	1.01	1.09	0.97	0.96	1.11	–	–	1.00*	8.77	–	–
1424-418	H	3	1.01	1.02	0.99	0.96	1.10	–	–	1.00*	9.10	–	–
1424-418	H	4	1.01	1.01	0.99	0.96	1.13	–	–	1.00*	9.88	–	–
1440-389	L	1	0.91	1.01	0.87	1.29	2.32	–	–	1.02	–	17.51	4.27
1440-389	L	2	0.94	1.09	0.85	0.98	1.76	–	–	1.00	–	5.38	2.57
1440-389	L	3	0.88	1.06	0.96	0.94	1.39	–	–	1.07	–	6.18	5.14
1440-389	L	4	0.87	1.06	0.97	0.96	1.74	–	–	1.11	–	9.14	2.51
1454-354	A	1	1.10	1.00	0.97	1.02	1.17	–	–	–	1.03	–	–
1454-354	A	2	1.12	1.03	0.97	0.99	1.15	–	–	–	1.01	–	–
1454-354	F	1	2.98	0.95	1.00	0.96	0.97	–	–	–	0.59	–	–
1454-354	F	2	3.07	0.94	1.00	0.96	0.99	–	–	–	0.76	–	–
1454-354	I	1	0.93	1.06	8.28	0.96	1.02	–	0.99	–	–	1.11	1.63
1454-354	I	2	0.92	1.06	3.41	0.95	0.95	–	0.99	–	–	1.03	0.94

Continued on the next page

Source name	*Epoch*	IF	Parkes	ATCA	Mopra	Hobart	Ceduna	DSS34	DSS43	DSS45	Hartebeesthoek	O'Higgins	TIGO
1454-354	I	3	0.92	1.11	1.84	0.99	0.96	–	0.97	–	–	0.97	1.00*
1454-354	I	4	1.00*	1.14	1.28	0.97	1.00	–	1.00*	–	–	1.00*	1.00*
1501-343	A	1	1.07	1.03	1.03	1.06	0.97	–	–	–	0.85	–	–
1501-343	A	2	1.07	1.04	1.04	1.05	0.96	–	–	–	0.85	–	–
1501-343	E	1	1.02	0.95	0.95	1.04	4.74	–	1.00*	–	1.01	–	–
1501-343	E	2	1.02	0.95	0.96	1.04	4.80	–	1.00*	–	1.01	–	–
1501-343	H	1	1.00	1.09	1.00	0.97	1.18	–	–	1.00*	4.71	–	–
1501-343	H	2	1.01	1.10	0.98	0.97	1.11	–	–	1.00*	3.94	–	–
1501-343	H	3	1.01	1.04	1.00	0.94	1.10	–	–	1.00*	7.39	–	–
1501-343	H	4	1.02	1.04	1.00	0.94	1.12	–	–	1.00*	4.00	–	–
1505-496	L	1	1.36	1.13	1.23	0.88	1.38	–	–	1.00*	–	1.00*	62.64
1505-496	L	2	1.41	1.17	1.23	0.84	1.31	–	–	1.00*	–	1.00*	196.36
1505-496	L	3	1.38	1.20	1.41	0.86	1.43	–	–	1.00*	–	1.00*	198.78
1505-496	L	4	1.00	1.05	1.18	0.93	1.16	–	–	1.00*	–	1.00*	96.21
1549-790	C	1	1.23	1.72	0.88	1.05	1.30	–	1.00*	–	2.68	–	–
1549-790	C	2	1.26	1.75	0.74	1.04	1.25	–	1.00*	–	2.03	–	–
1549-790	C	3	1.00*	1.00*	1.00*	1.00*	1.00*	–	1.00*	–	1.00*	–	–
1549-790	I	1	0.91	1.57	1.29	0.98	1.45	–	0.86	–	–	1.12	2.54
1549-790	I	2	0.91	1.60	1.09	1.01	1.27	–	0.93	–	–	1.16	1.68
1549-790	I	3	0.93	1.54	1.18	1.02	1.27	–	0.91	–	–	0.97	1.00*
1549-790	I	4	1.00*	1.11	1.53	1.94	1.43	–	1.00*	–	–	1.00*	1.00*
1600-489	K	1	1.09	0.99	1.14	1.01	2.04	1.00*	–	1.22	–	2.22	1.00*
1600-489	K	2	1.07	1.19	1.08	1.16	1.40	27.33	–	1.19	–	2.75	4.43
1600-489	K	3	1.04	0.99	1.17	1.04	1.68	27.66	–	1.27	–	1.86	3.76
1600-489	K	4	1.08	0.98	1.23	1.06	1.59	150.93	–	1.24	–	4.76	2.98
1600-489	L	1	0.90	1.22	0.93	0.96	1.90	–	–	1.18	–	13.31	9.92
1600-489	L	2	0.93	1.15	0.87	0.92	1.66	–	–	1.22	–	56.58	2.09
1600-489	L	3	0.97	1.30	1.04	0.90	1.45	–	–	1.15	–	6.47	2.42
1600-489	L	4	0.96	1.24	0.97	0.90	1.94	–	–	1.23	–	17.20	2.77
1600-489	N	1	0.98	1.00*	0.91	0.95	1.17	–	1.20	–	–	–	12.18
1600-489	N	2	1.00	1.00*	0.91	1.02	1.13	–	1.30	–	–	–	1.78
1600-489	N	3	0.98	1.00*	0.99	1.02	1.20	–	1.14	–	–	–	2.84
1600-489	N	4	0.95	1.00*	1.06	1.00	1.21	–	1.10	–	–	–	2.21
1600-445	N	1	1.09	1.00*	1.08	1.01	1.20	–	1.10	–	–	–	2.37
1600-445	N	2	1.11	1.00*	1.06	0.99	1.16	–	1.12	–	–	–	1.29
1600-445	N	3	1.10	1.00*	1.10	0.96	1.21	–	1.14	–	–	–	1.41

Continued on the next page

Source name	*Epoch*	IF	Parkes	ATCA	Mopra	Hobart	Ceduna	DSS34	DSS43	DSS45	Hartebeesthoek	O'Higgins	TIGO
1600-445	N	4	1.08	1.00*	1.08	0.99	1.24	–	1.13	–	–	–	1.39
1600-489	R	1	1.02	1.01	0.97	1.04	1.48	–	5589.12	–	–	–	1.17
1600-489	R	2	1.03	1.02	0.96	1.03	1.39	–	841.67	–	–	–	1.11
1600-489	R	3	1.02	1.03	0.99	1.01	1.42	–	1502.97	–	–	–	1.42
1600-489	R	4	1.01	1.04	0.99	1.01	1.39	–	1194.37	–	–	–	0.88
1606-667	L	1	1.03	1.28	3.18	1.65	2.13	–	–	1.00*	–	1.00*	9.52
1606-667	L	2	1.31	1.28	3.80	1.25	2.26	–	–	1.00*	–	1.00*	2.62
1606-667	L	3	1.16	1.20	1.68	1.73	5.47	–	–	1.00*	–	1.00*	1.87
1606-667	L	4	1.03	1.86	1.50	2.10	2.99	–	–	1.00*	–	1.00*	2.45
1610-771	C	1	1.71	1.07	0.98	1.02	1.45	–	1.00*	–	0.89	–	–
1610-771	C	2	1.80	1.08	0.85	1.03	1.47	–	1.00*	–	0.87	–	–
1610-771	C	3	1.00*	1.00*	1.00*	1.00*	1.00*	–	1.00*	–	1.00*	–	–
1610-771	E	1	1.03	0.99	0.96	1.03	4.66	–	4.11	–	1.01	–	–
1610-771	E	2	1.03	0.99	0.97	1.03	4.79	–	1.00*	–	1.01	–	–
1610-771	H	1	1.12	1.34	0.84	1.01	1.24	–	–	1.03	106.81	–	–
1610-771	H	2	1.05	1.23	0.94	0.94	1.19	–	–	1.05	139.78	–	–
1610-771	H	3	1.17	1.61	0.97	0.84	1.14	–	–	0.99	96.03	–	–
1610-771	H	4	1.13	1.16	0.91	0.92	1.21	–	–	1.08	101.71	–	–
1613-586	N	1	0.92	1.00*	0.98	0.99	1.59	–	1.02	–	–	–	1.94
1613-586	N	2	0.95	1.00*	0.98	1.04	1.54	–	1.03	–	–	–	1.29
1613-586	N	3	0.94	1.00*	1.04	0.97	1.56	–	1.01	–	–	–	1.23
1613-586	N	4	0.96	1.00*	1.04	0.97	1.60	–	1.02	–	–	–	1.26
1656-332	C	1	1.02	1.22	1.12	1.08	100.63	–	1.00*	–	1.00*	–	–
1656-332	C	2	1.02	1.23	0.95	1.06	263.13	–	1.00*	–	1.00*	–	–
1656-332	C	3	1.00*	1.00*	1.00*	1.00*	1.00*	–	1.00*	–	1.00*	–	–
1714-336	A	1	1.02	1.01	0.99	1.04	1.03	–	–	–	1.00*	–	–
1714-336	A	2	1.02	1.01	1.00	1.03	1.03	–	–	–	1.00*	–	–
1714-336	I	1	0.95	1.10	1.16	1.10	1.05	–	0.92	–	–	1.00*	1.00*
1714-336	I	2	0.95	1.08	1.17	1.10	1.03	–	0.91	–	–	1.00*	1.00*
1714-336	I	3	0.98	1.14	2.36	1.18	1.09	–	0.88	–	–	1.00*	1.00*
1714-336	I	4	1.00*	1.15	1.12	1.22	1.07	–	1.00*	–	–	1.00*	1.00*
1716-771	A	1	1.00	0.98	0.97	1.03	1.10	–	–	–	1.27	–	–
1716-771	A	2	1.00	0.98	0.97	1.02	1.10	–	–	–	1.27	–	–
1716-771	E	1	1.02	0.97	0.97	1.05	4.40	–	6.05	–	0.99	–	–
1716-771	E	2	1.03	0.97	0.99	1.04	4.44	–	1.00*	–	0.98	–	–
1716-771	H	1	0.99	1.09	0.98	0.98	1.25	–	–	0.99	9.93	–	–

Continued on the next page

Source name	*Epoch*	IF	Parkes	ATCA	Mopra	Hobart	Ceduna	DSS34	DSS43	DSS45	Hartebeesthoek	O'Higgins	TIGO
1716-771	H	2	0.99	1.09	0.98	0.97	1.17	–	–	1.01	9.72	–	–
1716-771	H	3	1.01	1.04	0.99	0.97	1.17	–	–	1.00	11.70	–	–
1716-771	H	4	1.02	1.03	0.99	0.96	1.18	–	–	1.03	9.68	–	–
1718-649	C	1	1.01	1.11	1.32	0.94	1.37	–	1.00*	–	1.10	–	–
1718-649	C	2	1.03	1.10	1.00	0.93	1.33	–	1.00*	–	1.24	–	–
1718-649	C	3	1.00*	1.00*	1.00*	1.00*	1.00*	–	1.00*	–	1.00*	–	–
1718-649	F	1	12.98	0.95	1.10	1.02	1.03	–	–	–	6.58	–	–
1718-649	F	2	12.87	0.96	1.09	1.01	1.02	–	–	–	7.02	–	–
1718-649	I	1	0.81	1.40	0.98	0.94	1.05	–	0.86	–	–	1.50	3.33
1718-649	I	2	0.81	1.42	0.99	0.94	0.97	–	0.86	–	–	1.47	1.65
1718-649	I	3	0.81	1.43	1.08	0.98	1.01	–	0.86	–	–	1.35	1.00*
1718-649	I	4	1.00*	1.54	1.10	0.92	1.09	–	1.00*	–	–	1.00*	1.00*
1718-649	S	1	1.02	0.98	0.99	0.98	1.26	–	1.06	–	–	–	2.00
1718-649	S	2	1.02	0.98	0.99	0.97	1.17	–	1.06	–	–	–	1.80
1718-649	S	3	0.99	1.05	1.01	0.96	1.22	–	1.05	–	–	–	1.45
1718-649	S	4	0.99	1.05	1.01	0.95	1.24	–	1.05	–	–	–	1.83
1733-565	C	1	1.04	1.20	1.09	0.97	1.31	–	1.00*	–	1.05	–	–
1733-565	C	2	1.04	1.23	0.96	0.96	1.32	–	1.00*	–	1.05	–	–
1733-565	C	3	1.00*	1.00*	1.00*	1.00*	1.00*	–	1.00*	–	1.00*	–	–
1733-565	E	1	1.05	0.97	1.00	1.01	4.58	–	7.09	–	1.04	–	–
1733-565	E	2	1.04	0.98	1.00	1.00	4.97	–	1.00*	–	1.03	–	–
1733-565	H	1	1.04	3.03	0.99	0.95	1.25	–	–	1.03	9.44	–	–
1733-565	H	2	1.02	3.01	1.00	0.95	1.21	–	–	1.04	8.47	–	–
1733-565	H	3	1.05	2.88	1.00	0.93	1.18	–	–	1.04	8.87	–	–
1733-565	H	4	1.04	2.80	1.01	0.92	1.22	–	–	1.08	10.40	–	–
1759-396	A	1	1.50	1.13	0.92	1.02	1.32	–	–	–	0.80	–	–
1759-396	A	2	1.42	1.12	0.93	1.01	1.44	–	–	–	0.81	–	–
1759-396	I	1	10.89	1.40	4.18	0.83	1.27	–	1.15	–	–	0.99	1.87
1759-396	I	2	12.32	1.32	2.61	0.79	1.03	–	1.16	–	–	0.84	1.21
1759-396	I	3	8.79	1.36	6.25	0.76	1.07	–	1.22	–	–	0.77	1.00*
1759-396	I	4	1.00*	1.38	1.46	0.94	1.04	–	1.00*	–	–	1.00*	1.00*
1804-502	A	1	1.11	1.02	1.03	1.06	1.14	–	–	–	0.82	–	–
1804-502	A	2	1.10	1.01	1.04	1.06	1.13	–	–	–	0.81	–	–
1804-502	E	1	1.06	0.96	1.00	1.04	4.42	–	3.79	–	1.00	–	–
1804-502	E	2	1.05	0.96	0.99	1.00	4.18	–	1.00*	–	1.00	–	–
1804-502	H	1	1.01	1.12	1.00	0.94	1.27	–	–	0.98	4.96	–	–

Continued on the next page

Source name	*Epoch*	IF	Parkes	ATCA	Mopra	Hobart	Ceduna	DSS34	DSS43	DSS45	Hartebeesthoek	O'Higgins	TIGO
1804-502	H	2	1.02	1.14	0.99	0.94	1.21	–	–	0.99	5.58	–	–
1804-502	H	3	1.04	1.08	1.01	0.94	1.19	–	–	0.99	5.90	–	–
1804-502	H	4	1.04	1.08	1.01	0.93	1.26	–	–	1.01	5.04	–	–
1814-637	C	1	1.25	1.13	1.45	0.91	1.39	–	1.00*	–	0.94	–	–
1814-637	C	2	1.23	1.11	1.31	0.90	1.39	–	1.00*	–	0.93	–	–
1814-637	C	3	1.00*	1.00*	1.00*	1.00*	1.00*	–	1.00*	–	1.00*	–	–
1814-637	I	1	2.69	1.54	1.83	0.46	1.47	–	3.17	–	–	2.44	4.15
1814-637	I	2	1.80	1.30	2.08	0.65	1.52	–	5.34	–	–	1.77	3.02
1814-637	I	3	1.21	1.05	1.56	1.16	1.28	–	11.65	–	–	2.45	1.00*
1814-637	I	4	1.00*	1.46	1.51	1.30	1.02	–	1.00*	–	–	1.00*	1.00*
1933-400	A	1	1.98	1.09	0.92	0.97	1.21	–	–	–	0.95	–	–
1933-400	A	2	2.05	1.06	0.94	0.99	1.21	–	–	–	0.95	–	–
1933-400	E	1	1.04	0.98	0.97	1.03	3.50	–	6.43	–	0.99	–	–
1933-400	E	2	1.03	0.98	0.98	1.03	3.59	–	1.00*	–	0.99	–	–
1933-400	H	1	1.04	1.04	0.95	1.32	1.28	–	–	1.00	9.87	–	–
1933-400	H	2	1.03	1.06	0.95	1.30	1.23	–	–	1.02	10.07	–	–
1933-400	H	3	1.02	1.03	0.98	0.96	1.15	–	–	0.99	9.12	–	–
1933-400	H	4	1.02	1.02	0.99	0.96	1.16	–	–	1.01	11.38	–	–
1934-638	C	1	1.69	3.05	0.91	0.61	9.34	–	1.00*	–	4.29	–	–
1934-638	C	2	1.11	1.74	0.60	0.96	4.48	–	1.00*	–	1.93	–	–
1934-638	C	3	1.00*	1.00*	1.00*	1.00*	1.00*	–	1.00*	–	1.00*	–	–
1934-638	E	1	1.32	1.18	1.17	0.96	3.04	–	5.85	–	2.13	–	–
1934-638	E	2	1.43	1.18	1.17	0.95	3.23	–	1.00*	–	2.65	–	–
1934-638	F	1	18.69	0.99	1.14	1.37	1.11	–	–	–	1.00*	–	–
1934-638	F	2	11.46	0.96	1.15	1.42	1.09	–	–	–	1.00*	–	–
1934-638	I	1	1.23	2.15	0.90	1.00	1.21	–	1.00	–	–	1.09	1.00*
1934-638	I	2	1.12	2.15	0.96	0.98	3.35	–	1.06	–	–	1.83	1.00*
1934-638	I	3	1.07	1.83	1.08	1.04	4.13	–	1.03	–	–	1.78	1.00*
1934-638	I	4	1.00*	1.57	1.21	0.95	6.63	–	1.00*	–	–	1.00*	1.00*
1934-638	K	1	1.44	1.00	1.37	1.06	1.28	16.27	–	1.00*	–	1.00*	1.00*
1934-638	K	2	1.23	1.07	1.42	1.10	1.37	26.09	–	1.00*	–	1.00*	1.00*
1934-638	K	3	1.28	1.05	1.49	1.22	1.26	24.57	–	1.00*	–	1.00*	1.00*
1934-638	K	4	1.38	1.04	1.48	1.15	1.25	15.93	–	1.00*	–	1.00*	1.00*
1934-638	L	1	0.85	1.28	0.94	1.19	1.99	–	–	1.00*	–	7.76	1.00*
1934-638	L	2	0.83	1.32	0.94	1.22	2.26	–	–	1.00*	–	101.98	1.00*
1934-638	L	3	0.88	1.25	1.06	1.63	2.30	–	–	1.00*	–	9.50	1.00*

Continued on the next page

Source name	*Epoch*	IF	Parkes	ATCA	Mopra	Hobart	Ceduna	DSS34	DSS43	DSS45	Hartebeesthoek	O'Higgins	TIGO
1934-638	L	4	0.84	1.32	1.09	1.23	2.10	–	–	1.00*	–	24.15	1.00*
1954-388	C	1	1.57	4.10	0.84	0.79	1.57	–	1.00*	–	0.68	–	–
1954-388	C	2	1.54	4.11	0.75	0.80	1.68	–	1.00*	–	0.68	–	–
1954-388	C	3	1.00*	1.00*	1.00*	1.00*	1.00*	–	1.00*	–	1.00*	–	–
1954-388	I	1	0.93	1.11	1.08	0.96	1.04	–	0.98	–	–	1.15	3.17
1954-388	I	2	0.93	1.14	1.21	0.97	1.11	–	0.97	–	–	1.04	1.32
1954-388	I	3	0.95	1.16	1.22	0.99	0.99	–	0.96	–	–	1.01	1.00*
1954-388	I	4	1.00*	1.10	1.17	1.01	0.98	–	1.00*	–	–	1.00*	1.00*
2004-447	T	1	1.02	1.00	0.95	0.98	1.37	1.00*	–	1.00*	1.24	–	1.00*
2004-447	T	2	1.03	1.00	0.94	0.98	1.27	1.00*	–	1.00*	1.26	–	1.00*
2004-447	T	3	1.04	0.99	0.96	0.97	1.27	1.00*	–	1.00*	1.31	–	1.00*
2004-447	T	4	1.05	0.99	0.96	0.97	1.29	1.00*	–	1.00*	1.24	–	1.00*
2005-489	A	1	1.46	1.07	0.90	0.96	1.13	–	–	–	1.18	–	–
2005-489	A	2	1.43	1.06	0.92	0.96	1.15	–	–	–	1.23	–	–
2005-489	E	1	0.86	0.81	0.79	0.78	2.76	–	1.92	–	0.98	–	–
2005-489	E	2	0.85	0.81	0.80	0.78	2.72	–	1.00*	–	0.93	–	–
2005-489	H	1	0.95	1.02	0.93	0.95	1.22	–	–	0.93	7.51	–	–
2005-489	H	2	0.95	1.03	0.93	0.94	1.15	–	–	0.94	5.66	–	–
2005-489	H	3	0.96	0.98	0.95	0.93	1.14	–	–	0.94	8.15	–	–
2005-489	H	4	0.97	0.97	0.95	0.93	1.15	–	–	0.97	5.83	–	–
2027-308	F	1	1.08	0.88	1.26	1.31	0.88	–	–	–	3.23	–	–
2027-308	F	2	1.07	0.88	1.25	1.30	0.88	–	–	–	2.53	–	–
2052-474	C	1	2.09	2.38	0.91	0.99	7.76	–	1.00*	–	0.79	–	–
2052-474	C	2	2.18	2.20	0.96	0.99	8.25	–	1.00*	–	0.79	–	–
2052-474	C	3	1.00*	1.00*	1.00*	1.00*	1.00*	–	1.00*	–	1.00*	–	–
2052-474	E	1	1.03	0.99	0.97	1.08	3.97	–	6.79	–	1.00	–	–
2052-474	E	2	1.02	0.99	0.98	1.07	4.10	–	1.00*	–	1.00	–	–
2052-474	H	1	1.01	1.03	0.95	2.93	1.25	–	–	0.99	9.96	–	–
2052-474	H	2	1.02	1.04	0.94	2.71	1.19	–	–	1.01	9.93	–	–
2052-474	H	3	1.00	1.02	0.98	0.95	1.14	–	–	0.97	12.87	–	–
2052-474	H	4	1.00	1.01	0.98	0.94	1.17	–	–	0.99	11.76	–	–
2106-413	C	1	2.72	3.04	1.00	0.85	4.69	–	1.00*	–	0.86	–	–
2106-413	C	2	2.50	4.37	1.04	0.85	7.43	–	1.00*	–	0.80	–	–
2106-413	C	3	1.00*	1.00*	1.00*	1.00*	1.00*	–	1.00*	–	1.00*	–	–
2106-413	I	1	1.03	1.09	0.98	0.99	1.29	–	1.07	–	–	1.17	1.00*
2106-413	I	2	1.16	1.05	1.02	0.87	1.17	–	4.02	–	–	0.89	1.00*

Continued on the next page

Source name	*Epoch*	IF	Parkes	ATCA	Mopra	Hobart	Ceduna	DSS34	DSS43	DSS45	Hartebeesthoek	O'Higgins	TIGO
2106-413	I	3	1.22	1.12	1.09	0.86	1.13	–	3.66	–	–	0.82	1.00*
2106-413	I	4	1.00*	1.08	1.13	1.03	1.14	–	1.00*	–	–	1.00*	1.00*
2136-428	O	1	1.05	1.10	0.97	1.14	1.00*	–	–	–	–	–	3.79
2136-428	O	2	1.02	1.00	1.00	1.12	1.00*	–	–	–	–	–	7.57
2136-428	O	3	1.06	1.10	1.01	1.15	1.00*	–	–	–	–	–	4.26
2136-428	O	4	1.03	1.02	1.01	1.18	1.00*	–	–	–	–	–	2.47
2149-306	E	1	1.04	1.01	0.97	1.00	4.07	–	6.85	–	1.01	–	–
2149-306	E	2	1.03	1.00	0.99	0.99	4.04	–	1.00*	–	0.99	–	–
2149-306	H	1	0.99	1.09	0.97	1.00	1.20	–	–	0.98	8.55	–	–
2149-306	H	2	0.99	1.10	0.97	0.99	1.15	–	–	0.99	8.88	–	–
2149-306	H	3	1.00	1.05	0.99	0.96	1.12	–	–	0.99	8.10	–	–
2149-306	H	4	1.01	1.03	0.99	0.95	1.17	–	–	1.01	9.13	–	–
2152-699	C	1	1.01	1.04	0.95	1.02	1.15	–	1.00*	–	1.02	–	–
2152-699	C	2	1.00	1.06	0.97	1.01	1.12	–	1.00*	–	1.00	–	–
2152-699	C	3	1.00*	1.00*	1.00*	1.00*	1.00*	–	1.00*	–	1.00*	–	–
2152-699	I	1	3.79	0.95	0.97	0.96	1.04	–	1.29	–	–	1.26	1.00*
2152-699	I	2	3.58	0.95	0.93	1.00	1.04	–	1.29	–	–	1.08	8.27
2152-699	I	3	3.51	0.96	1.06	0.97	1.08	–	1.31	–	–	1.22	1.00*
2152-699	I	4	1.00*	0.98	1.05	1.05	1.08	–	1.00*	–	–	1.00*	1.00*
2155-304	E	1	1.03	0.98	0.98	1.02	3.92	–	5.17	–	0.98	–	–
2155-304	E	2	1.02	0.99	0.99	1.02	3.96	–	1.00*	–	0.98	–	–
2155-304	H	1	0.98	1.06	0.96	1.02	1.32	–	–	0.97	6.25	–	–
2155-304	H	2	0.98	1.07	0.96	1.02	1.28	–	–	0.98	5.71	–	–
2155-304	H	3	0.99	1.02	0.97	0.98	1.25	–	–	0.98	6.07	–	–
2155-304	H	4	1.00	1.01	0.98	0.98	1.29	–	–	1.00	6.31	–	–
2155-304	L	1	0.87	1.12	1.00	1.09	1.32	–	–	1619.90	–	1.88	1.54
2155-304	L	2	0.88	1.13	0.98	1.08	1.24	–	–	2321.25	–	1.75	1.00
2155-304	L	3	0.91	1.18	1.07	1.05	1.31	–	–	216.25	–	1.46	0.95
2155-304	L	4	0.89	1.20	1.09	1.10	1.24	–	–	1284.31	–	1.73	1.01
2155-304	N	1	0.93	1.00*	1.01	1.00	1.67	–	1.06	–	–	–	1.76
2155-304	N	2	0.93	1.00*	1.00	1.01	1.57	–	1.08	–	–	–	1.05
2155-304	N	3	0.95	1.00*	1.06	1.00	1.68	–	1.05	–	–	–	1.01
2155-304	N	4	0.96	1.00*	1.06	1.00	1.61	–	1.05	–	–	–	0.99
2204-540	C	1	1.87	2.91	1.16	0.94	0.87	–	1.00*	–	0.82	–	–
2204-540	C	2	1.79	2.04	1.17	0.96	0.85	–	1.00*	–	0.86	–	–
2204-540	C	3	1.00*	1.00*	1.00*	1.00*	1.00*	–	1.00*	–	1.00*	–	–

Continued on the next page

Source name	*Epoch*	IF	Parkes	ATCA	Mopra	Hobart	Ceduna	DSS34	DSS43	DSS45	Hartebeesthoek	O'Higgins	TIGO
2204-540	I	1	3.20	1.06	0.95	0.80	2.24	–	1.71	–	–	0.74	1.31
2204-540	I	2	3.45	1.03	0.93	0.82	4.44	–	1.44	–	–	0.75	0.90
2204-540	I	3	3.83	1.12	1.06	0.76	2.16	–	1.54	–	–	0.68	1.00*
2204-540	I	4	1.00*	1.22	1.28	1.00	3.90	–	1.00*	–	–	1.00*	1.00*
2326-477	A	1	1.01	0.99	0.98	1.03	1.09	–	–	–	0.96	–	–
2326-477	A	2	1.01	0.99	0.96	1.03	1.08	–	–	–	0.96	–	–
2326-477	E	1	1.08	0.99	0.97	1.05	3.23	–	3.69	–	0.97	–	–
2326-477	E	2	1.07	1.00	0.99	1.05	3.37	–	1.00*	–	0.97	–	–
2326-477	H	1	0.99	1.09	0.99	1.01	1.25	–	–	1.02	23.82	–	–
2326-477	H	2	0.99	1.10	0.98	1.00	1.18	–	–	1.03	31.37	–	–
2326-477	H	3	1.00	1.05	1.00	0.97	1.17	–	–	1.03	25.29	–	–
2326-477	H	4	1.01	1.04	1.00	0.97	1.19	–	–	1.06	34.93	–	–
2355-534	C	1	0.99	1.07	1.02	1.00	2.64	–	1.00*	–	1.03	–	–
2355-534	C	2	0.97	1.21	1.02	1.01	2.77	–	1.00*	–	1.04	–	–
2355-534	C	3	1.00*	1.00*	1.00*	1.00*	1.00*	–	1.00*	–	1.00*	–	–
2355-534	I	1	1.71	1.04	0.68	0.93	1.13	–	1.51	–	–	0.83	2.87
2355-534	I	2	1.68	0.99	0.87	0.83	1.21	–	1.65	–	–	0.73	1.62
2355-534	I	3	5.34	1.06	0.94	0.87	1.12	–	1.43	–	–	0.74	1.00*
2355-534	I	4	1.00*	1.00	1.04	0.99	0.97	–	1.00*	–	–	1.00*	1.00*

Table A.1.: Gain correction factors from amplitude self-calibration for each telescope in the X-band (8.4GHz) for each sources' observation. Values with asteriks indicate dismissed data, wherefore no gain correction is given. See section 3.1 for further explanation.

Source name	*Epoch*	IF	Parkes	ATCA	Mopra	Hobart	Ceduna	DSS43	Hartebeesthoek
0047-579	D	1	1.09	1.15	1.13	1.22	1.67	1.00*	–
0047-579	D	2	1.10	1.16	1.13	1.21	1.62	1.00*	–
0047-579	G	1	0.94	0.97	0.98	0.74	3.06	–	1.00*
0047-579	G	2	0.95	0.95	1.00	0.76	3.22	–	1.00*
0208-512	J	1	1.04	1.08	1.10	0.90	2.17	2.14	–
0208-512	J	2	1.03	1.08	1.15	0.90	2.25	2.15	–
0244-470	Q	1	0.97	0.95	1.06	1.03	2.05	–	–
0244-470	Q	2	0.97	0.95	1.05	1.01	2.00	–	–
0302-623	Q	1	1.01	1.00	1.08	1.12	2.49	–	–
0302-623	Q	2	1.01	1.01	1.08	1.13	2.45	–	–
0308-611	Q	1	0.99	0.95	1.07	1.11	2.16	–	–
0308-611	Q	2	0.98	0.96	1.07	1.12	2.04	–	–
0332-403	B	1	1.21	0.93	1.06	0.99	1.16	1.00*	–
0332-403	B	2	1.21	0.92	1.03	1.00	1.13	1.00*	–
0332-403	B	3	1.00*	1.00*	1.00*	1.00*	1.00*	1.00*	–
0332-403	D	1	1.04	1.06	1.17	1.14	1.36	1.00*	–
0332-403	D	2	1.04	1.07	1.19	1.14	1.37	1.00*	–
0332-403	G	1	0.76	1.66	1.21	0.98	4.45	–	5.32
0332-403	G	2	0.75	1.61	1.27	1.00	2.81	–	5.31
0405-385	B	1	1.21	0.89	0.97	1.26	1.62	1.00*	–
0405-385	B	2	1.21	0.89	0.97	1.30	1.60	1.00*	–
0405-385	B	3	1.00*	1.00*	1.00*	1.00*	1.00*	1.00*	–
0405-385	D	1	1.10	0.99	1.15	1.20	1.64	1.00*	–
0405-385	D	2	1.11	1.00	1.17	1.17	1.50	1.00*	–
0438-436	B	1	1.22	0.87	1.14	1.29	1.58	1.00*	–
0438-436	B	2	1.22	0.86	1.16	1.25	1.62	1.00*	–
0438-436	B	3	1.00*	1.00*	1.00*	1.00*	1.00*	1.00*	–
0438-436	J	1	0.93	1.01	0.93	0.97	2.09	3.19	–
0438-436	J	2	0.92	1.01	0.96	0.97	1.86	3.47	–
0454-463	J	1	1.07	1.04	0.98	1.07	4.20	4.20	–
0454-463	J	2	1.09	1.03	1.04	1.06	4.37	4.17	–
0506-612	D	1	0.95	1.04	1.11	1.23	1.47	1.00*	–
0506-612	D	2	0.94	1.04	1.15	1.19	1.38	1.00*	–
0506-612	G	1	0.94	1.29	0.90	1.03	2.16	–	1.00*
0506-612	G	2	0.98	1.31	0.95	1.04	1.94	–	1.00*

Continued on the next page

Source name	*Epoch*	IF	Parkes	ATCA	Mopra	Hobart	Ceduna	DSS43	Hartebeesthoek
0516-621	Q	1	1.00	0.96	1.08	1.12	1.84	–	–
0516-621	Q	2	1.01	0.96	1.07	1.14	1.78	–	–
0518-458	J	1	0.96	1.00	0.93	0.96	1.46	1.80	–
0518-458	J	2	0.97	1.00	0.96	0.97	1.45	1.80	–
0521-365	D	1	1.10	1.13	1.10	1.09	1.29	1.00*	–
0521-365	D	2	1.10	1.14	1.13	1.09	1.29	1.00*	–
0521-365	G	1	1.03	1.48	0.90	1.10	2.04	–	17.66
0521-365	G	2	1.06	1.38	0.91	1.10	2.10	–	13.23
0537-441	D	1	1.04	1.15	1.07	1.18	1.12	1.00*	–
0537-441	D	2	1.04	1.15	1.09	1.18	1.15	1.00*	–
0537-441	G	1	1.16	1.97	1.32	0.91	2.77	–	13.23
0537-441	G	2	1.30	1.95	1.48	0.85	2.46	–	12.97
0537-441	Q	1	0.98	0.97	1.05	1.17	2.56	–	–
0537-441	Q	2	0.97	0.98	1.05	1.16	2.58	–	–
0625-354	B	1	1.19	0.85	1.01	1.20	1.37	1.00*	–
0625-354	B	2	1.18	0.79	1.02	1.29	1.37	1.00*	–
0625-354	B	3	1.00*	1.00*	1.00*	1.00*	1.00*	1.00*	–
0625-354	J	1	0.94	1.07	0.82	1.26	1.88	1.67	–
0625-354	J	2	0.93	1.08	0.86	1.26	1.88	1.67	–
0637-752	B	1	1.07	0.99	1.00	1.07	1.39	1.00*	–
0637-752	B	2	1.07	0.99	1.01	1.06	1.43	1.00*	–
0637-752	B	3	1.00*	1.00*	1.00*	1.00*	1.00*	1.00*	–
0637-752	D	1	0.94	1.02	1.28	1.10	1.45	1.00*	–
0637-752	D	2	0.96	1.01	1.33	1.08	1.38	1.00*	–
0637-752	G	1	1.00	1.06	1.06	1.06	0.87	–	14.46
0637-752	G	2	1.00	1.06	1.09	1.06	0.87	–	10.10
1104-445	B	1	1.11	1.18	0.95	1.16	2.13	1.00*	–
1104-445	B	2	1.12	1.16	0.92	1.17	1.89	1.00*	–
1104-445	B	3	1.00*	1.00*	1.00*	1.00*	1.00*	1.00*	–
1104-445	J	1	0.96	0.94	0.93	1.01	1.27	1.56	–
1104-445	J	2	0.94	0.94	0.99	1.01	1.27	1.59	–
1144-379	B	1	1.01	1.04	1.03	0.94	1.10	1.00*	–
1144-379	B	2	1.01	1.04	1.03	0.96	1.25	1.00*	–
1144-379	B	3	1.00*	1.00*	1.00*	1.00*	1.00*	1.00*	–
1144-379	D	1	1.15	0.93	1.00	1.17	1.41	1.00*	–
1144-379	D	2	1.09	0.96	1.01	1.13	1.26	1.00*	–

Continued on the next page

Source name	*Epoch*	IF	Parkes	ATCA	Mopra	Hobart	Ceduna	DSS43	Hartebeesthoek
1144-379	G	1	0.89	2.34	0.92	0.61	1.86	–	1.00*
1144-379	G	2	0.90	2.34	0.94	0.61	2.00	–	1.00*
1257-326	B	1	1.00*	1.00*	1.00*	1.00*	1.00*	1.00*	–
1257-326	B	2	1.00*	1.00*	1.00*	1.00*	1.00*	1.00*	–
1257-326	B	3	1.00*	1.00*	1.00*	1.00*	1.00*	1.00*	–
1257-326	J	1	0.89	1.04	0.99	1.06	1.00*	1.77	–
1257-326	J	2	0.88	1.03	0.95	1.11	1.00*	2.44	–
1313-333	B	1	1.04	1.14	1.07	0.99	1.27	1.00*	–
1313-333	B	2	1.03	1.15	1.07	0.97	1.35	1.00*	–
1313-333	B	3	1.00*	1.00*	1.00*	1.00*	1.00*	1.00*	–
1313-333	D	1	1.07	1.03	0.99	1.10	1.35	1.00*	–
1313-333	D	2	1.06	1.04	1.01	1.06	1.14	1.00*	–
1313-333	G	1	0.99	1.91	1.05	0.90	1.64	–	16.56
1313-333	G	2	1.00	1.93	1.08	0.90	1.56	–	15.38
1322-428	J	1	1.04	1.14	0.98	1.17	1.65	2.56	–
1322-428	J	2	1.02	1.16	1.02	1.18	1.64	2.59	–
1323-526	B	1	1.18	1.05	0.99	0.90	2.63	1.00*	–
1323-526	B	2	1.18	1.08	1.00	0.89	3.57	1.00*	–
1323-526	B	3	1.00*	1.00*	1.00*	1.00*	1.00*	1.00*	–
1323-526	D	1	1.01	1.03	1.01	0.92	1.82	1.00*	–
1323-526	D	2	0.99	1.04	1.04	0.93	1.62	1.00*	–
1323-526	G	1	1.05	1.17	1.05	0.91	1.82	–	1.00*
1323-526	G	2	1.04	1.22	1.10	0.92	1.95	–	1.00*
1333-337	B	1	1.09	1.11	0.99	1.16	1.00*	1.00*	–
1333-337	B	2	1.07	1.09	1.03	0.98	4.14	1.00*	–
1333-337	B	3	1.00*	1.00*	1.00*	1.00*	1.00*	1.00*	–
1333-337	J	1	0.91	1.06	0.88	0.91	2.02	1.58	–
1333-337	J	2	0.92	1.07	0.92	0.90	1.68	1.52	–
1424-418	D	1	1.05	1.00	0.97	1.08	1.62	1.00*	–
1424-418	D	2	1.05	1.01	0.98	1.09	1.43	1.00*	–
1424-418	G	1	0.94	1.44	0.97	1.05	2.64	–	1.00*
1424-418	G	2	0.94	1.44	1.01	1.07	2.68	–	1.00*
1454-354	J	1	0.97	0.99	0.85	0.86	1.66	2.08	–
1454-354	J	2	0.98	1.00	0.88	0.85	1.64	2.09	–
1501-343	D	1	0.92	1.23	1.01	1.30	1.00*	1.00*	–
1501-343	D	2	1.00*	1.00*	1.00*	1.00*	1.00*	1.00*	–

Continued on the next page

Source name	*Epoch*	IF	Parkes	ATCA	Mopra	Hobart	Ceduna	DSS43	Hartebeesthoek
1501-343	G	1	0.99	1.12	1.02	0.83	1.69	–	1.00*
1501-343	G	2	0.99	1.10	1.04	0.87	1.56	–	1.00*
1549-790	B	1	1.11	1.09	1.15	1.07	1.94	1.00*	–
1549-790	B	2	1.11	1.11	1.14	1.09	2.27	1.00*	–
1549-790	B	3	1.00*	1.00*	1.00*	1.00*	1.00*	1.00*	–
1549-790	J	1	0.89	1.14	0.86	1.16	1.12	2.12	–
1549-790	J	2	0.97	1.14	0.92	1.20	1.14	1.87	–
1600-489	Q	1	1.11	1.03	1.17	0.99	2.61	–	–
1600-489	Q	2	1.11	1.02	1.17	0.98	4.85	–	–
1600-445	Q	1	1.01	0.93	1.12	1.13	2.67	–	–
1600-445	Q	2	1.01	0.94	1.12	1.13	2.95	–	–
1610-771	B	1	1.32	1.07	1.35	1.56	1.54	1.00*	–
1610-771	B	2	1.30	1.09	1.32	1.60	1.56	1.00*	–
1610-771	B	3	1.00*	1.00*	1.00*	1.00*	1.00*	1.00*	–
1610-771	D	1	1.08	1.25	0.91	1.44	1.72	1.00*	–
1610-771	D	2	1.08	1.30	0.94	1.41	1.74	1.00*	–
1610-771	G	1	1.04	1.00	1.00	1.28	1.58	–	1.00*
1610-771	G	2	1.05	0.99	1.03	1.28	1.59	–	1.00*
1714-336	J	1	1.11	1.41	1.04	1.05	1.77	1.76	–
1714-336	J	2	1.09	1.38	1.09	1.02	1.63	1.72	–
1716-771	D	1	1.34	1.07	1.08	1.07	1.82	1.00*	–
1716-771	D	2	1.37	1.14	1.05	1.07	2.26	1.00*	–
1716-771	G	1	1.04	1.03	1.08	1.02	2.31	–	1.00*
1716-771	G	2	1.03	1.03	1.12	1.00	2.12	–	1.00*
1718-649	B	1	1.05	1.23	1.01	1.18	1.42	1.00*	–
1718-649	B	2	1.09	1.22	1.03	1.21	1.43	1.00*	–
1718-649	B	3	1.00*	1.00*	1.00*	1.00*	1.00*	1.00*	–
1718-649	J	1	0.96	1.00	0.95	0.98	2.01	2.13	–
1718-649	J	2	0.96	1.00	1.00	1.00	1.82	2.55	–
1733-565	B	1	1.26	1.08	1.14	0.87	1.93	1.00*	–
1733-565	B	2	1.22	1.15	1.25	0.70	1.79	1.00*	–
1733-565	B	3	1.00*	1.00*	1.00*	1.00*	1.00*	1.00*	–
1733-565	D	1	1.27	1.00	1.34	0.96	1.62	1.00*	–
1733-565	D	2	1.16	1.00	1.14	1.06	1.88	1.00*	–
1733-565	G	1	1.03	0.97	1.06	0.91	1.99	–	1.00*
1733-565	G	2	1.07	0.98	1.06	0.86	2.35	–	1.00*

Continued on the next page

Source name	*Epoch*	IF	Parkes	ATCA	Mopra	Hobart	Ceduna	DSS43	Hartebeesthoek
1759-396	J	1	1.65	1.22	1.24	0.90	1.38	3.37	–
1759-396	J	2	1.70	1.22	1.31	0.84	1.31	2.89	–
1804-502	D	1	1.17	1.04	1.03	1.01	2.10	1.00*	–
1804-502	D	2	1.16	1.06	1.04	1.02	2.86	1.00*	–
1804-502	G	1	1.04	1.06	1.06	0.89	2.76	–	1.00*
1804-502	G	2	1.05	1.06	1.09	0.89	2.49	–	1.00*
1814-637	B	1	0.95	1.08	1.21	1.88	1.00*	1.00*	–
1814-637	B	2	0.92	1.15	1.09	1.31	1.00*	1.00*	–
1814-637	B	3	1.00*	1.00*	1.00*	1.00*	1.00*	1.00*	–
1814-637	J	1	0.98	1.15	1.02	1.10	1.00*	1.00*	–
1814-637	J	2	1.05	1.13	1.13	1.10	1.00*	1.00*	–
1933-400	D	1	1.31	0.89	1.03	1.29	1.80	1.00*	–
1933-400	D	2	1.31	0.88	1.05	1.25	1.63	1.00*	–
1933-400	G	1	1.02	1.03	1.05	1.01	1.99	–	16.48
1933-400	G	2	1.02	1.03	1.08	1.01	1.81	–	16.23
1934-638	B	1	1.00*	1.00*	1.00*	1.00*	1.00*	1.00*	–
1934-638	B	2	1.00*	1.00*	1.00*	1.00*	1.00*	1.00*	–
1934-638	B	3	1.00*	1.00*	1.00*	1.00*	1.00*	1.00*	–
1934-638	D	1	1.00*	1.00*	1.00*	1.00*	1.00*	1.00*	–
1934-638	D	2	1.00*	1.00*	1.00*	1.00*	1.00*	1.00*	–
1934-638	G	1	1.08	1.02	0.99	1.53	1.00*	–	1.00*
1934-638	G	2	1.08	1.03	1.01	1.45	1.00*	–	1.00*
1934-638	J	1	1.00*	1.00*	1.00*	1.00*	1.00*	1.00*	–
1934-638	J	2	1.12	1.05	0.96	0.95	1.00*	1.00*	–
1954-388	B	1	1.03	1.03	1.16	0.77	2.03	1.00*	–
1954-388	B	2	1.02	1.03	1.17	0.76	2.23	1.00*	–
1954-388	B	3	1.00*	1.00*	1.00*	1.00*	1.00*	1.00*	–
1954-388	J	1	0.89	1.19	0.88	0.86	1.16	5.08	–
1954-388	J	2	0.89	1.19	0.91	0.87	1.09	4.57	–
2005-489	D	1	1.47	0.97	1.12	1.07	2.70	1.00*	–
2005-489	D	2	1.52	0.99	1.08	1.08	2.02	1.00*	–
2005-489	G	1	1.07	1.07	0.98	0.97	1.58	–	1.00*
2005-489	G	2	1.07	1.05	1.01	0.99	1.39	–	1.00*
2052-474	B	1	1.21	1.26	1.20	0.63	1.61	1.00*	–
2052-474	B	2	1.20	1.24	1.18	0.65	1.67	1.00*	–
2052-474	B	3	1.00*	1.00*	1.00*	1.00*	1.00*	1.00*	–

Continued on the next page

Source name	*Epoch*	IF	Parkes	ATCA	Mopra	Hobart	Ceduna	DSS43	Hartebeesthoek
2052-474	D	1	1.07	1.17	1.17	0.97	1.64	1.00*	–
2052-474	D	2	1.05	1.20	1.24	0.96	1.55	1.00*	–
2052-474	G	1	0.96	1.17	1.14	0.89	3.17	–	15.23
2052-474	G	2	0.96	1.17	1.17	0.89	2.95	–	19.77
2106-413	B	1	1.17	1.12	1.15	0.67	2.01	1.00*	–
2106-413	B	2	1.17	1.12	1.14	0.66	1.89	1.00*	–
2106-413	B	3	1.00*	1.00*	1.00*	1.00*	1.00*	1.00*	–
2106-413	J	1	0.96	1.22	0.82	0.78	1.53	3.92	–
2106-413	J	2	0.95	1.22	0.87	0.77	1.85	4.12	–
2149-306	D	1	1.12	1.18	0.93	1.00	1.58	1.00*	–
2149-306	D	2	1.12	1.17	0.94	0.98	1.45	1.00*	–
2149-306	G	1	1.03	1.06	1.03	1.01	2.60	–	16.60
2149-306	G	2	1.03	1.06	1.06	1.01	2.59	–	15.05
2152-699	B	1	1.02	1.13	1.25	0.89	1.66	1.00*	–
2152-699	B	2	1.03	1.25	1.12	0.86	1.69	1.00*	–
2152-699	B	3	1.00*	1.00*	1.00*	1.00*	1.00*	1.00*	–
2152-699	J	1	1.15	0.97	0.77	0.93	1.78	2.22	–
2152-699	J	2	1.09	1.03	0.76	0.96	1.74	2.46	–
2155-304	D	1	0.97	1.22	0.91	0.99	2.31	1.00*	–
2155-304	D	2	0.99	1.23	0.95	0.98	2.48	1.00*	–
2155-304	G	1	0.96	0.94	0.95	0.86	2.58	–	1.00*
2155-304	G	2	0.96	0.95	0.98	0.87	2.45	–	1.00*
2155-304	Q	1	1.10	0.96	1.03	1.16	2.02	–	–
2155-304	Q	2	1.12	0.97	1.02	1.14	2.69	–	–
2204-540	B	1	1.11	1.05	1.18	0.92	1.22	1.00*	–
2204-540	B	2	1.11	1.07	1.16	0.91	1.21	1.00*	–
2204-540	B	3	1.00*	1.00*	1.00*	1.00*	1.00*	1.00*	–
2204-540	J	1	1.12	1.16	0.88	0.98	2.01	9.28	–
2204-540	J	2	1.11	1.15	0.92	0.99	2.01	1.00*	–
2326-477	D	1	0.99	1.11	1.03	1.03	1.33	1.00*	–
2326-477	D	2	0.95	1.13	1.10	1.03	1.38	1.00*	–
2326-477	G	1	0.99	1.06	1.07	0.92	2.45	–	1.00*
2326-477	G	2	1.00	1.05	1.09	0.92	2.03	–	1.00*
2355-534	B	1	1.16	1.04	1.16	0.92	1.10	1.00*	–
2355-534	B	2	1.17	1.04	1.18	0.91	1.10	1.00*	–
2355-534	B	3	1.00*	1.00*	1.00*	1.00*	1.00*	1.00*	–

Continued on the next page

Source name	*Epoch*	IF	Parkes	ATCA	Mopra	Hobart	Ceduna	DSS43	Hartebeesthoek
2355-534	J	1	0.87	1.15	1.07	0.97	1.63	2.26	–
2355-534	J	2	0.90	1.08	1.15	0.97	1.62	2.12	–

Table A.2.: Gain correction factors from amplitude self-calibration for each telescope in the K-band (22.3GHz) for each sources' observation. Values with asteriks indicate dismissed data, wherefore no gain correction is given. See section 3.1 for further explanation.

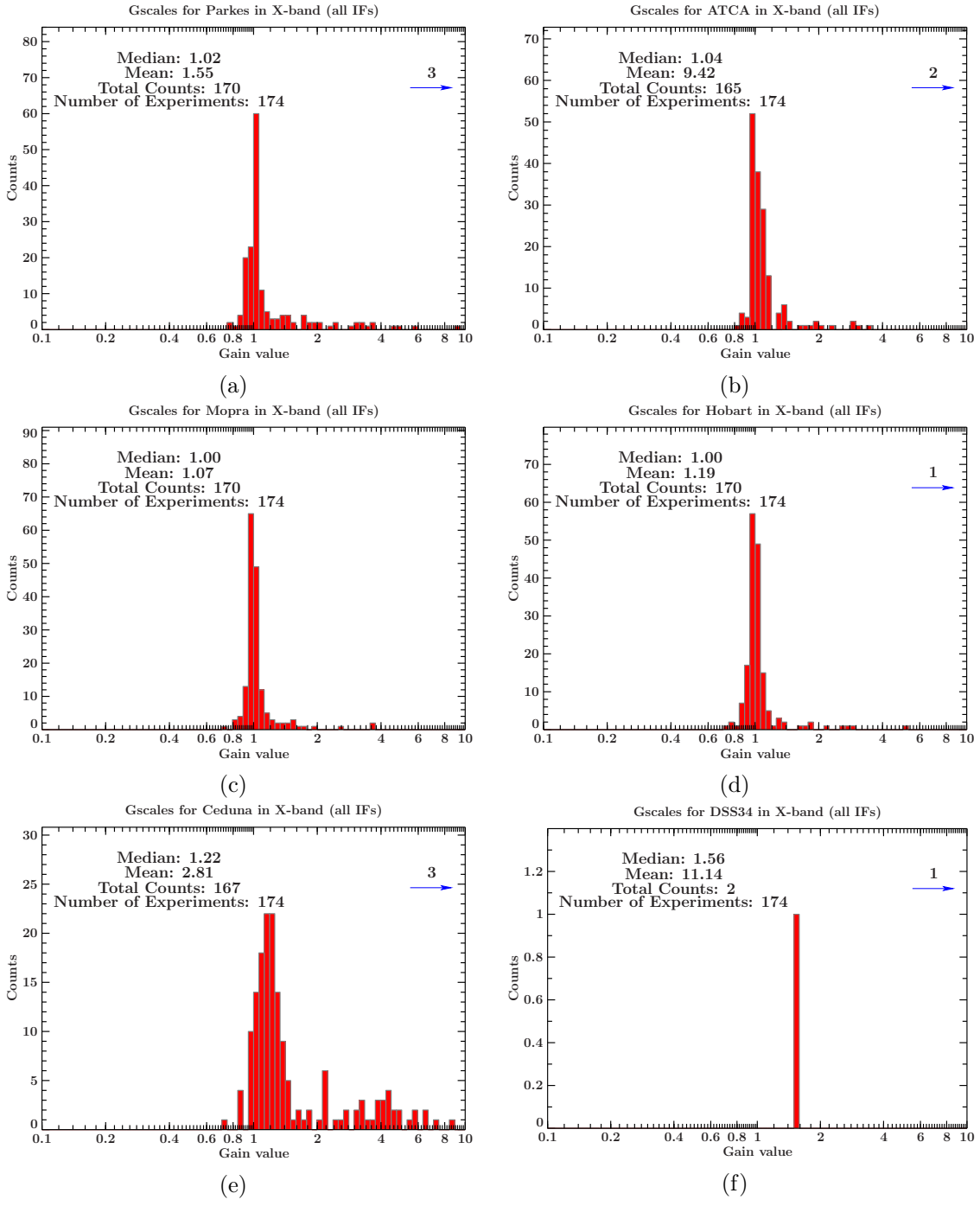

Figure A.1.: The gain value distribution as histogram for the telescope Parkes (A.1a), ATCA (A.1b), Mopra (A.1c), Hobart (A.1d), Ceduna (A.1e) and DSS34 (A.1f) in the X-band.

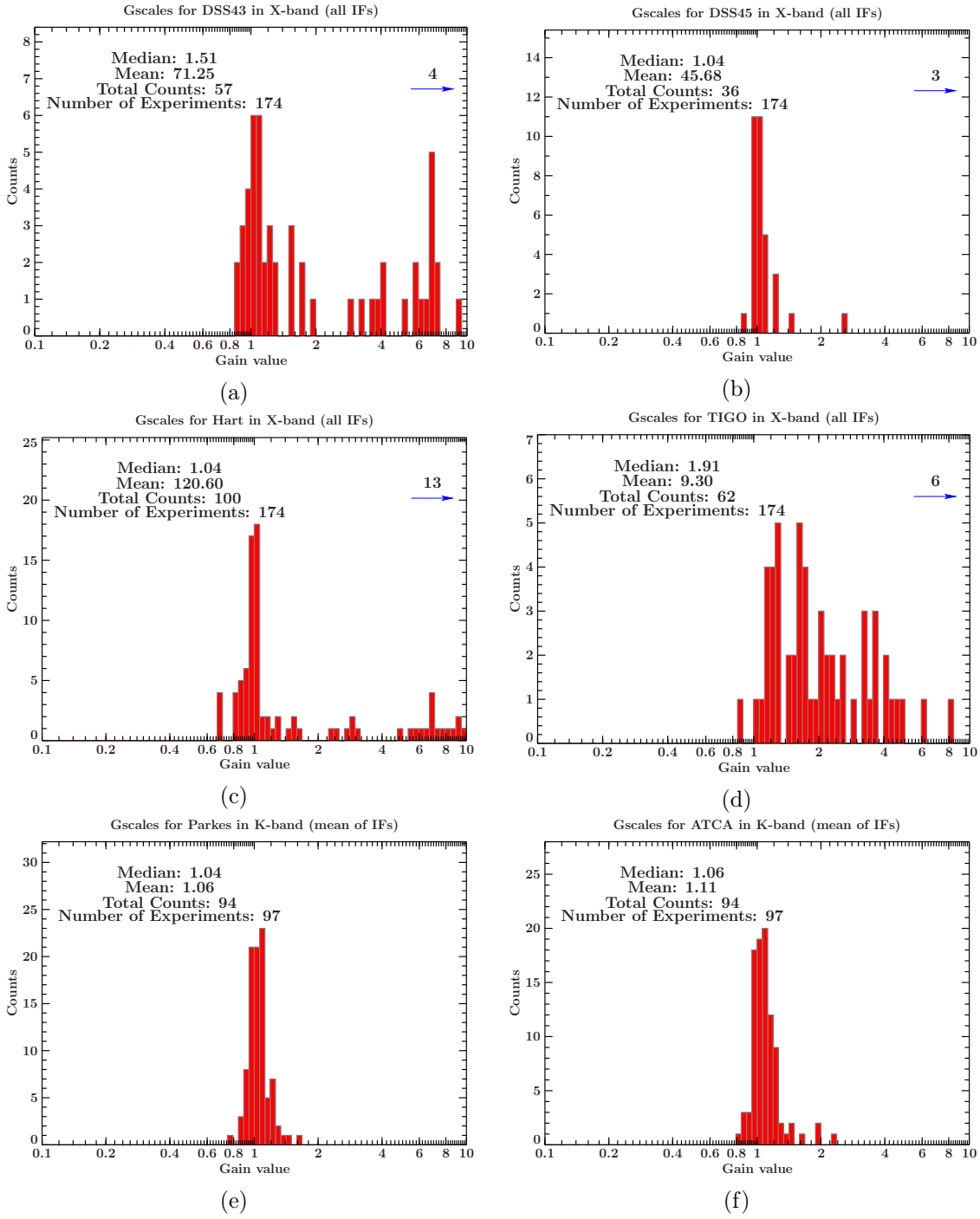

Figure A.2.: The gain value distribution as histogram for the telescope DSS43 (A.2a), DSS45 (A.2b), Hartebeesthoek (A.2c) and TIGO (A.2d) in the X-band, followed by Parkes (A.2e) and ATCA (A.2f) in the K-band.

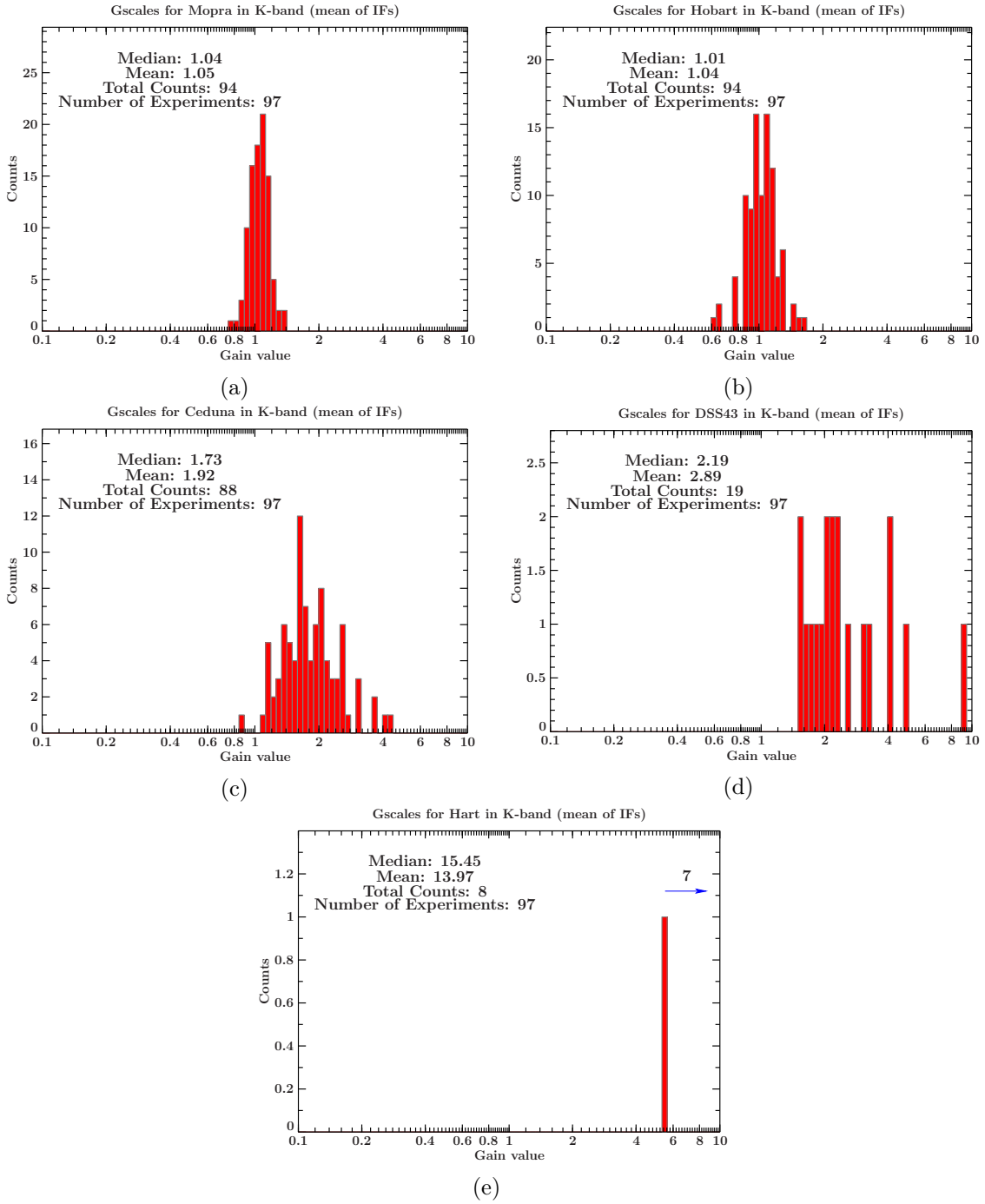

Figure A.3.: The gain value distribution as histogram for the telescope Mopra (A.3a), Hobart (A.3b), Ceduna (A.3c), DSS43 (A.3d) and Hartebeesthoek (A.3e) in the K-band.

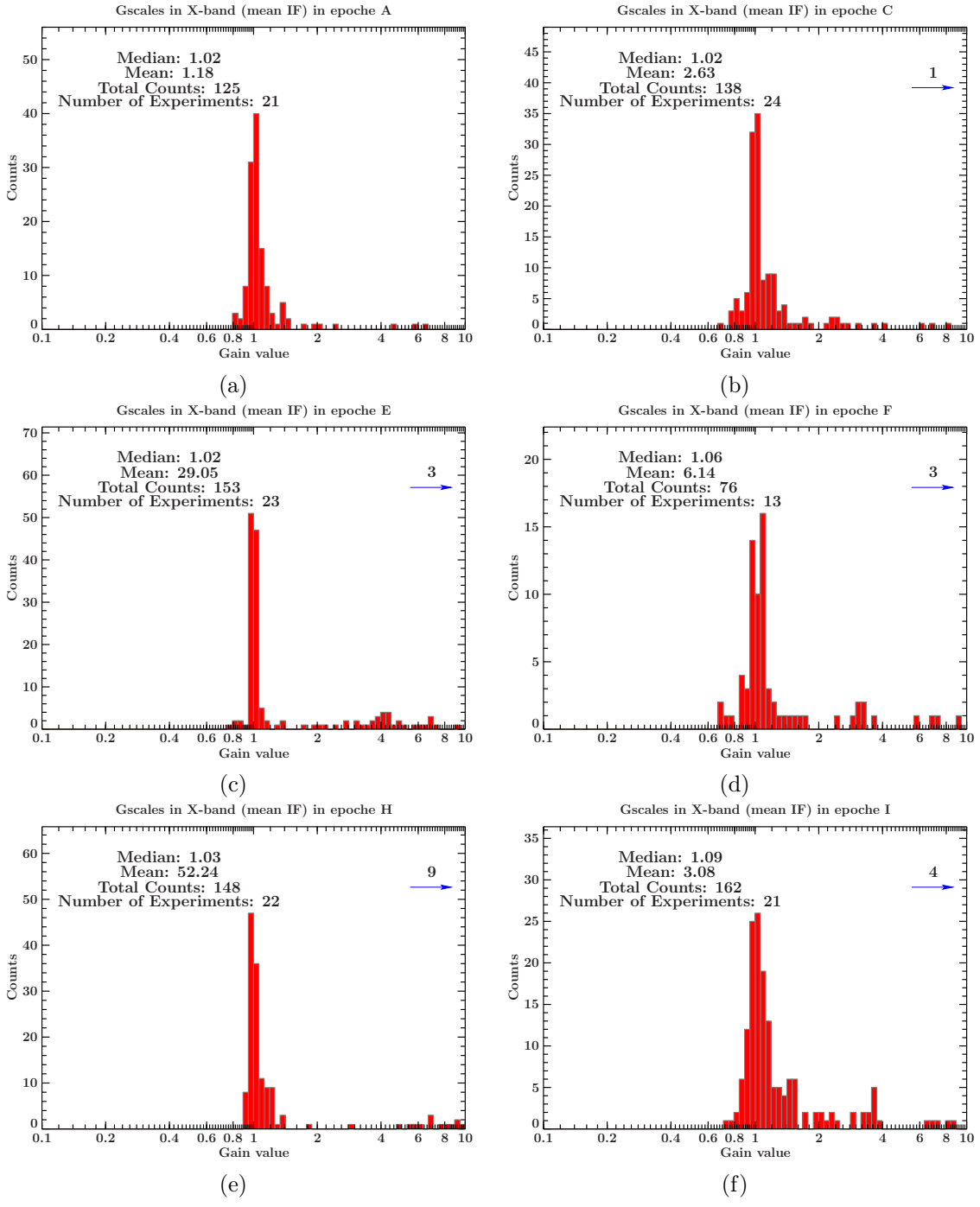

Figure A.4.: The gain value distribution as histogram for the observation cycles A (A.4a), C (A.4b), E (A.4c), F (A.4d), H (A.4e) and I (A.4f) (X-band).

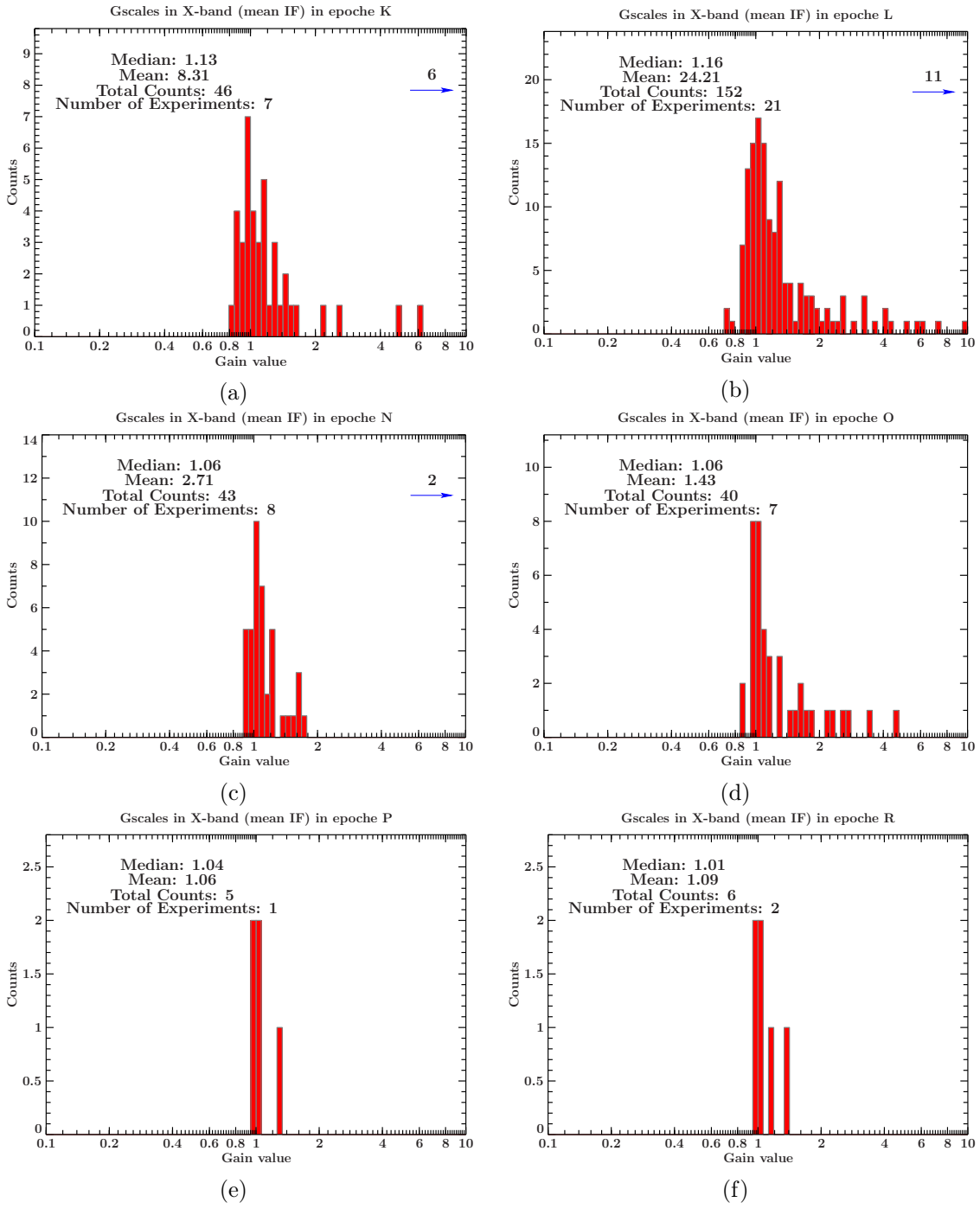

Figure A.5.: The gain value distribution as histogram for the observation cycles K (A.5a), L (A.5b), N (A.5c), O (A.5d), P (A.5e) and R (A.5f) (X-band).

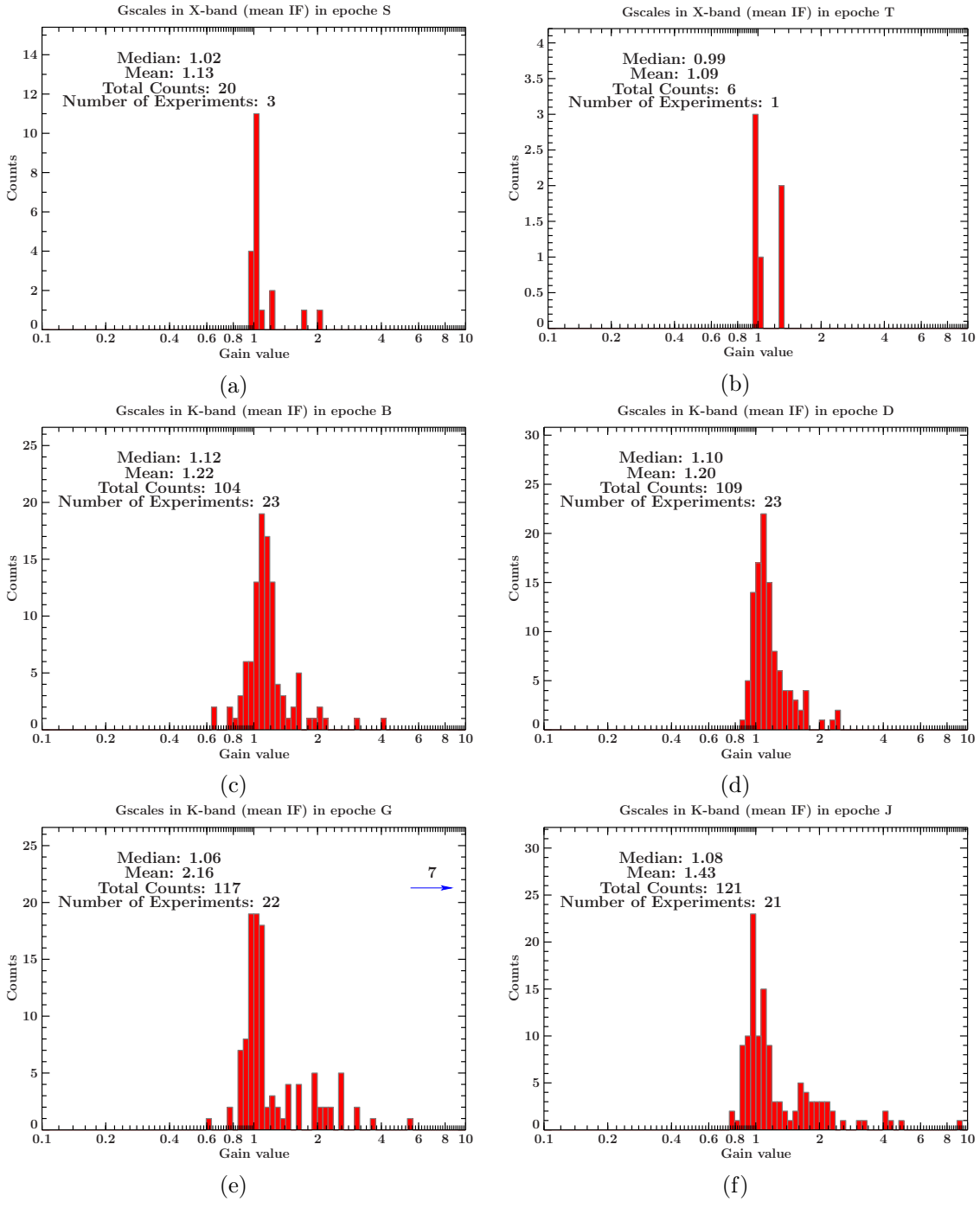

Figure A.6.: The gain value distribution as histogram for the observation cycles S (A.6a) and T (A.6b)(X-band), followed by B (A.6c), D (A.6d), G (A.6e) and J (A.6f) (K-band).

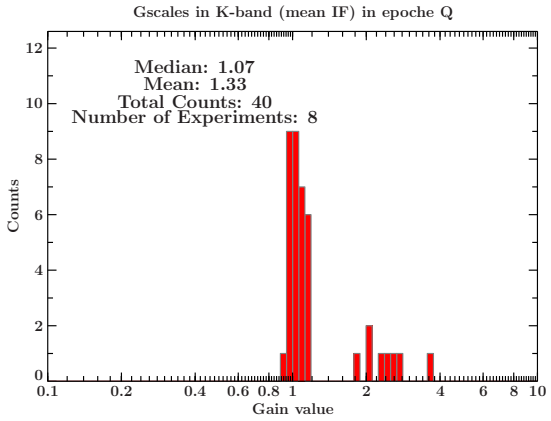

(a)

Figure A.7.: The gain value distribution as histogram for the observation cycle Q (A.7a) (K-band).

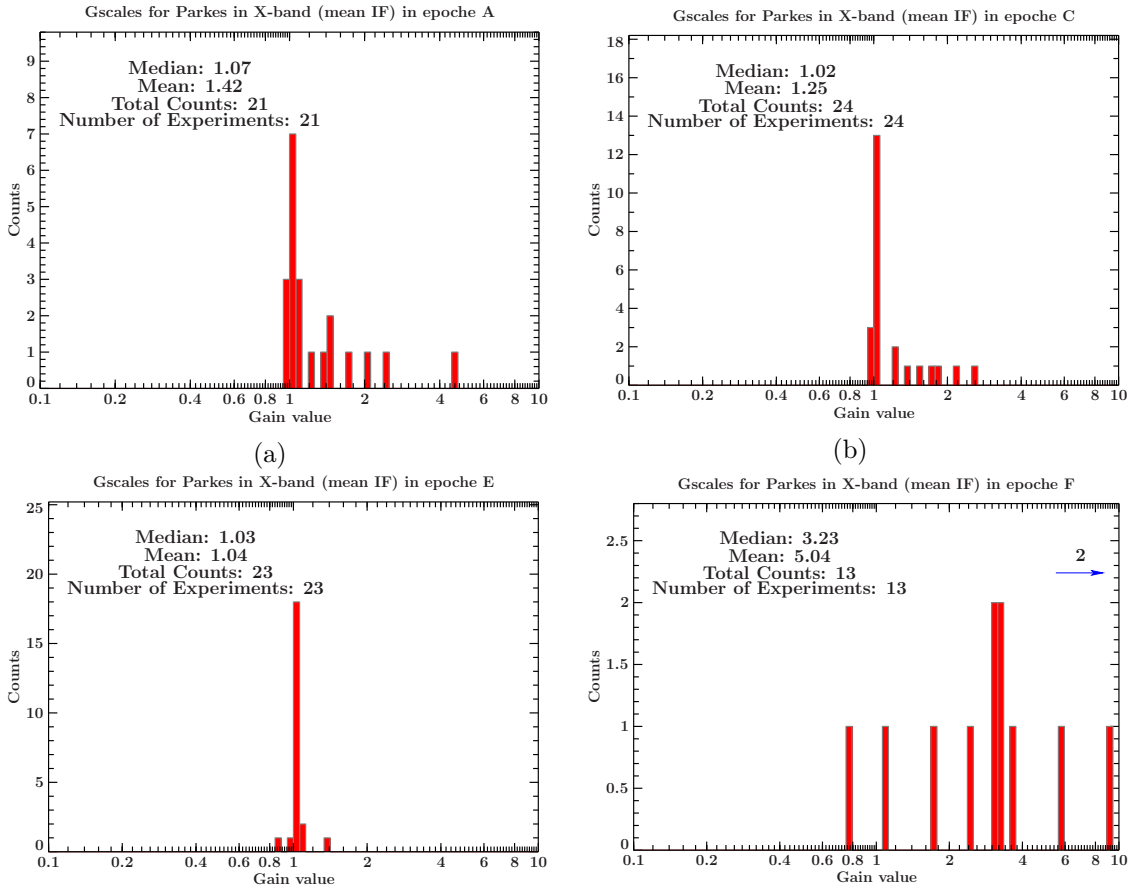

(a) (b) (c) (d)

Figure A.8.: The gain value distribution as histogram for the Parkes telescope in the observation cycles A (A.8a), C (A.8b), E (A.8c) and F (A.8d) (X-band).

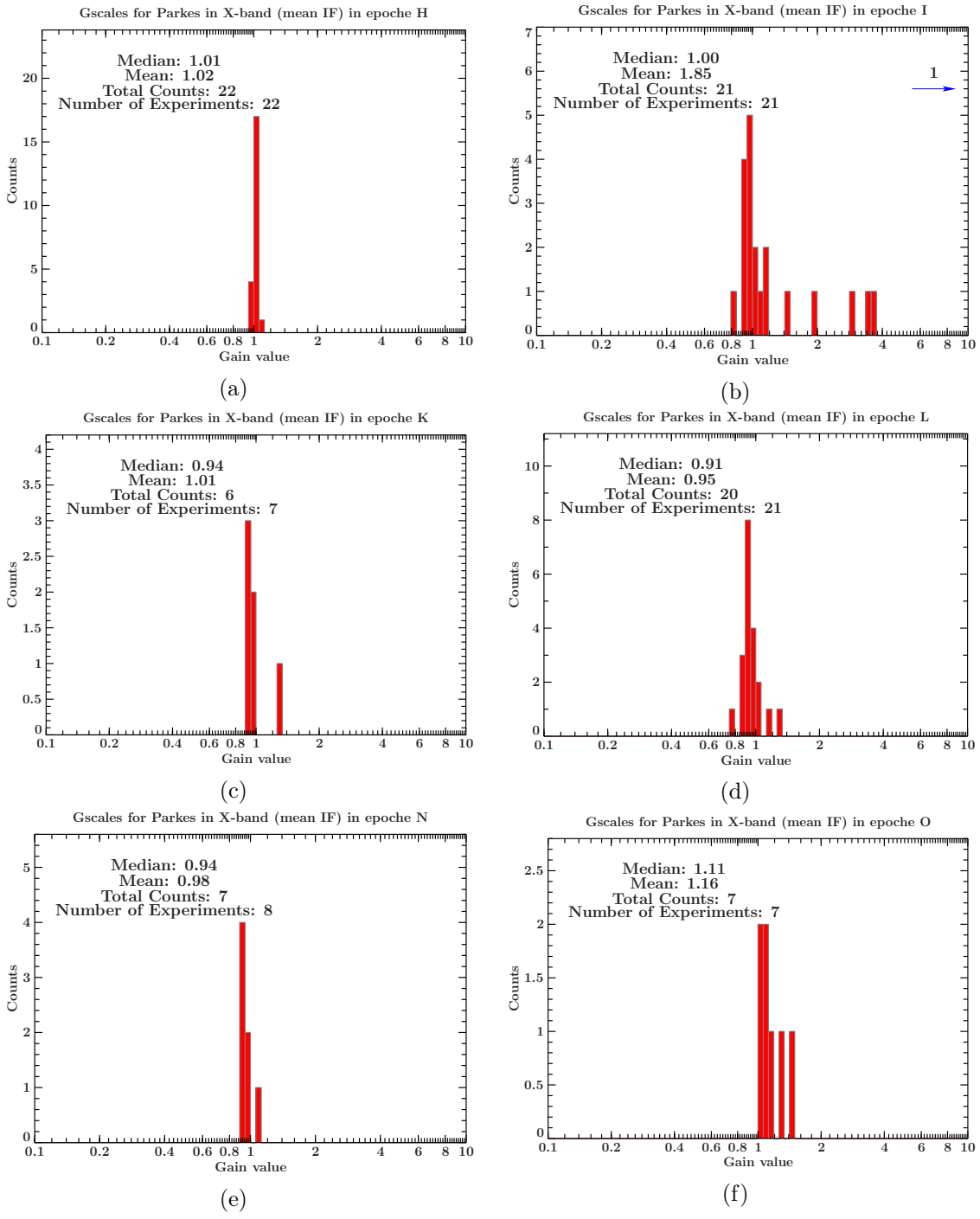

Figure A.9.: The gain value distribution as histogram for the Parkes telescope in the observation cycles H (A.9a), I (A.9b), K (A.9c), L (A.9d), N (A.9e) and O (A.9f) (X-band).

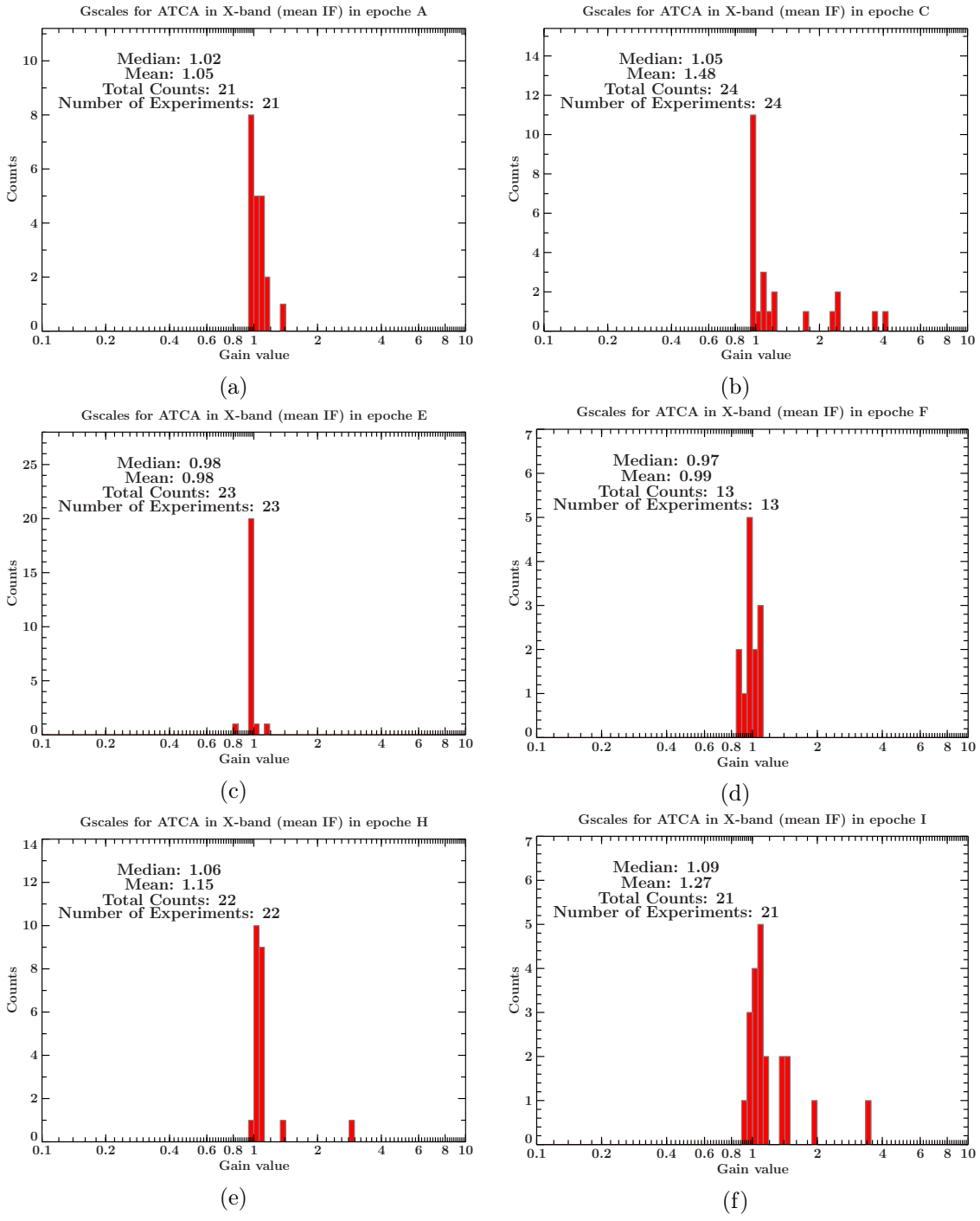

Figure A.10.: The gain value distribution as histogram for the ATCA telescope in the observation cycles A (A.10a), C (A.10b), E (A.10c), F (A.10d), H (A.10e) and I (A.10f) (X-band).

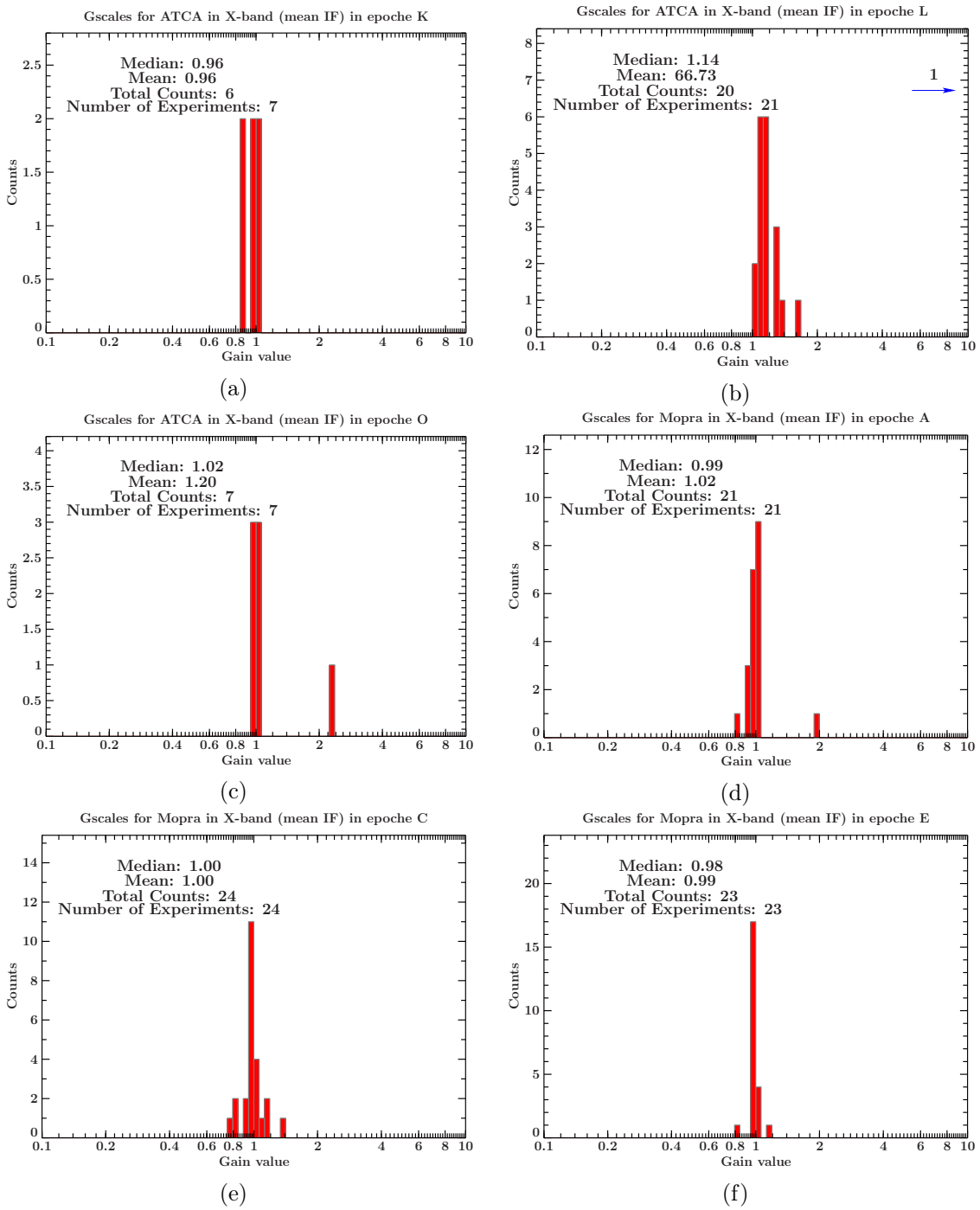

Figure A.11.: The gain value distribution as histogram for the ATCA telescope in the observation cycles K (A.11a), L (A.11b) and O (A.11c)(X-band), followed by the Mopra telescope in the cycles A (A.11d), C (A.11e) and E (A.11f) (X-band).

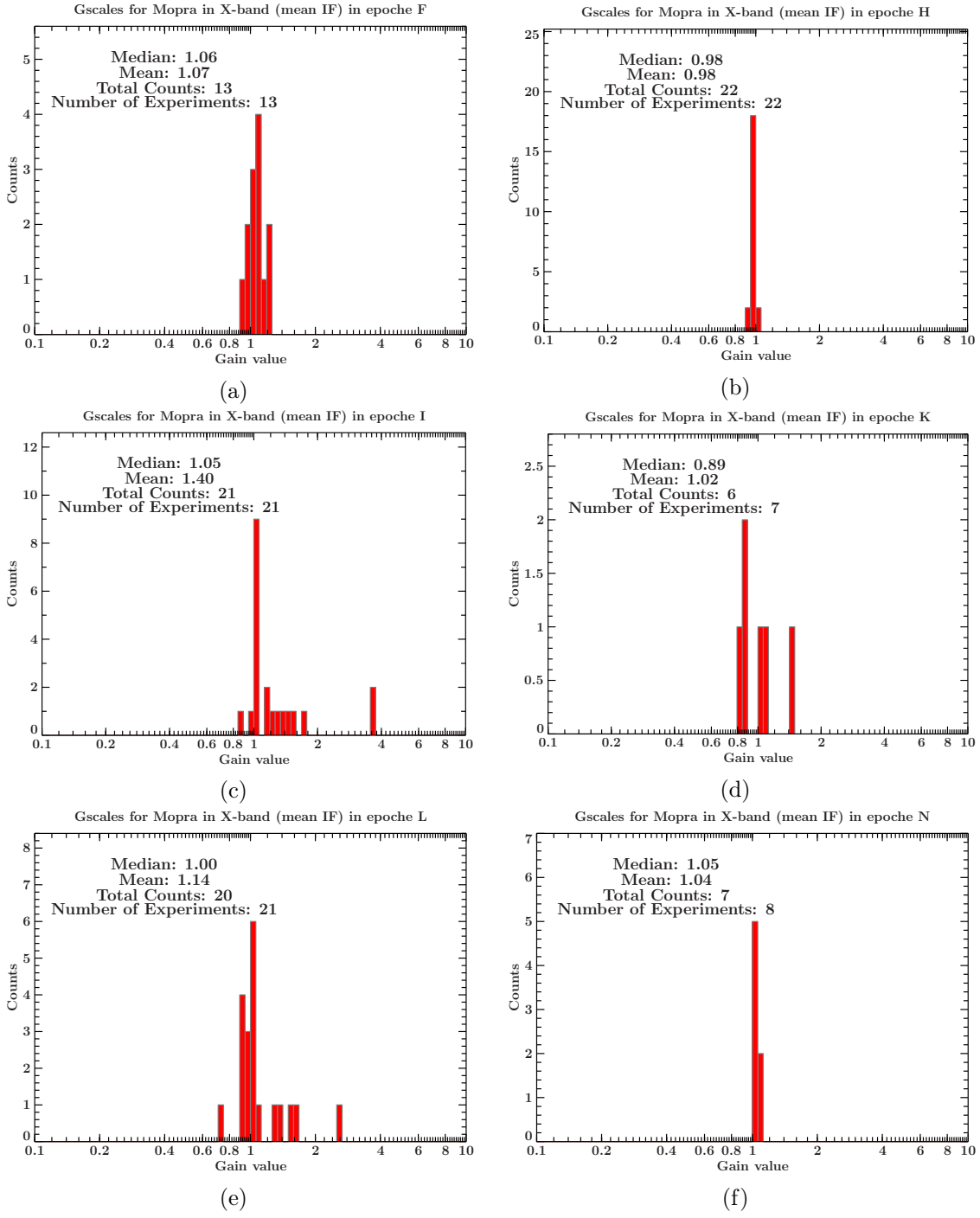

Figure A.12.: The gain value distribution as histogram for the Mopra telescope in the observation cycles F (A.12a), H (A.12b), I (A.12c), K (A.12d), L (A.12e) and N (A.12f) (X-band).

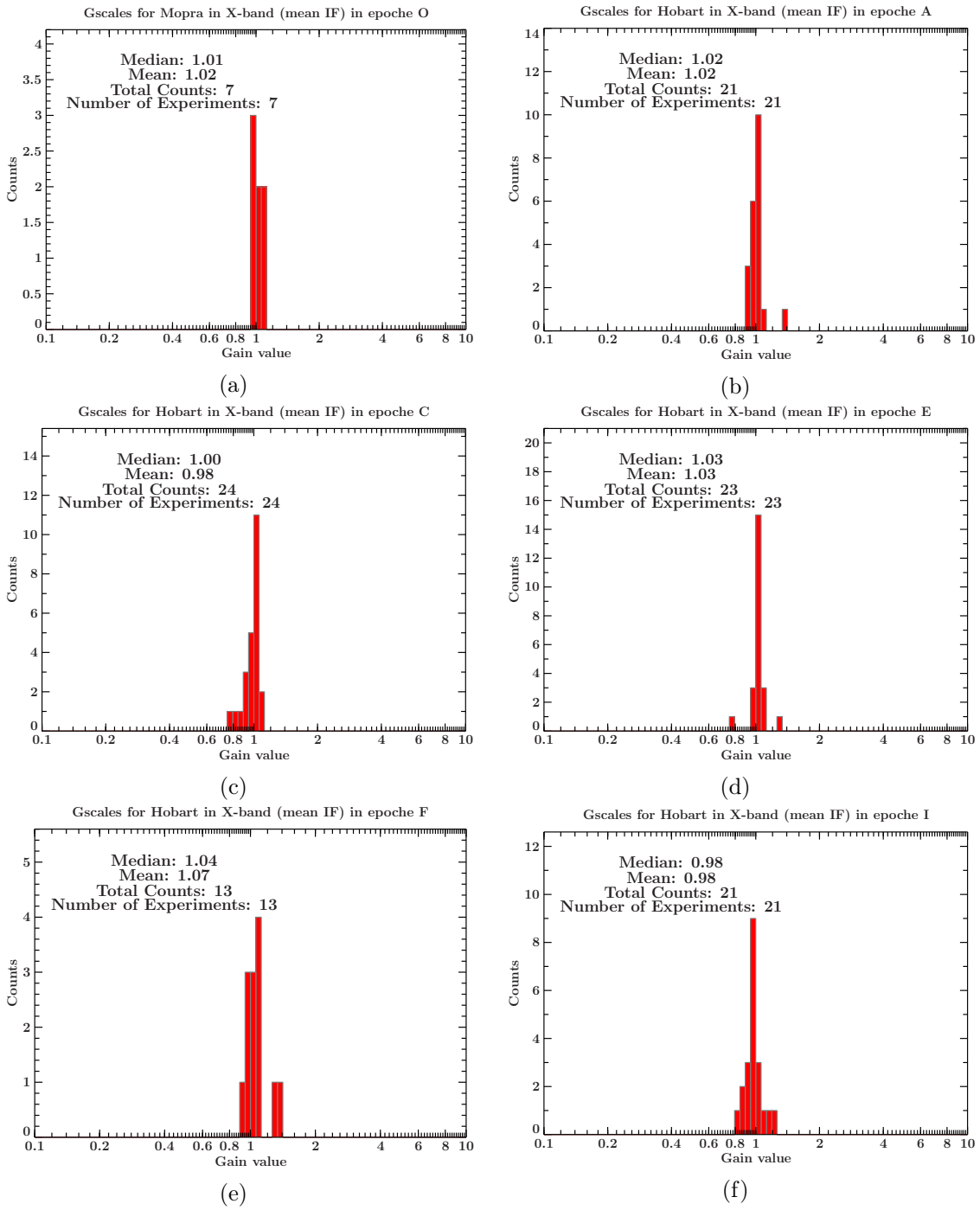

Figure A.13.: The gain value distribution as histogram for the Mopra telescope in the observation cycle O (A.13a) (X-band), followed by the Hobart telescope in the cycles A (A.13b), C (A.13c), E (A.13d), F (A.13e) and I (A.13f) (X-band).

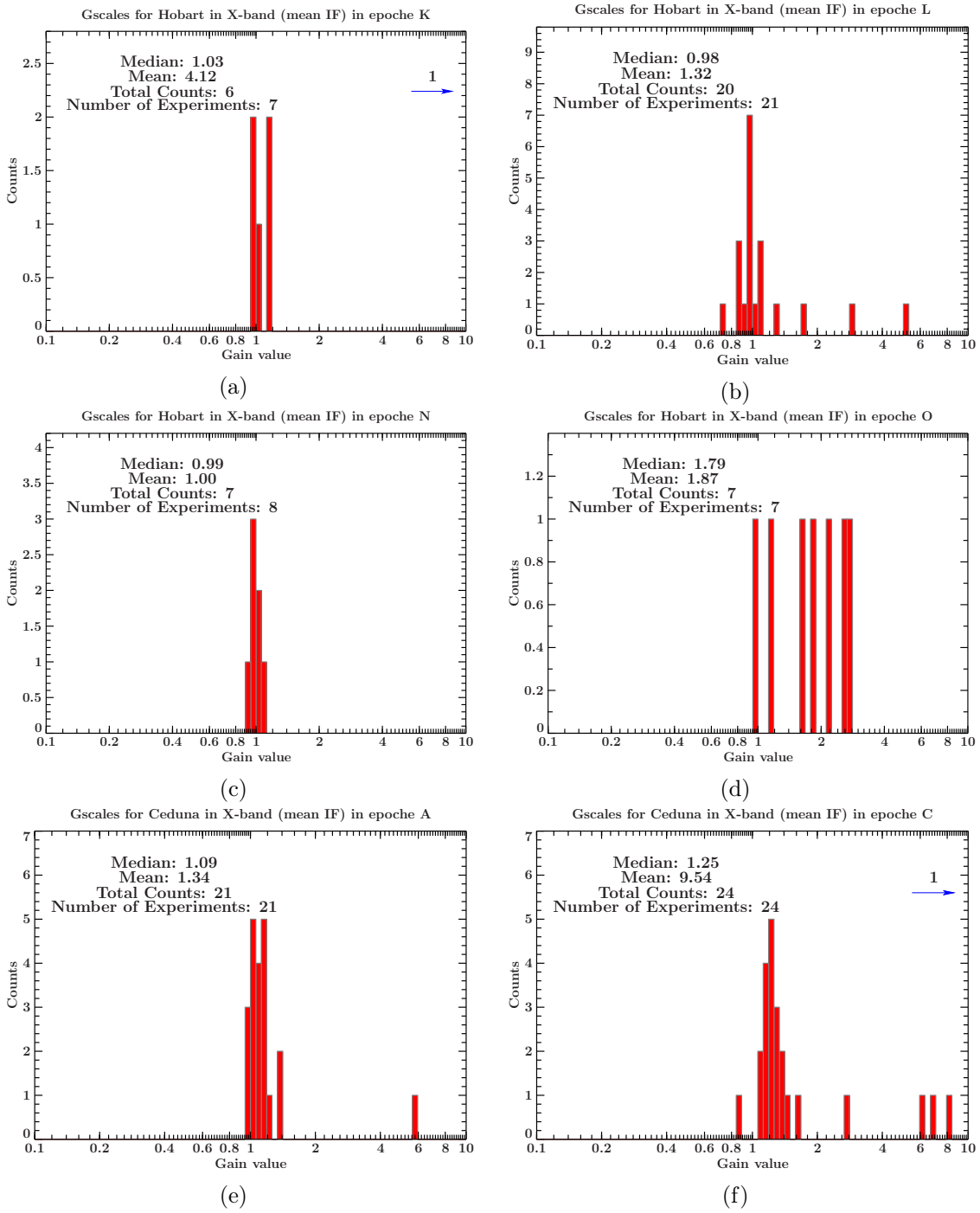

Figure A.14.: The gain value distribution as histogram for the Hobart telescope in the observation cycles K (A.14a), L (A.14b), N(A.14c) and O (A.14d)(X-band), followed by the Ceduna telescope in the cycles A (A.14e) and C (A.14f) (X-band).

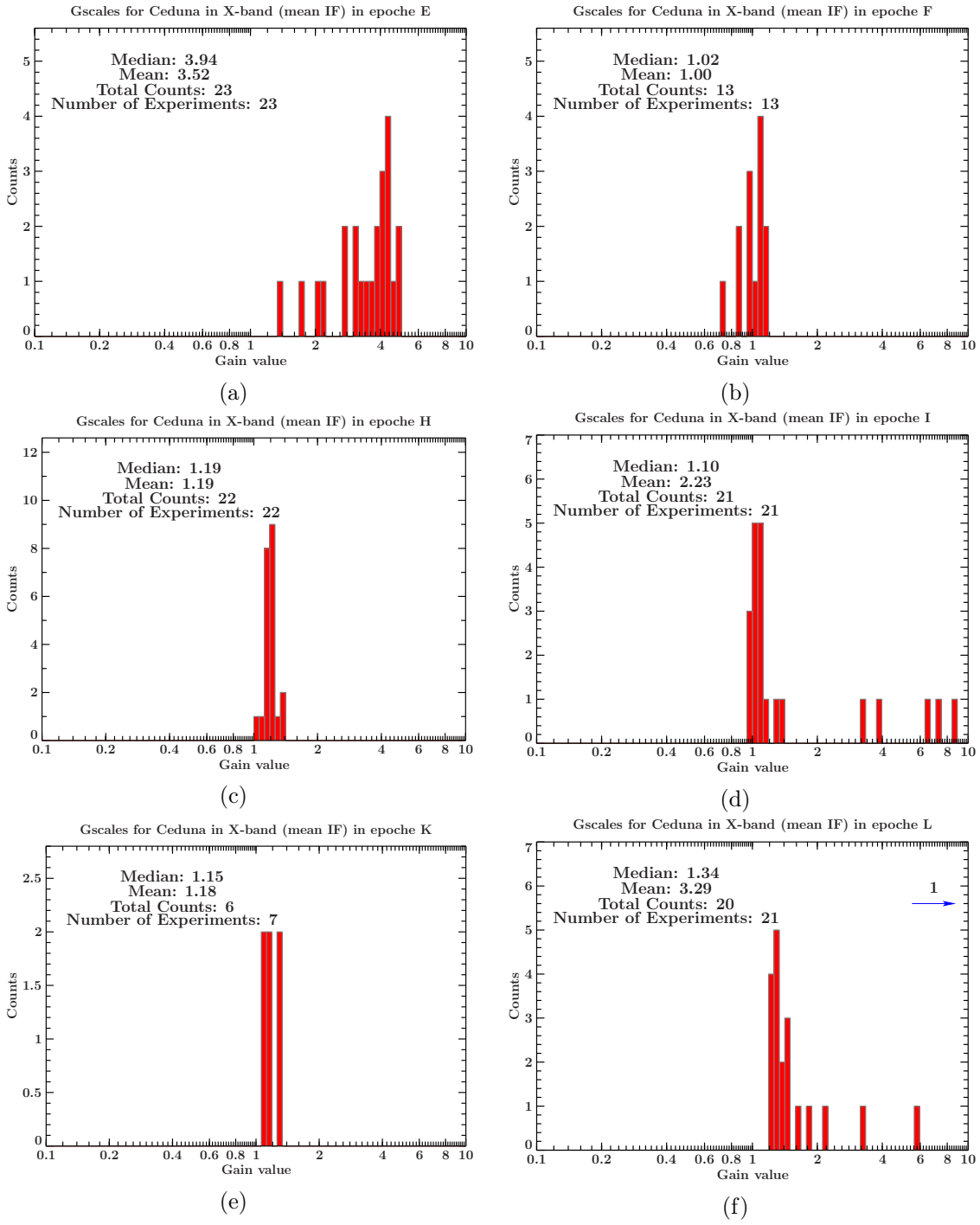

Figure A.15.: The gain value distribution as histogram for the Ceduna telescope in the observation cycles E (A.15a), F (A.15b), H (A.15c), I (A.15d), K (A.15e) and L (A.15f) (X-band).

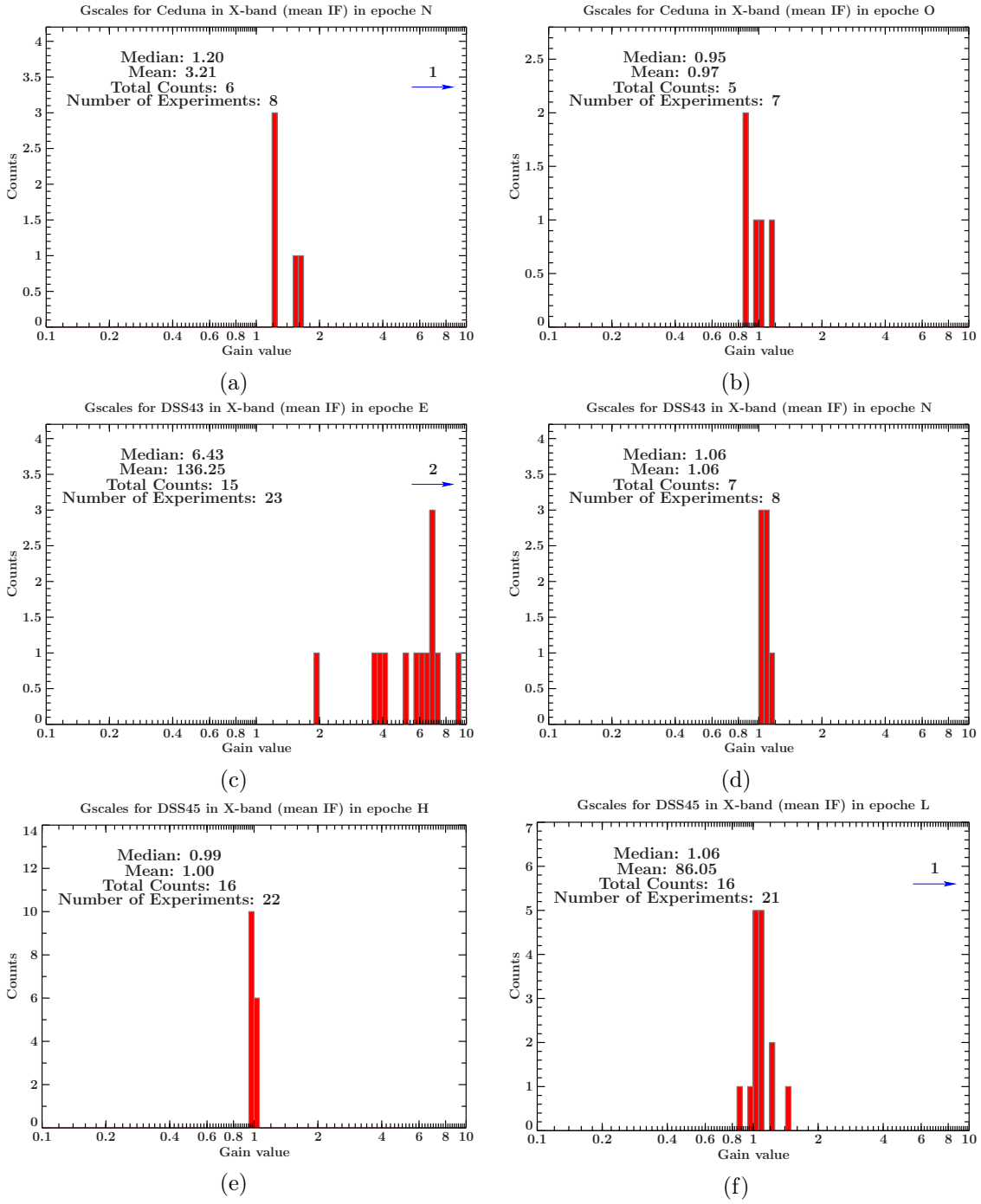

Figure A.16.: The gain value distribution as histogram for the Ceduna telescope in the observation cycles N (A.16a) and O (A.16b) (X-band),followed by the DSS43 telescope in the cycles E(A.16c) and N (A.16d)(X-band), and the DSS45 telescope in the cycles H (A.16e) and L (A.16f) (X-band).

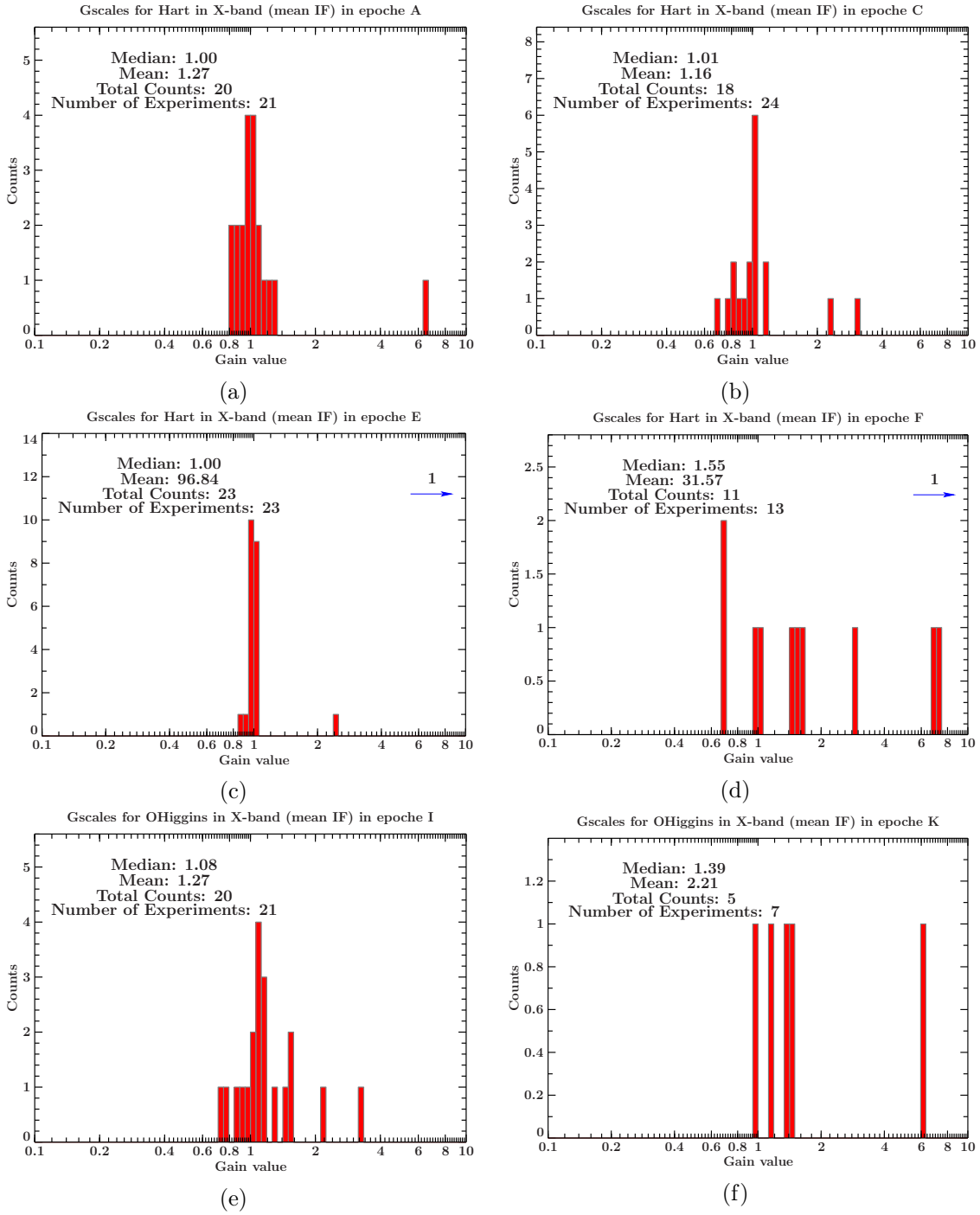

Figure A.17.: The gain value distribution as histogram for the Hartebeesthoek telescope in the observation cycles A (A.17a), C (A.17b), E (A.17c) and F (A.17d)(X-band), followed by the O'Higgins telescope in the cycles I (A.17e) and K (A.17f) (X-band).

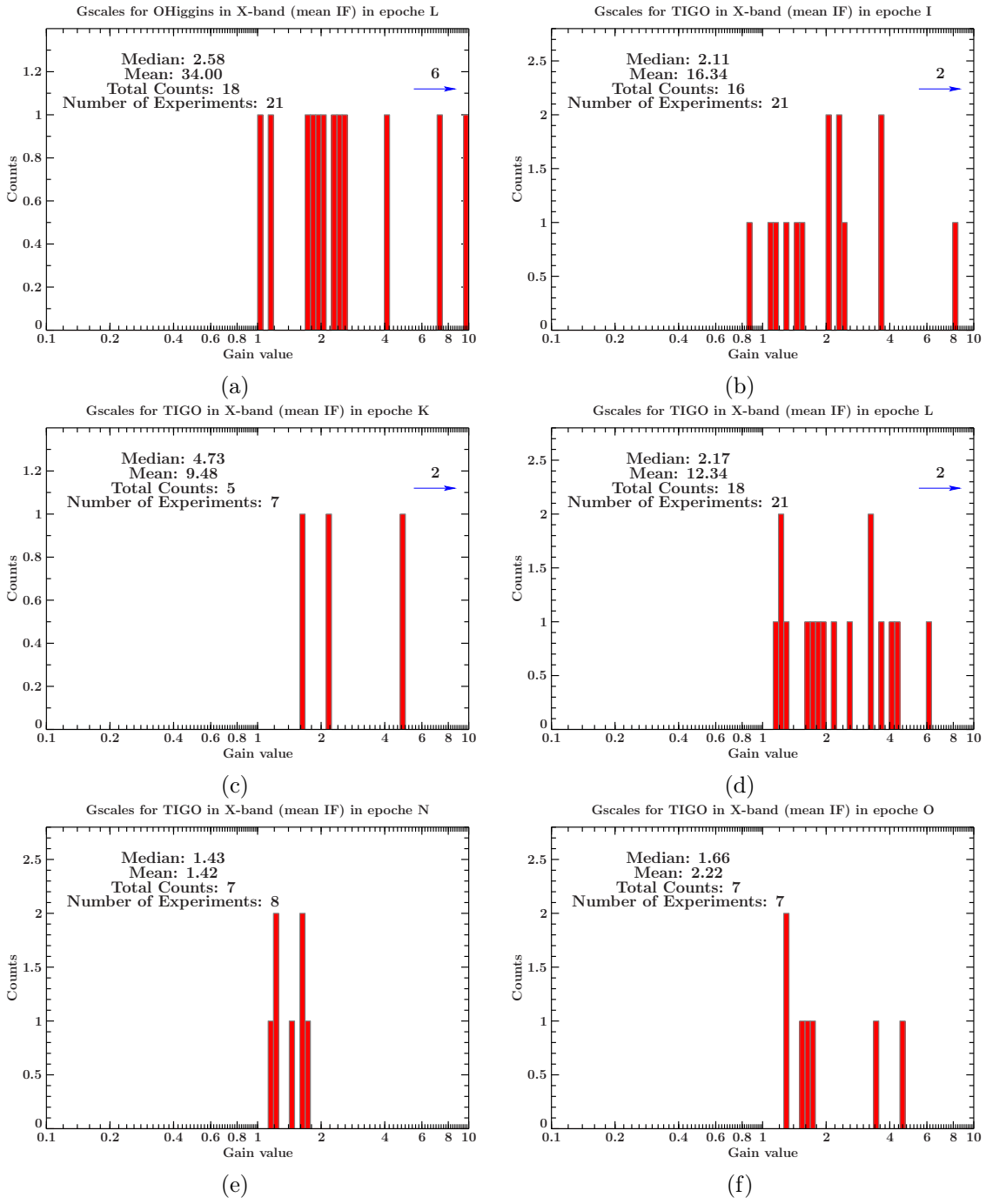

Figure A.18.: The gain value distribution as histogram for the O'Higgins telescope in the observation cycle L (A.18a) (X-band), followed by the TIGO telescope in the cycles I (A.18b), K (A.18c), L (A.18d), N (A.18e) and O (A.18f) (X-band).

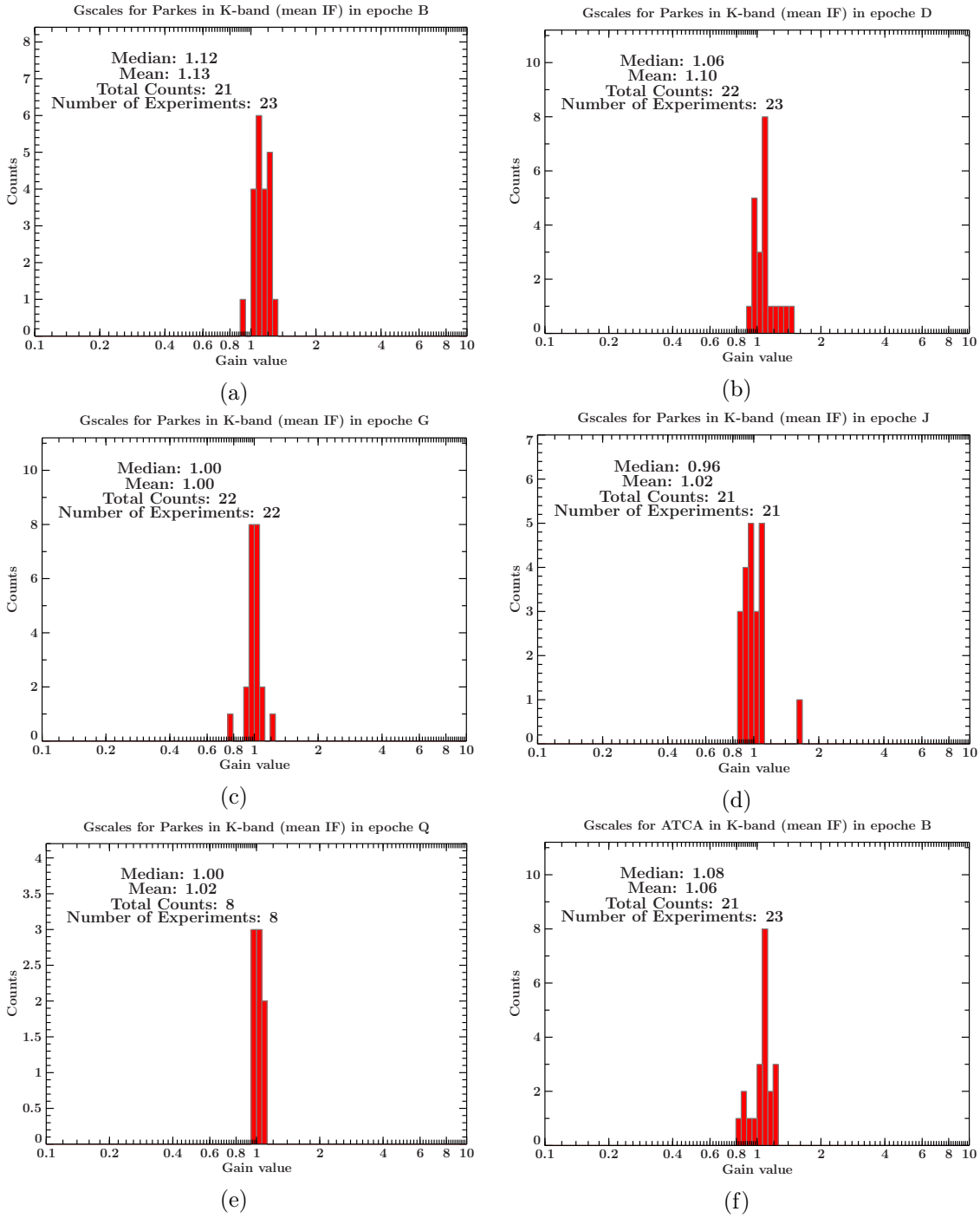

Figure A.19.: The gain value distribution as histogram for the Parkes telescope in the observation cycles B (A.19a) , D (A.19b), G (A.19c), J (A.19d) and Q (A.19e) (K-band), followed by the ATCA telescope in the cycle B (A.19f) (K-band).

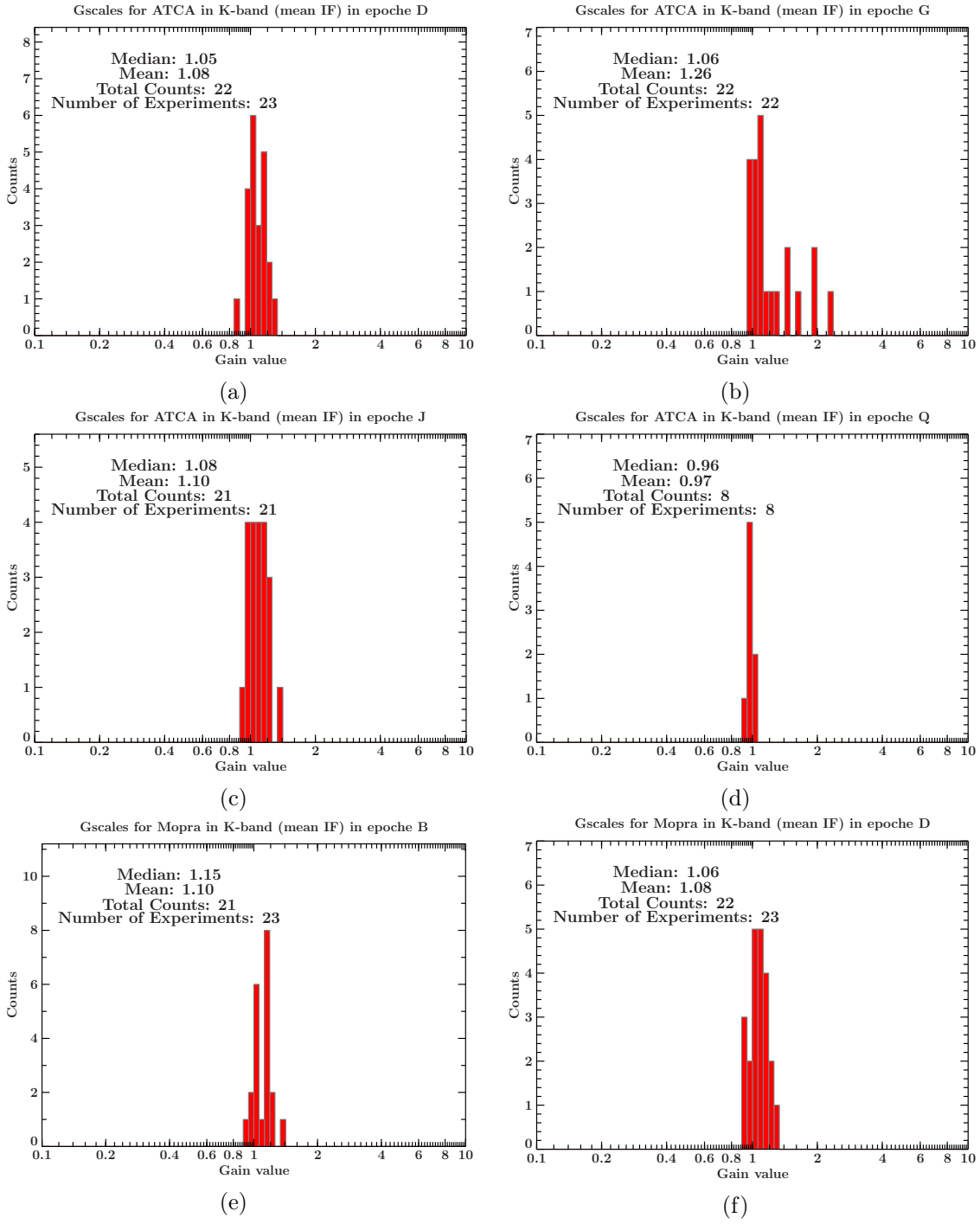

Figure A.20.: The gain value distribution as histogram for the ATCA telescope in the observation cycles B (A.20a), D (A.20b), J (A.20c) and Q (A.20d)(K-band), followed by the Mopra telescope in the cycles B (A.20e) and D (A.20f) (K-band).

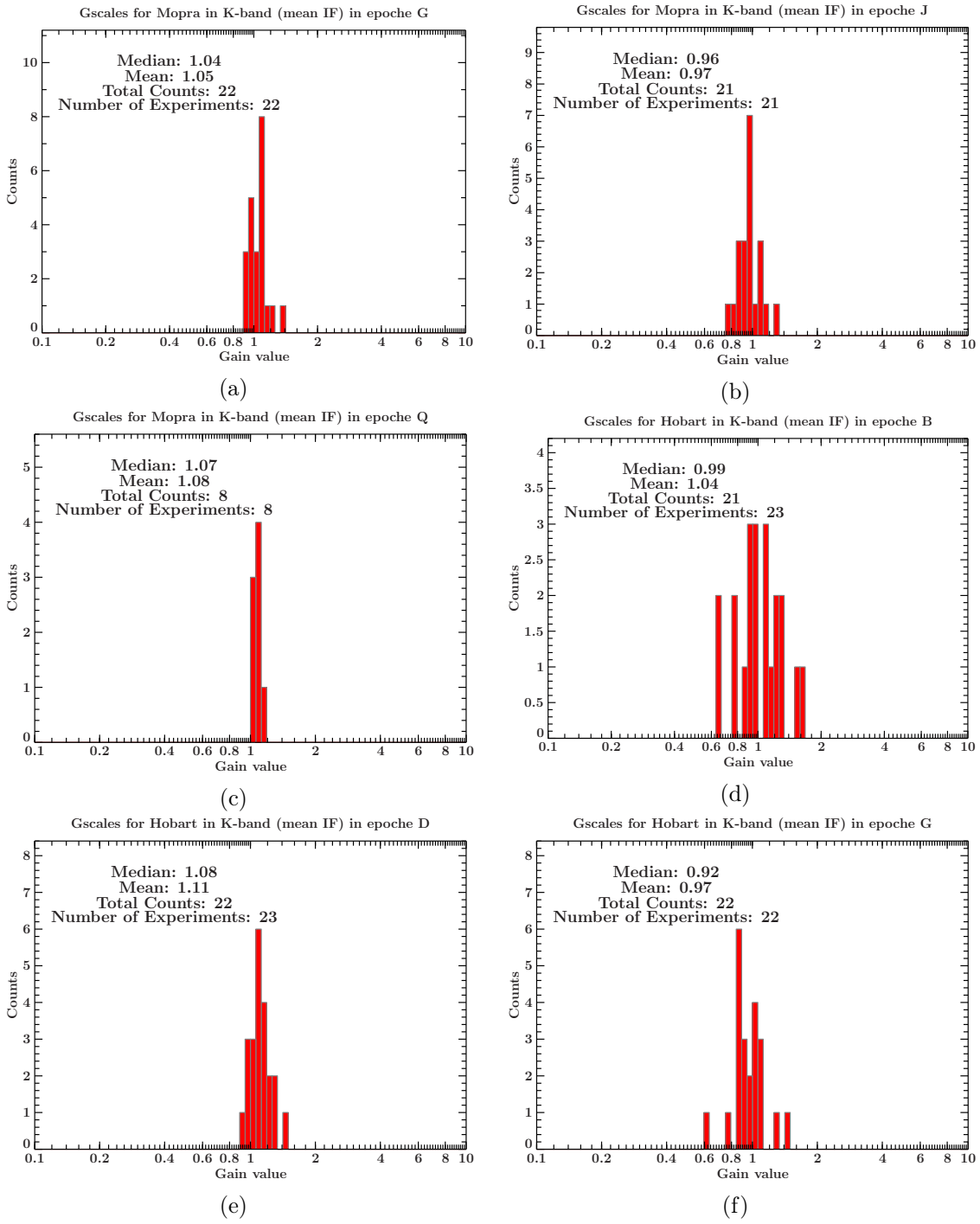

Figure A.21.: The gain value distribution as histogram for the Mopra telescope in the observation cycles G (A.21a), J (A.21b) and Q (A.21c) (K-band), followed by the Hobart telescope in the cycles B (A.21d), D (A.21e) and G (A.21f) (K-band).

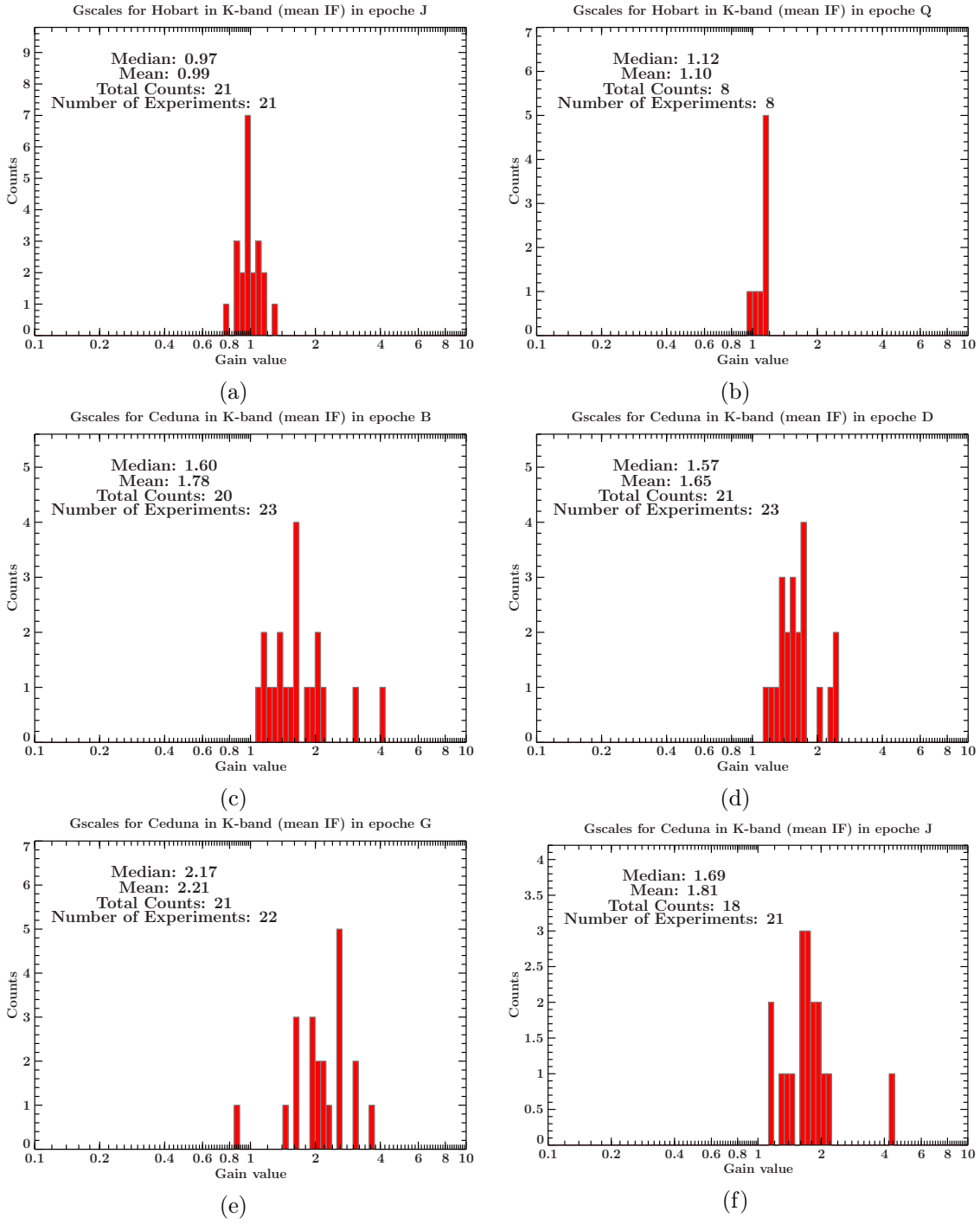

Figure A.22.: The gain value distribution as histogram for the Hobart telescope in the observation cycles J (A.22a) and Q (A.22b) (K-band), followed by the Ceduna telescope in the cycles B (A.22c), D (A.22d), G (A.22e) and J (A.22f) (K-band).

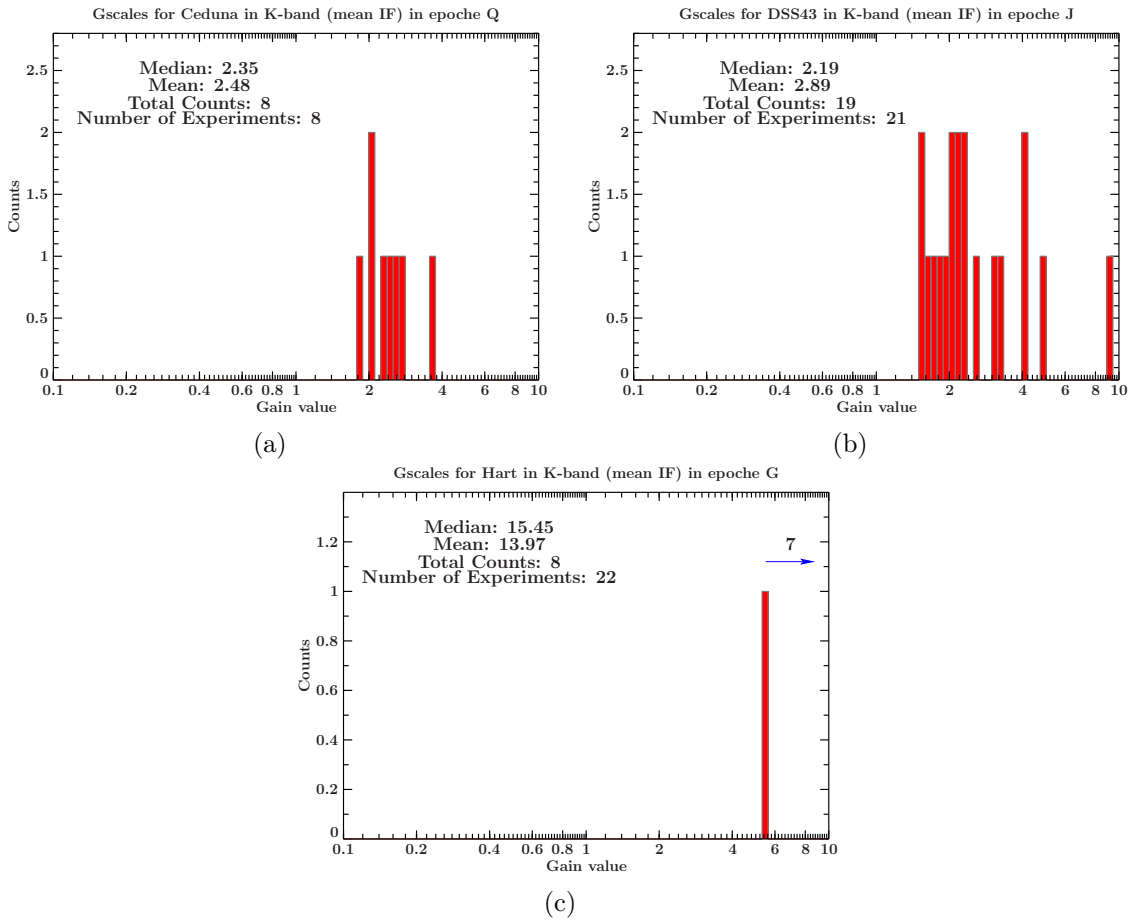

Figure A.23.: The gain value distribution as histogram for the Ceduna telescope in the observation cycle Q (A.23a) (K-band), followed by the DSS43 telescope in the cycle J (A.23b) (K-band) and the Hartebeesthoek telescope in the cycle G (A.23c) (K-band).

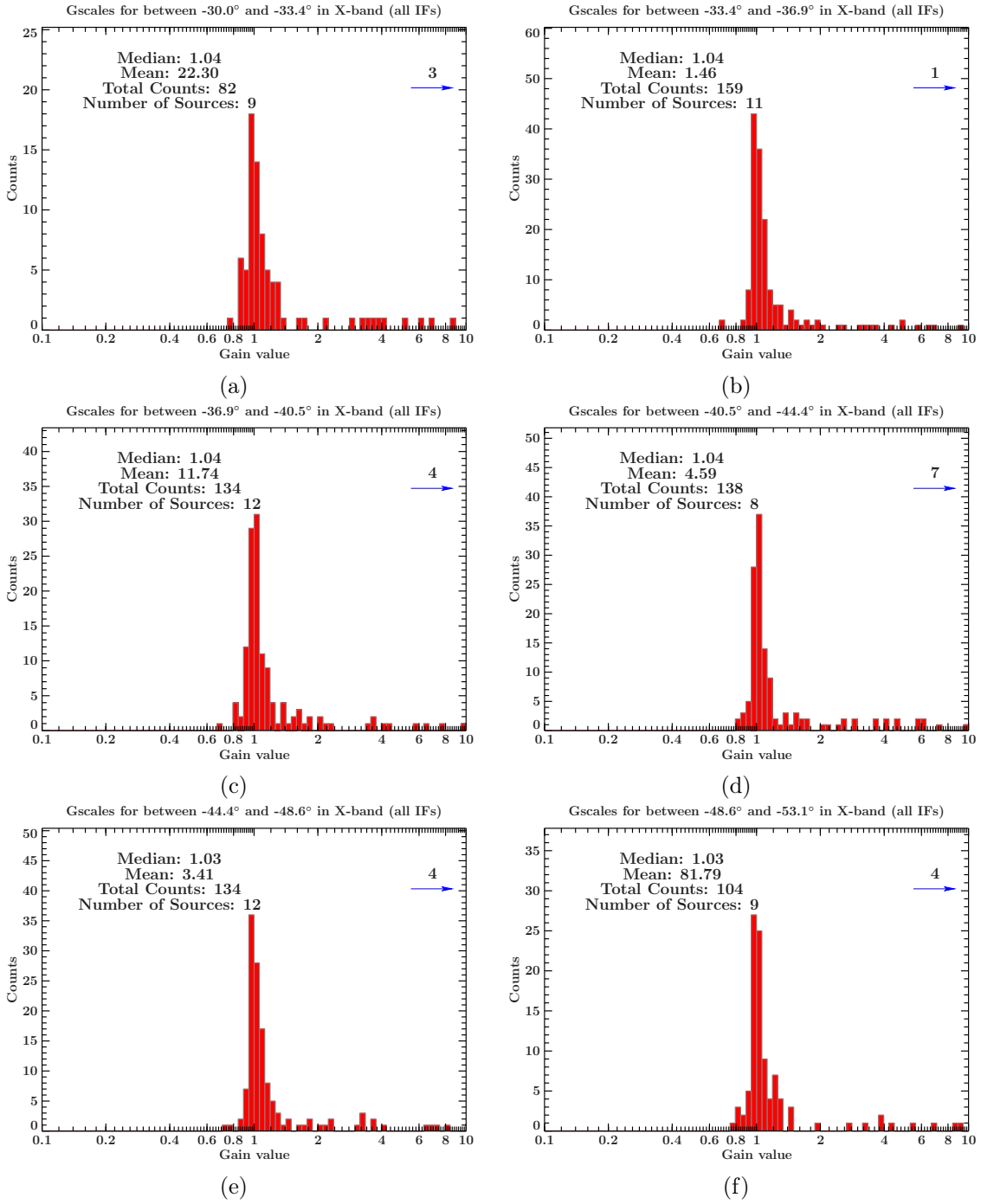

Figure A.24.: The gain value distribution as histogram for sources' declinations between -30.0° to -33.4° (A.24a), -33.4° to -36.9° (A.24b), -36.9° to -40.5° (A.24c), -40.9° to -44.4° (A.24d), -44.4° to -48.6° (A.24e) and -48.6° to -53.1° (A.24f) in X-band.

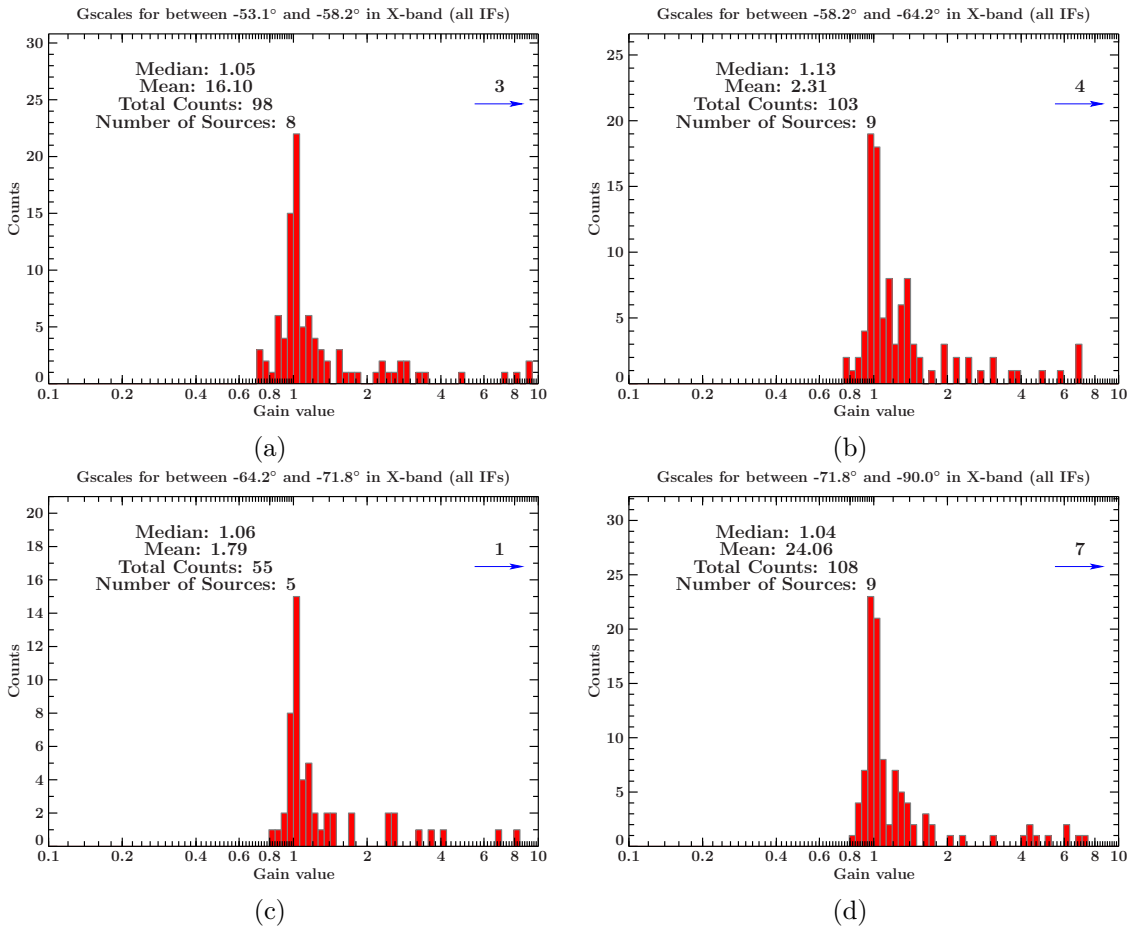

Figure A.25.: The gain value distribution as histogram for sources' declinations between -53.1.0° to -58.2° (A.25a), -58.2° to -64.2° (A.25b), -64.2° to -71.8° (A.25c) and -71.8° to -90.0° (A.25d) in X-band.

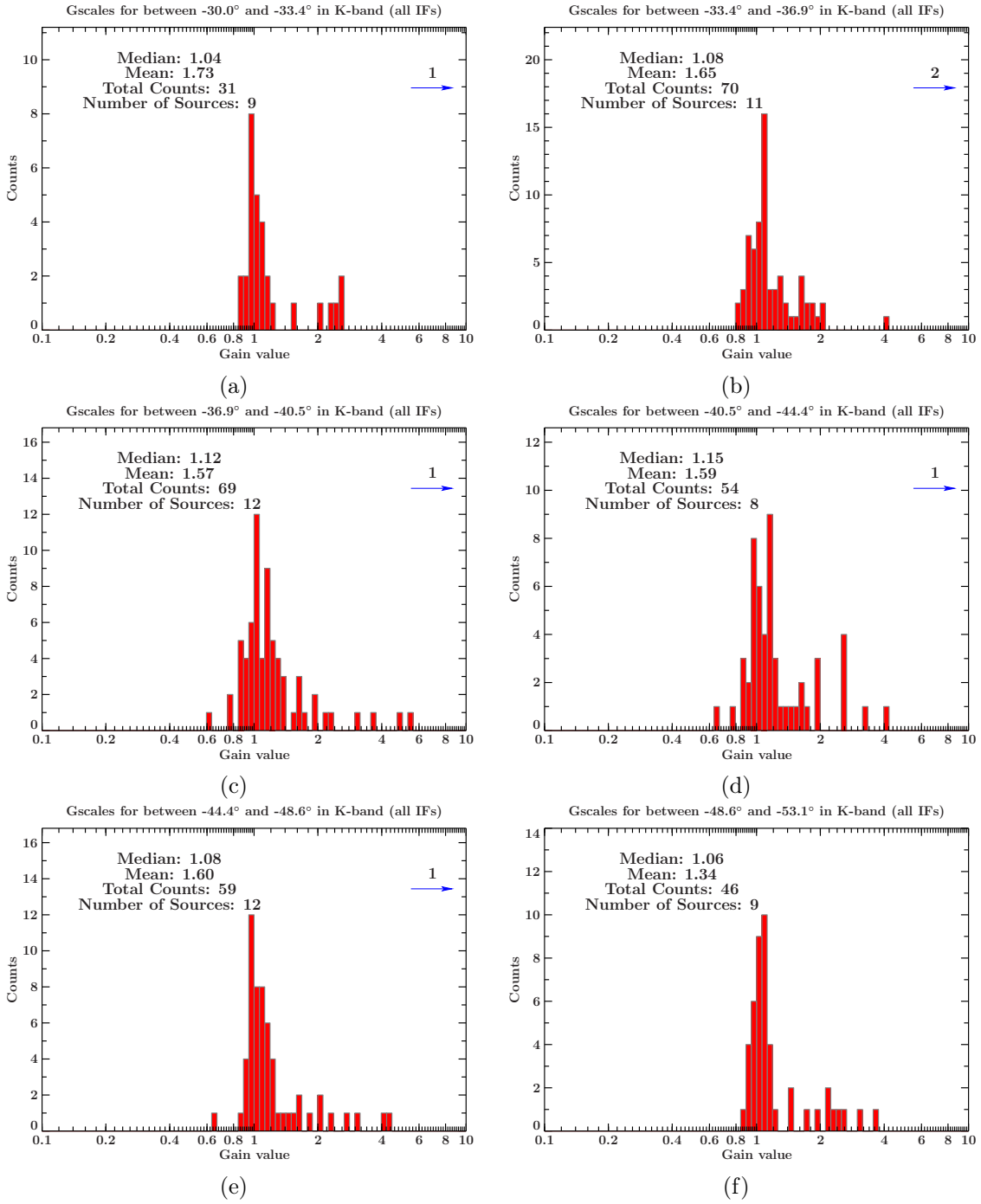

Figure A.26.: The gain value distribution as histogram for sources' declinations between -30.0° to -33.4° (A.26a), -33.4° to -36.9° (A.26b), -36.9° to -40.5° (A.26c), -40.9° to -44.4° (A.26d), -44.4° to -48.6° (A.26e) and -48.6° to -53.1° (A.26f) in K-band.

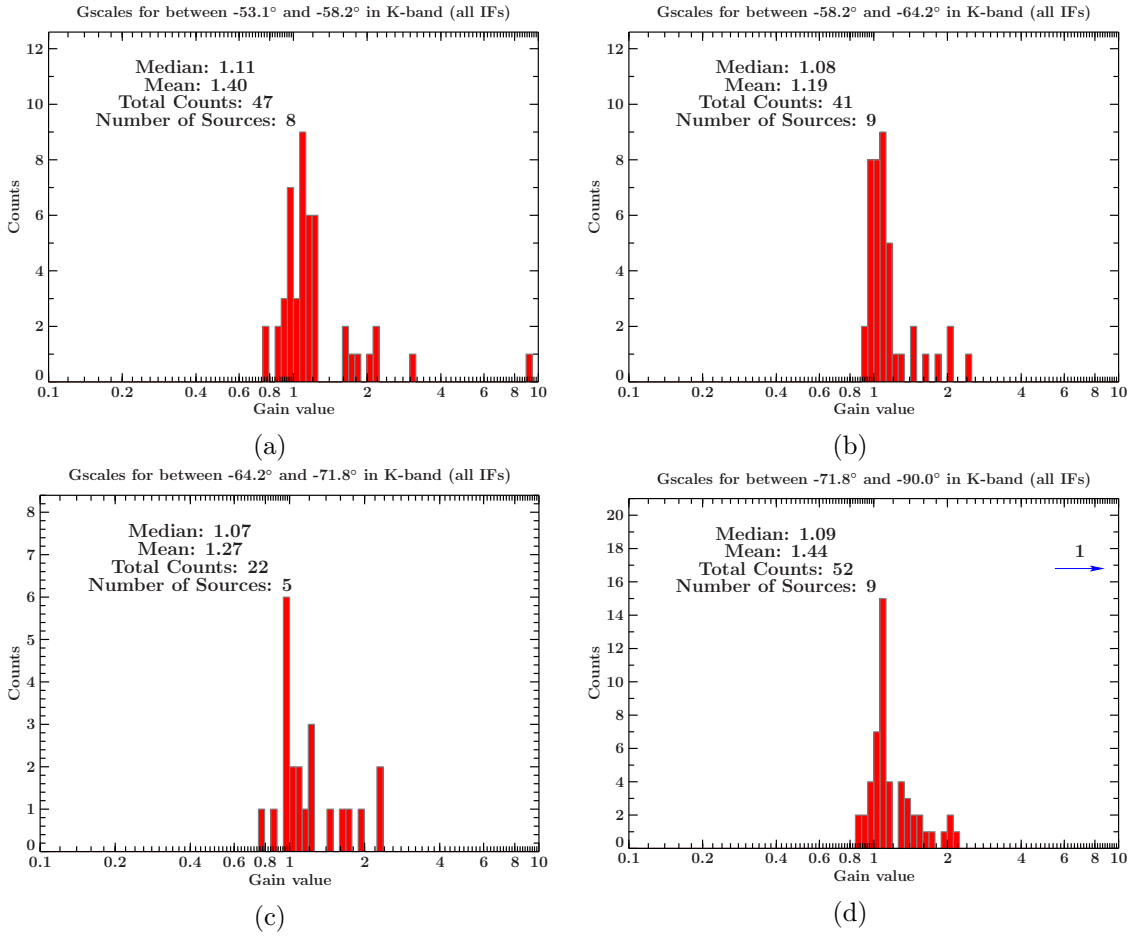

Figure A.27.: The gain value distribution as histogram for sources' declinations between -53.1.0° to -58.2° (A.27a), -58.2° to -64.2° (A.27b), -64.2° to -71.8° (A.27c) and -71.8° to -90.0° (A.27d) in K-band.

B. Danksagung

An dieser Stelle möchte ich meine Dankbarkeit an folgende Personen ausdrücken, die zum Gelingen dieser Bachelorarbeit beigetragen haben.

- Zu Beginn adressiere ich einen herzlichen Dank an Prof. Dr. Matthias Kadler für die Bereitstellung sowie auch Betreuung dieses interessanten Projektes. Bei aufkommenden Problemen, sowie aufschlussreichen Diskussionen war er zugegen und unterstützte mich mit seinem Fachwissen und hilfreichen Ratschlägen. Das Wissen und die Erfahrung die ich dabei über die Astronomie mitnehmen durfte haben mich zudem darin bestärkt mich weiter in diesem hochinteressanten Bereich der Physik zu beschäftigen.

- Ein besonderer Dank geht an meine Betreuer Robert Schulz und Jonas Trüstedt. Immer wenn Fragen oder Probleme aufkamen halfen sie mir bereitwillig und konnten mir überdies hilfreiche Tipps aus ihren Erfahrungen mitgeben. Hilfsbereit übernahmen sie ebenfalls das Korrekturlesen, was für mich eine sehr große Hilfe darstellte, nochmals ein Feedback von einer Fachkundigen Seite zu erhalten.

- Ohne weitere Namen zu nennen (da dies einfach zu viele wären), möchte ich mich bei der ganzen AG Kadler bedanken, die mich ohne Umwege mit meinem Projekt in ihre Struktur eingebunden hat und für ein überaus angenehmes Arbeitsklima sorgte.

- Darüber hinaus möchte ich ebenfalls meinen Eltern danken, welche mich in allen meinen Entscheidungen und insbesondere meinem Studium in besonderem Maße unterstützen und mir ein auf den Lerninhalt konzentriertes Studium ermöglichen.

Abschließend möchte ich meine Anerkennung für meine Freunde und Kommilitonen äußern, die nicht explizit erwähnt sind und zu dieser Arbeit in Form von inspirativen Diskussionen und Vorschlägen beitrugen.

List of Figures

Acronyms

AGN Active Galactic Nuclei. v, vi, 1, 2, 5, 35

ATNF Australia Telescope National Facility. 3

BKG *Bundesamt für Kartographie und Geodäsie*. 3

EGRET Energetic Gamma Ray Experiment Telescope. 2

EM electromagnetic. 1, 5

EVN European VLBI Network. 2, 4, 93

FFT Fast Fourier transformation. 10

FWHM full width at half maximum. 10, 12

LBA Long Baseline Array. 2, 3

MOJAVE Monitoring Of Jets in Active galactic nuclei with VLBA Experiments. 2, 4, 93

NASA National Aeronautics and Space Administration. 3

PKS Parkes Radio Cataloge. 15

SMBH Super Massive Black Hole. 1

TANAMI Tracking Active Galactic Nuclei with Austral Milliarcsecond Interferometry. v, vi, 2–4, 9, 11, 17, 30, 35, 93

VLBA Very Long Baseline Array. 4

VLBI Very Long Baseline Interferometry. v, vi, 1, 2, 4, 5, 9, 10, 93